Ordering forces would be expected to affect M_s from Zener's calculations.[4] Nearest-neighbour distances are little affected during (110)[$\bar{1}$10] shear, but ordering is significantly affected and M_s would be expected to be depressed. This constraint is likely to be readily observed in elastic modulus measurements. Robertson[19] has recently reviewed most of the available information on elastic moduli and has pointed to the considerable assistance to be gained from such values in predicting transformation behaviour. He notes that instability is promoted in the b.c.c. phase by a large elastic anisotropy. Zirinsky[9] reports that elastic anisotropy of $AuCd^{47.5}$ in the β′ phase, just above M_s, may be decreased by quenching to give a value similar to that of the annealed $AuCd^{50}$ alloy and a similar transformation product. The reason for this is not clear but has been discussed by Nakanishi[20] in terms of a stabilizing effect from a decreased ionic repulsion due to the production of vacancies on quenching.

It is interesting to compare the transformation behaviour of AgCd β-phase alloys[21] with those of AuCd. In the former an orthorhombic phase, structurally intermediate between b.c.c. and h.c.p., is formed on cooling. However, if this phase is deformed, ordering constraints are reduced and a hexagonal structure results. Further, it is known that when h.c.p. phases become ordered they often undergo an orthorhombic distortion.[5] Since ordering forces would be expected to be a maximum in AuCd at the 1 : 1 ratio it was considered that the trigonal phase might be metastable to the orthorhombic phase in that ordering forces stabilize the trigonal form. However, deformation of the $AuCd^{50}$ trigonal phase by filing at 20° C produces only line broadening of the X-ray powder pattern.

Work is proceeding to determine the elastic anisotropy of various β-phase alloys in order to correlate this information with bulk-transformation data and microstructural features.

Acknowledgements

Grateful thanks are extended to Professor G. V. Raynor for providing laboratory facilities. This research has been sponsored in part by the Air Force Office of Scientific Research under Grant AF EOAR 67-4 through the European Office of Aerospace Research (OAR), United States Air Force.

References

1. W. Hume-Rothery, P. W. Reynolds, and G. V. Raynor, *J. Inst. Metals*, 1940, **66,** 191.
2. G. V. Raynor and T. B. Massalski, *Acta Met.*, 1955, **3,** 480.
3. H. Warlimont, "Physical Properties of Martensite and Bainite" (Iron Steel Inst. Special Rep. No. 93), p. 58. **1965:** London (Iron Steel Inst.).
4. C. Zener, *Phys. Rev.*, 1947, **71,** 846.
5. T. B. Massalski and H. W. King, *Progress Materials Sci.*, 1961, **10,** (1), 1.
6. H. Pops and T. B. Massalski, *Trans. Met. Soc. A.I.M.E.*, 1964, **230,** 1662.
7. M. E. Brookes and R. W. Smith, *Metal Sci. J.*, to be published.
8. M. S. Wechsler, *Acta Met.*, 1957, **5,** 150.
9. S. Zirinsky, *ibid.*, 1956, **4,** 164.
10. L. C. Chang, *Acta Cryst.*, 1951, **4,** 320.
11. L. C. Chang and T. A. Read, *Trans. Amer. Inst. Min. Met. Eng.*, 1951, **191,** 47.
12. J. F. Breedis, D. S. Lieberman, and T. A. Read, to be published (quoted in Ref. 13).
13. N. Nakanishi and C. M. Wayman, *Trans. Met. Soc. A.I.M.E.*, 1963, **227,** 500.
14. F. Rothwarf and L. Muldawer, *J. Appl. Physics*, 1962, **33,** 2531.
15. M. E. Brookes and R. W. Smith, *J. Sci. Instruments*, 1967, **44,** 75.
16. W. Lovick, *Electronic Eng.*, 1962, **34,** 332.
17. P. R. Swann and H. Warlimont, *Acta Met.*, 1963, **11,** 511.
18. L. Muldawer, *J. Appl. Physics*, 1966, **37,** 2062.
19. W. D. Robertson, Ref. 3, p. 26.
20. N. Nakanishi, *J. Japan Inst. Metals*, 1965, **6,** 222.
21. D. B. Masson, *Trans. Met. Soc. A.I.M.E.*, 1960, **218,** 1940.

On the Problem of the Definitions and the Mechanisms of the Bainite Reaction

H. I. Aaronson

Bainite is shown to have three principal definitions, each quite different from and often incompatible with the other two. The *microstructural* definition considers that bainite is formed by the precipitation of a non-lamellar dispersion of carbides (from austenite and/or from ferrite) in association with proeutectoid ferrite. On this view, bainite is the product of non-lamellar eutectoid reactions, and is thus the counterpart of the lamellar or pearlite reaction. The *kinetic* definition describes bainite as formed largely in the temperature region between those of the pearlite and martensite reactions, characterized by its own C-curve and increasingly incomplete as the highest temperature of this curve is approached. Recent evidence indicates, however, that these phenomena develop only in the presence of certain alloying elements that retard the kinetics of the proeutectoid ferrite reaction through an interface reaction effect, particularly at intermediate transformation temperatures. The *surface-relief* definition terms bainite any precipitate plate which has a composition different from that of its matrix and exhibits a martensitic relief effect at a free surface. A shear-type growth mechanism is customarily inferred. It is shown, however, that the most probable mechanism for the growth of a ferrite crystal is the diffusional jumping of atoms across disordered areas of interphase boundary at its edges and at the risers of ledges on its broad faces. Thus, the recommendations are offered that the microstructural definition be accepted as the definition of bainite, that the kinetic definition be considered to describe an effect of alloying elements upon the proetutectoid ferrite reaction, and that the surface-relief definition be discarded.

The bainite reaction, which was the last of the major modes of austenite decomposition to be discovered, has been hard pressed, almost from the beginning, to establish and retain a definite identity. As a result of repeated changes not only of definition but also, it will be shown, of the transformation phenomena described, an aura of confusion has come to envelop the term bainite. An attempt will accordingly be made to clarify the problem of definition. This will provide a framework for the principal concern of this paper, namely, a critical examination of the various explanations proposed for the phenomena encompassed by each of the main definitions of bainite now in use.

Manuscript received 24 April 1968. H. I. Aaronson, Ph.D., is in the Metallurgy Department of the Scientific Laboratory, Ford Motor Company, Dearborn, Michigan, U.S.A.

Summary of the Three Principal Definitions of Bainite

The *microstructural* definition[1,2] characterizes bainite as Widmanstätten ferrite which is precipitated from austenite and contains a (normally) non-lamellar dispersion of carbides (Fig. 1).

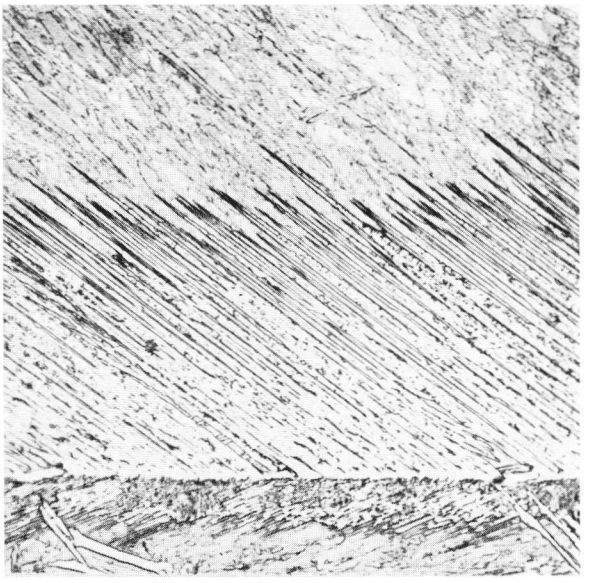

Fig. 1 *Representative microstructurally defined bainite in* 0·29% *C,* 0·76% *Mn steel reacted* 4 *sec at* 525° *C.* × 1000.

The *kinetic* definition describes bainite in terms of the following behaviours of the overall kinetics of isothermal reaction.[3–14]

(1) On a *TTT* diagram, the bainite reaction has its own C - curve for the initiation of transformation. Most of this curve usually lies in the temperature range between the C - curve for the pearlite reaction and the M_s temperature. In plain carbon steels, the bainite and pearlite C - curves overlap extensively (Fig. 2(*a*)), whereas in steels containing an appreciable proportion of an alloying element that is a strong carbide former, e.g. Mo or Cr, the curves can be quite well separated (Fig. 2(*b*)).

(2) The upper temperature of the bainite C - curve, here denoted as the " kinetic-bainite start " or " kinetic-B_s " temperature, represents the highest temperature at which bainite can form, and usually lies 100–300 degC below the eutectoid temperature range.

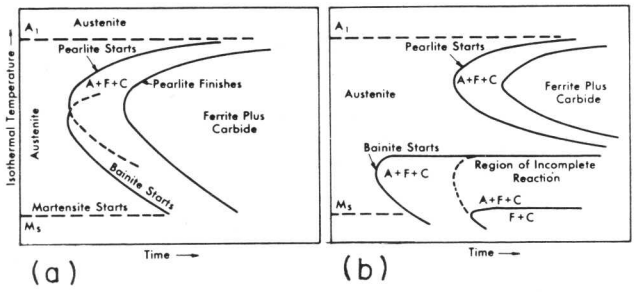

[*Courtesy "Metal Progress"*.

Fig. 2 (a) *Relative disposition of the C-curves for pearlite and for bainite in a steel in which they overlap extensively, and* (b) *in a steel in which they are well separated.*[15]

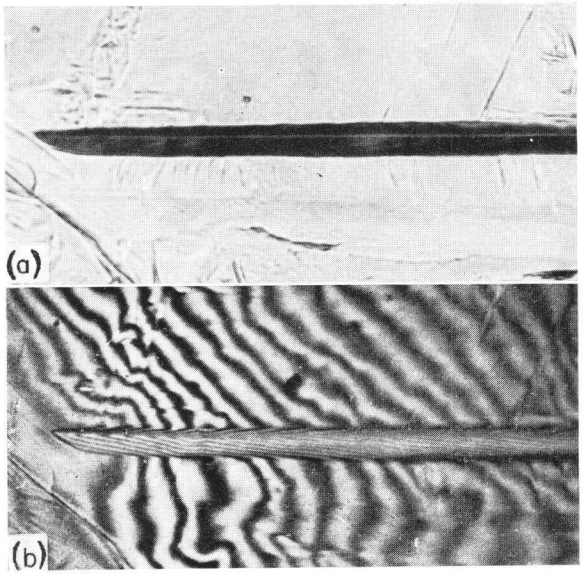

Fig. 3 *" Surface-relief bainite "; a Widmanstätten ferrite plate formed in an Fe–0·11% C alloy reacted* 12 *sec at* 730° *C shown under* (a) *ordinary illumination, and* (b) *by interferometry, with the martensite-like relief effect displayed with exceptional clarity. (Courtesy Dr. K. R. Kinsman.)*

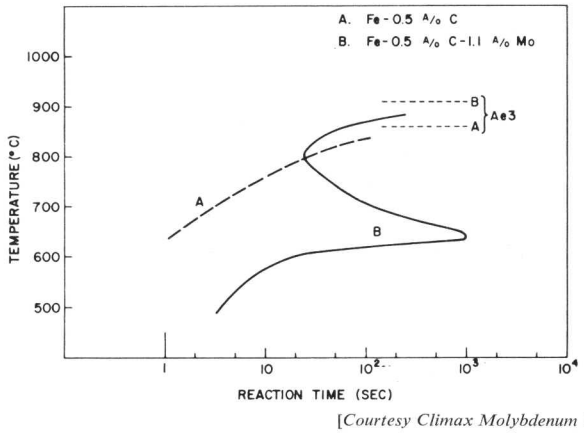

[*Courtesy Climax Molybdenum Co*

Fig. 4 TTT *curves for initiation of transformation in Fe–0·11% C–1·95% Mo (solid curve) and Fe–0·11% C (broken curve).*[51]

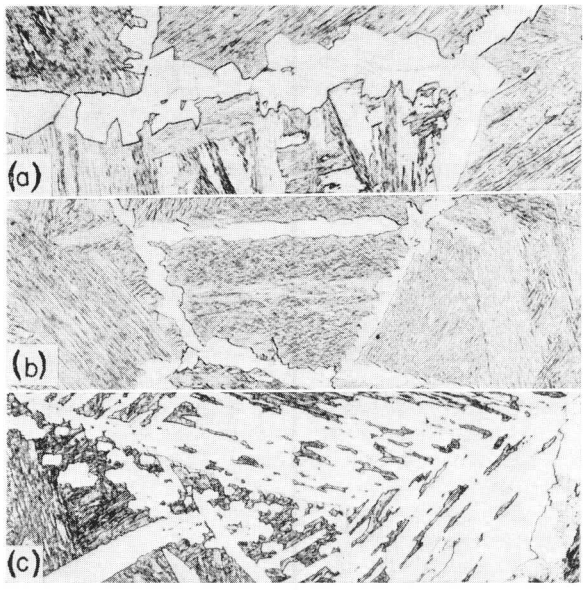

Fig. 5 *Proeutectoid ferrite as the only transformation product at temperatures* (a) *above*, (b) *at, and* (c) *below that of the bay in Fe–0·11% C–1·95% Mo.* (a) *Reacted* 5 *min at* 700° *C*, (b) *reacted* 90 *min at* 650° *C*, (c) *reacted* 2 *h at* 630° *C. All* × 150.

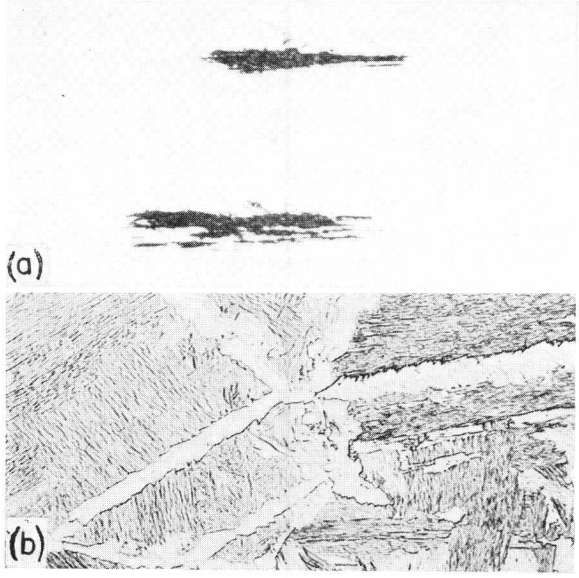

Fig. 6 (a) *Microstructural bainite formed* 50 *degC above the kinetic-*B_S *in Fe–0·41% C–2·99% Cr; reacted* 50 *min at* 600° *C.* × 1000. (b) *Only grain- and twin-boundary allotriomorphs of proeutectoid ferrite in Fe–0·11% C–1·95% Mo,* 10 *degC below the kinetic-*B_S*; reacted* 150 *min at* 640° *C.* × 150.

(3) Austenite can be completely transformed to bainite at and below a characteristic temperature, inappropriately termed the " bainite-finish " or B_f temperature. At higher temperatures, transformation ceases entirely after the austenite matrix has been only partially decomposed. The proportion of the austenite transformed to bainite decreases with increasing temperature, becoming zero at the kinetic-B_S.

On the *surface-relief* definition,[16,17] bainite consists simply of ferrite plates that exhibit a martensite-like relief effect when formed at a free surface (Fig. 3).

Conflicts among the Three Definitions of Bainite

As Ko[17] has clearly stated, surface-relief bainite need not contain carbides. Ferrite plates are a major feature of the microstructure at temperatures above that of the eutectoid within an appreciable temperature–composition region in plain carbon steels.[18] Since carbide formation is thermodynamically impossible in this region, a major conflict is thus established between the surface-relief and the microstructural definitions.

The *TTT* curve for the beginning of transformation in a Fe–0·11% C–1·95% Mo alloy[19] is given in Fig. 4 as a solid curve. Comparison with Fig. 5 shows that proeutectoid ferrite is the transformation product at temperatures above, at, and below that of the kinetic-B_s. An equivalent conflict between the microstructural and the kinetic definitions can be demonstrated in a low-carbon 3% Cr steel.[13] Conversely, Fig. 6(*a*) illustrates microstructural bainite at a temperature ~ 50 degC above that of the kinetic-B_s[20] in a higher-carbon 3% Cr steel.

Fig. 6(*b*) shows only carbide-free grain-boundary and twin-boundary allotriomorphs 10 degC below the kinetic-B_s. That allotriomorphs do not yield a martensitic surface relief has long been known.[17] Both this observation and that of Fig. 6(*a*) are illustrative of important conflicts between the surface-relief and the kinetic definitions of bainite. Even more striking examples of this situation are provided by the recent findings that the W_s (Widmanstätten-start) temperature in the Fe–C–Mo alloy of Fig. 4 is 200 degC higher than the kinetic-B_s temperature, and that nearly as large a difference exists in a low-carbon 3% Cr steel.[21]

The examples given in this section provide critical support for the view that the three definitions of bainite actually deal with essentially different transformation phenomena. In succeeding sections, these definitions will be individually considered from this standpoint.

The Microstructural Definition

The core aspect of the microstructural definition is the precipitation of carbides in association with proeutectoid ferrite. These carbides can precipitate from austenite at austenite/ferrite boundaries and from the proeutectoid ferrite itself.[22–29] In both cases, however, it is clear that what is taking place overall is simply the eutectoid reaction: austenite → ferrite + carbide. The pearlite and the bainite reactions can thus be regarded simply as alternative means of reaching equilibrium at temperatures where the formation of *two* precipitate phases is required to attain this condition.

A better perspective of the microstructural definition of bainite as a particular " internal " morphological form of the eutectoid reaction may be gained by consideration of the morphologies developed during eutectoid decomposition in alloy systems other than Fe–C.* From this point of view it is soon appreciated that the eutectoid reaction has two principal " internal " morphologies: the familiar pearlitic or *lamellar* one; and the " granular ", or " divorced ", or *non-lamellar* eutectoid morphology. The non-lamellar morphology evidently occurs less frequently, however, and is intrinsically subject to more extensive variations in form and mechanism; its significance has thus been less widely appreciated. When both low-temperature phases precipitate from the matrix and are able to form with little difficulty by repeated nucleation and/or by continued growth of one precipitate phase around crystals of the other, structures such as that of Fig. 7(*a*) develop. As in the case of pearlite, the

* The review by Spencer and Mack[30] is particularly useful in this context.

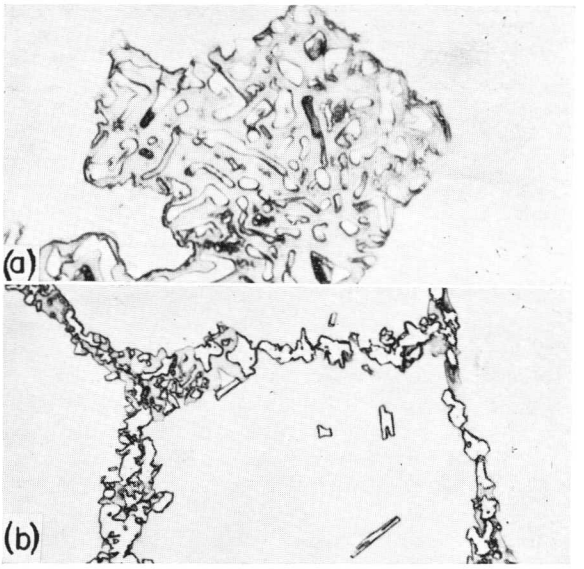

[*Courtesy Amer. Inst. Min. Met. Eng.*

Fig. 7 (a) *Largely non-lamellar eutectoid structure in Ti–17·42% Cr; reacted 8 days at 650° C.* × 2000. (b) *Comparison of proeutectoid $TiCr_2$ and eutectoid morphologies in the same alloy; reacted 5 days at 675° C.*[31] × 500.

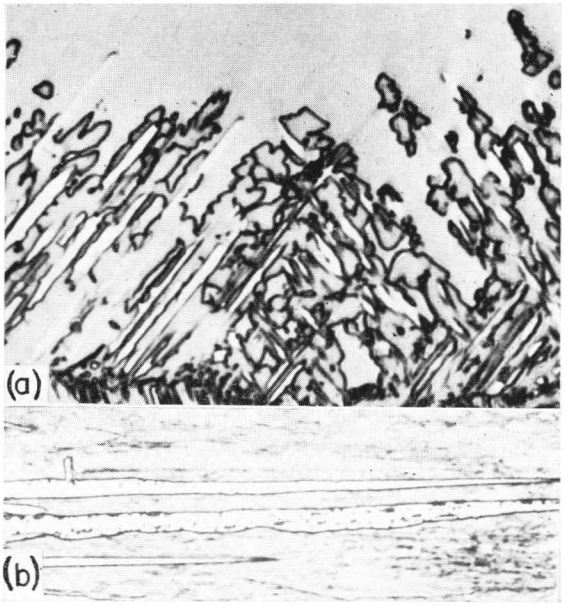

[*Courtesy John Wiley.*

Fig. 8 (a) *Non-lamellar eutectoid initiated by α needles in Cu–27·0% Sn; reacted 1 min at 500° C.*[30] × 2000. (b) *Demonstration that ferrite plates at which bainitic carbides have precipitated are thicker in Fe–0·29% C–0·76% Mn; reacted 7 sec at 500° C.* × 1000.

" external " morphology of a non-lamellar eutectoid structure formed in this manner usually differs markedly from that of any proeutectoid component of the microstructure (Fig. 7(*b*)). When both repeated nucleation and continued growth are inhibited, however, the " external " morphology of the eutectoid structure inevitably resembles more closely the morphology of the precipitate that, functioning as the proeutectoid phase, initiated the formation of this structure (Fig. 8(*a*)).

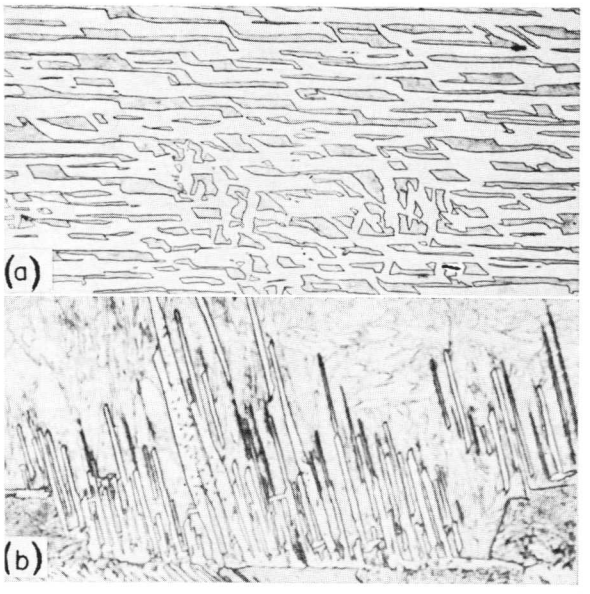

Fig. 9 Ferrite sideplates free of carbides at 600° C and containing a relatively small number of them at 550° C in a 0·29% C, 0·76% Mn steel. (a) *Reacted 4 sec at 600° C.* × 1000. (b) *Reacted 4 sec at 550° C.* × 1000.

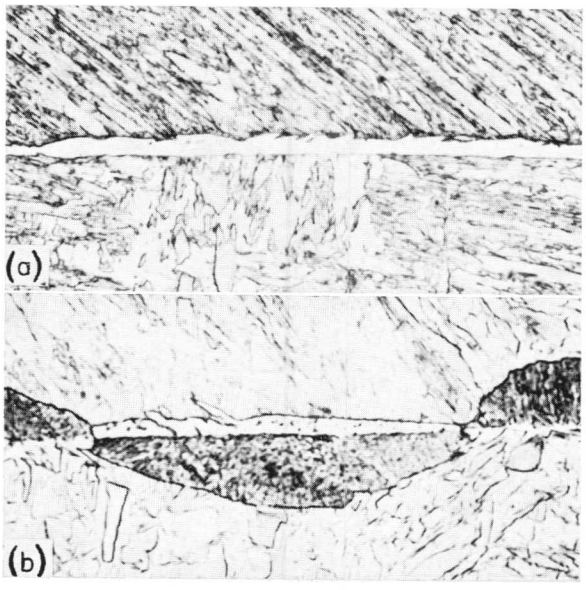

Fig. 10 Grain-boundary allotriomorphs of ferrite at 600° C and of bainite at 550° C in a 0·29% C, 0·76% Mn steel. (a) *Reacted 6 sec at 600° C.* × 1000. (b) *Reacted 2 sec at 550° C.* × 1500.

In the microstructural bainite reaction in steel, Fig. 8(*b*) indicates that both repeated nucleation of carbides and continued growth of proeutectoid ferrite around them occur readily. However, the size of the individual carbides is so small relative to that of the ferrite plates that continued growth of the ferrite does not normally produce important changes in the shape of the resulting aggregate structure. Should carbide precipitation take place wholly within proeutectoid ferrite, the external morphology of the eutectoid structure must of course be identical to that of its ferritic component.

If a non-lamellar eutectoid reaction happens to be initiated primarily by the formation of a particular proeutectoid morphology, and should this morphology develop at temperatures appreciably above that at which the second precipitate phase begins to nucleate at a significant rate, then one must expect that the proeutectoid structures will exhibit a continuous transition into non-lamellar eutectoid structures as the reaction temperature is decreased. Such a transition is readily observed in steel.[25] Figs. 9(*a*) and (*b*) exemplify proeutectoid ferrite sideplates entirely free of carbides, and containing carbides only in some plates, respectively, while Fig. 1 shows carbides associated with all sideplates in the microstructure; this sequence evolved as a plain carbon hypoeutectoid steel was reacted at successively lower temperatures.

Further evidence that the non-lamellar eutectoid reaction is the central aspect of microstructurally defined bainite is provided by the following demonstrations that the existence of this reaction is not dependent upon the Widmanstätten ferrite morphology. Since this morphology normally predominates at the temperatures at which the precipitation of bainitic carbides is observed, it has appeared reasonable to make the contrary assumption. However, Figs. 10(*a*) and (*b*) show grain-boundary allotriomorphs of proeutectoid ferrite free of carbides at one reaction temperature, and bainitic allotriomorphs at a somewhat lower temperature.

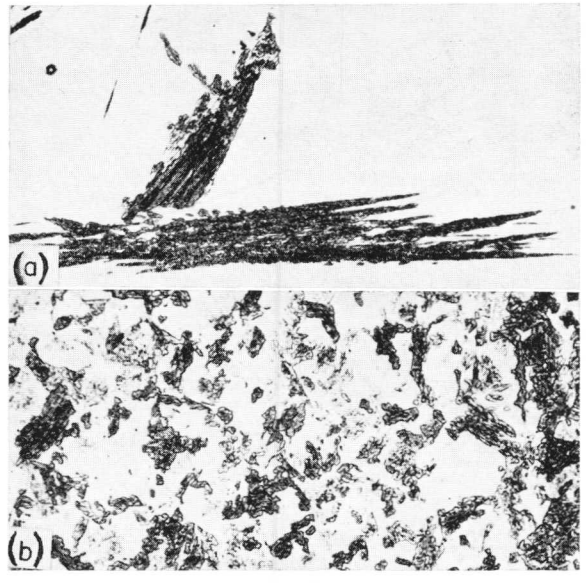

Fig. 11 Influence of austenite grain size upon the morphology of the ferritic component of bainite in Fe–0·39% C–2·96% Cr. (a) *Widmanstätten morphology in specimen with ASTM grain size larger than No. 0; reacted 2 min at 450° C.* × 250. (b) *Predominantly allotriomorphic morphology in specimen with ASTM grain size smaller than No. 8; reacted 2 min at 450° C.*[32] × 500.

Normally allotriomorphs are only a minor component of the microstructure at temperatures within the microstructural bainite range. Figs. 11(*a*) and (*b*) demonstrate that this situation can be reversed by sufficiently reducing the austenite grain size.[32] Bainitic carbides are still present in the microstructure shown in Fig. 11(*b*) despite the fact that allotriomorphs have become virtually the only ferrite morphology.

If one temporarily continues to restrict the use of the term bainite to structures in which the ferritic component has a plate or needle morphology, the microstructural B_s tem-

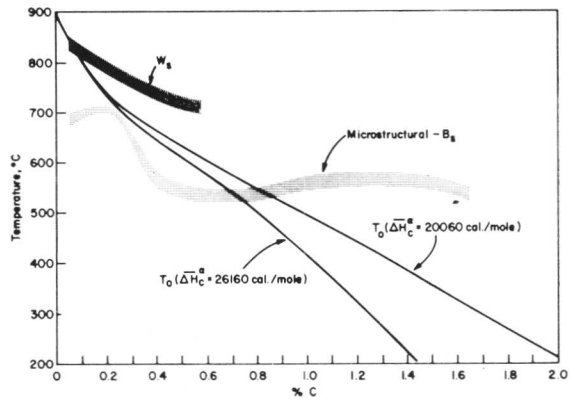

[*Courtesy Amer. Inst. Min. Met. Eng. and John Wiley.*

Fig. 12 *Microstructural-*B_s *temperature (requiring the ferrite to be in Widmanstätten form) and* W_s *temperature as a function of carbon content in high-purity Fe–C alloys*[33,51] *compared with two versions of* T_0 *vs.* % *C curve.*

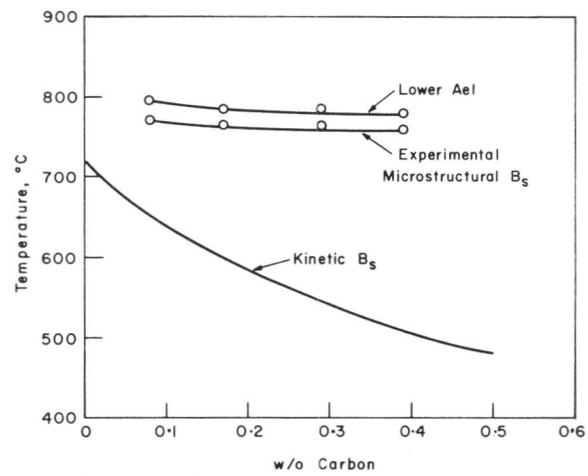

Fig. 14 *Effect of carbon content upon the lower Ae 1 temperature, the experimentally observed microstructural-*B_s*, and the* TTT *diagram or kinetic-*B_s *(as reported by Lyman and Troiano*[13]*) in* 3% *Cr steels.*[32]

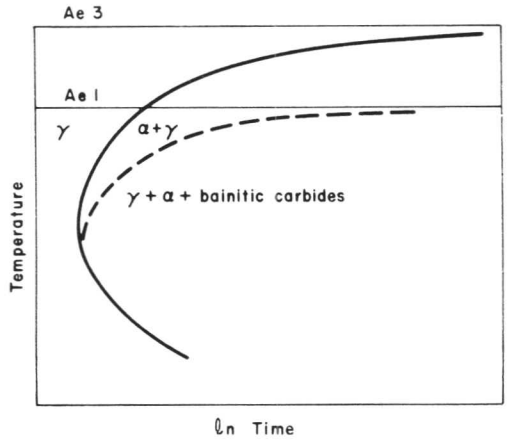

Fig. 15 *Schematic* TTT *diagram for the initiation of the proeutectoid ferrite reaction (solid curve) and of the associated precipitation of bainitic carbides (broken curve).*

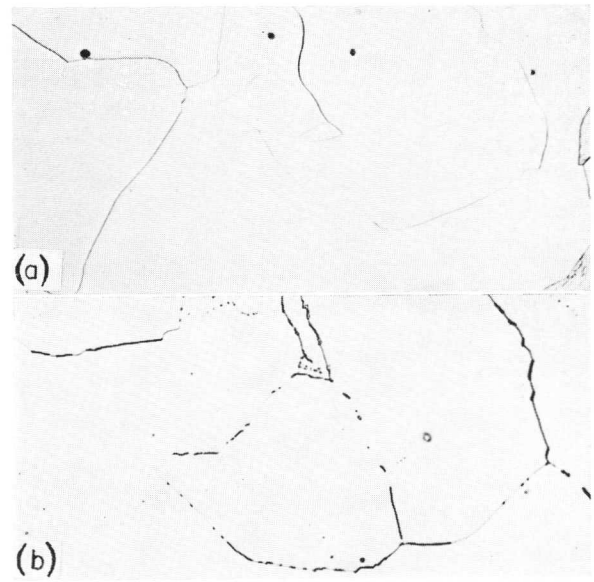

Fig. 13 *Precipitation of carbides within impinged aggregates of ferrite crystals at a temperature* 20 *degC below the lower Ae 1 in Fe–*0·17% *C–*2·92% *Cr.* (a) *Ferrite/ferrite boundaries are largely free of carbides after reaction for* 2 *h at* 765° *C.* × 250. (b) *Extensive carbide precipitation, primarily at ferrite/ferrite boundaries, after* 12 *h at* 765° *C.*[32] × 500.

perature varies with carbon content in high-purity Fe–C alloys in the manner shown in Fig. 12.[35] (The depression of this B_s temperature in the vicinity of the eutectoid composition is due to interference from the pearlite reaction.) When microstructurally defined bainite is freed of this morphological restriction, however, the microstructural B_s becomes identical to the eutectoid temperature for carbides precipitated both from austenite at austenite/ferrite boundaries and from ferrite. Figs. 13(*a*) and (*b*) support this conclusion by demonstrating carbide precipitation from impinged aggregates of proeutectoid ferrite allotriomorphs at a temperature only 20 degC below the lower eutectoid temperature in a 3% Cr steel.[32] Fig. 14 indicates that this result was obtained over a relatively wide range of carbon contents.[32]

Whether or not carbides actually do precipitate in association with proeutectoid ferrite at a given temperature, however, is clearly a complex question in competitive reaction kinetics, particularly at temperatures relatively close to the revised microstructural-B_s or eutectoid temperature. Alloying elements such as Si and Al, which inhibit carbide precipitation, act to reduce the temperature at which bainite is first observed.[28,29] Elements that preferentially inhibit the pearlite reaction, such as Cr and Mo, have the reverse effect (e.g. Fig. 13), since pearlite both removes sites at which carbides can precipitate from austenite and competitively drains excess carbon from proeutectoid ferrite. Experimental evidence of the latter process is provided by the observation that the tips of pearlitic carbide lamellæ in contact with proeutectoid ferrite are preferentially thickened.[34] Low carbon contents and large austenite grain sizes, which produce arrangements of proeutectoid ferrite crystals capable of interfering with the pearlite reaction in a variety of ways,[35] also encourage the formation of bainitic carbides.

These kinetic considerations can be summarized on the basis of the schematic *TTT* curve for the initiation of the bainite reaction shown in Fig. 15. This curve has been drawn

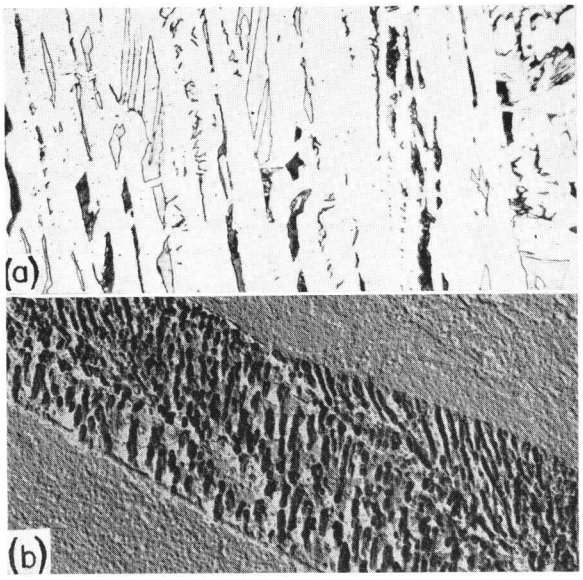

[*Courtesy Climax Molybdenum Co.*

Fig. 16 (a) *Precipitation of pearlite and of bainitic carbides from austenite trapped between ferrite plates during the closing stage of transformation in Fe–0·29% C–0·76% Mn; reacted 50 sec at 600° C.* × 1000. (b) *Lamellar distribution of bainitic carbides in Fe–0·69% C–2·00% Si–0·86% Mn; reacted at 345° C.*[37] × 5000.

asymptotic to a line just below the eutectoid temperature to indicate the location of the revised microstructural-B_s, and is broken at high temperatures to make clear that whether or not bainite actually appears at these temperatures depends sensitively upon the details of the proeutectoid ferrite and pearlite microstructures initially generated. Reflecting the fact that the time interval between the initiation of the proeutectoid ferrite reaction and the onset of bainitic carbide precipitation decreases as the reaction temperature is reduced (compare the interval of many seconds at 600° C, Figs. 9(*a*) and 16(*a*), with the negligible interval at 550° C, Fig. 10(*b*), in the same steel), the bainite curve is shown to approach asymptotically that for proeutectoid ferrite.

It remains to note that there appears to be some overlap between microstructural bainite and pearlite. The structure formed by the spheroidization of pearlite is a trivial example of this problem, since the definition of microstructural bainite applies only to *initially* non-lamellar carbides formed in association with *proeutectoid ferrite*. (These strictures should also rule out confusion with tempered martensite.) Degenerate pearlite[27,36] is a clearer example of overlap between the two types of structure, as Hillert[36] has remarked. More detailed studies may well show, however, that they do not merge in all respects. Although the lamellar carbides in the bainite of Fig. 16(*b*) appear to present a more serious problem in this regard, it should be noted that the " external " morphology of this structure is distinctly that of proeutectoid ferrite. This suggests that both the crystallographic relationships and the growth interactions between the ferrite and carbide phases in this type of structure are fundamentally different from those obtaining in pearlite. For example, the bainitic carbides may have grown allotriomorphically along austenite/ferrite boundaries or may even have precipitated from the ferrite at ferrite/ferrite boundaries.

The Kinetic Definition

The Pearlite vs. Bainite Explanation

As illustrated in Figs. 2(*a*) and (*b*), this explanation assumes that austenite has but two important modes of diffusional decomposition, the pearlite and the bainite reactions. Even in a eutectoid steel, however, it cannot explain the kinetic-B_s temperature (particularly when this temperature clearly lies far below that of the eutectoid, e.g. Fig. 2(*b*)), or account for the incompleteness of transformation at temperatures between kinetic-B_s and B_f. The most troublesome aspect of this explanation, of course, is the fact that it ignores the proeutectoid ferrite reaction. This explanation is clearly untenable in steels such as the Fe–C–Mo alloy of Figs. 4 and 5, in which proeutectoid ferrite forms both above and below the kinetic-B_s. An effort is sometimes made to circumvent this obvious objection by inserting a separate *TTT* curve for the proeutectoid ferrite reaction at shorter times than those for the pearlite and the bainite reactions. This procedure is certainly valid in the pearlite range, and has been shown to be correct at higher temperatures in the bainite range[7,8,28,29] if bainite is microstructurally defined, i.e. in terms of carbide precipitation in association with proeutectoid ferrite. However, there is no evidence for two different modes of ferrite formation at temperatures below the kinetic-B_s. For example, although various changes in morphology have been found to occur just when the reaction temperature is reduced below that of the kinetic-B_s,[37] Figs. 5(*a*), 5(*b*), and 6(*b*) show that this is not general; grain and twin-boundary allotriomorphs are the dominant morphology in this steel both above and just below the kinetic-B_s.

The Ortho- and Paraferrite Hypothesis

Hultgren[28] based his explanation of the kinetic bainite phenomena entirely upon the proeutectoid ferrite reaction. He proposed that the initial product of transformation at temperatures above that of the bay is " orthoferrite ". This product contains equilibrium (with austenite) proportions of both carbon and alloying element. At lower temperatures, it was postulated to be replaced by " paraferrite ", which contains a nearly equilibrium concentration of carbon but inherits the full alloy content of the parent austenite. A bay in the *TTT* diagram is readily derived from such a reaction sequence. However, electron-probe analysis of specimens of 3% Cr steels reacted at temperatures above and below that of the bay has disclosed no partition of chromium between austenite and ferrite in either the orthoferrite or the paraferrite temperature range.[20,38] This explanation must accordingly be discarded.

The Kinetic-$B_s = T_0$ Theory

This theory, due to Zener,[39] postulates that kinetic bainite inherits the carbon as well as the alloy content of the parent austenite. The kinetic-B_s temperature is thus identical to the T_0 temperature, at which austenite and ferrite of the same composition are in stress-free equilibrium. This theory explains, at least qualitatively, most of the kinetic bainite phenomena.

A straightforward theoretical test of this theory can be made by comparing calculated T_0 temperatures with experimentally determined kinetic-B_s temperatures. This is perhaps best done (at the present time) by using a relationship obtained by combining a statistical thermodynamic treatment of interstitial solid solutions due to Lacher[40] and Fowler and Guggenheim[41] with Zener's[42] treatment of the effects of alloying elements upon the magnetic and the non-magnetic

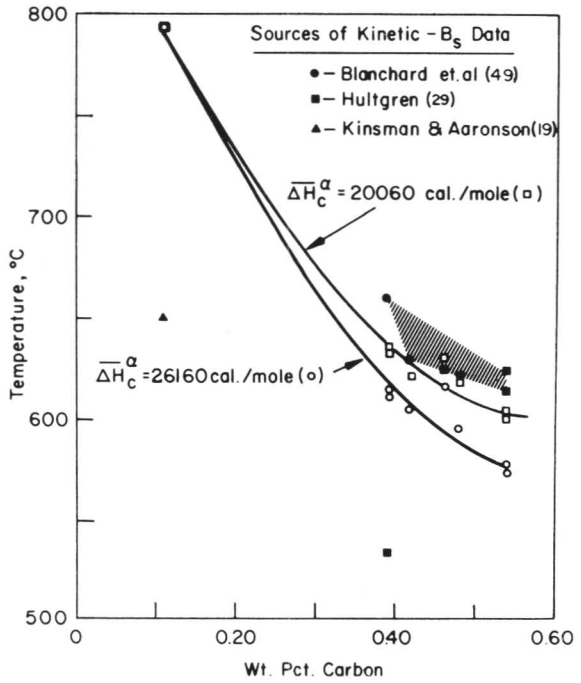

Fig. 17 Effect of carbon content upon the kinetic-B_s temperature and upon the T_0 temperature calculated with different values of ΔH_C^α in Mo steels. Influence of variable Mo contents is ignored in this plot.

components of the free-energy change accompanying the $\gamma \rightarrow \alpha$ transformation in pure iron.[19,43,44] This relationship includes the partial molar heat of solution of carbon in ferrite, ΔH_C^α. Since there is considerable dispute about the correct value of ΔH_C^α,[33,45–48] two "limiting" values will be employed. T_0 temperatures computed from this equation have been previously compared with the kinetic-B_s for an 0·50% C nickel steel and for an 0·60% C silicon steel, with reasonable agreement being obtained in both cases.[43] These comparisons are now extended to Mo steels. Data on kinetic-B_s temperatures obtained from published *TTT* diagrams[19,29,49] and the T_0 temperatures calculated for these steels are plotted as a function of carbon content in Fig. 17 without consideration of the proportion of Mo present. All but two of the kinetic-B_s data lie within the rather narrow shaded region, and are in reasonable agreement with the higher of the two T_0 curves; the steels in this group all contained between 0·39 and 0·54% C, and from 0·23 to 0·82% Mo. The two exceptions, however, lie far below the T_0 curves. Both are for steels containing ~ 2% Mo; the 0·11% C, 1·95% Mo alloy (Fig. 4), which also has much the lowest carbon content examined, exhibits the largest differences between the T_0 and the kinetic-B_s temperatures. Preliminary data on a 0·07% C, 2·88% Mo steel[21] indicate discrepancies at least as large. Although additional comparisons are needed, it appears that the agreement between the kinetic-B_s and T_0 found to date may be essentially coincidental, and that in general these temperatures are not identical. While it is still thermodynamically possible that kinetically defined bainite in the 2% Mo alloys of Fig. 17 inherits both the carbon and the alloy contents of the austenite phase, the incomplete agreement between the kinetic-B_s and T_0 indicates that this is unlikely.

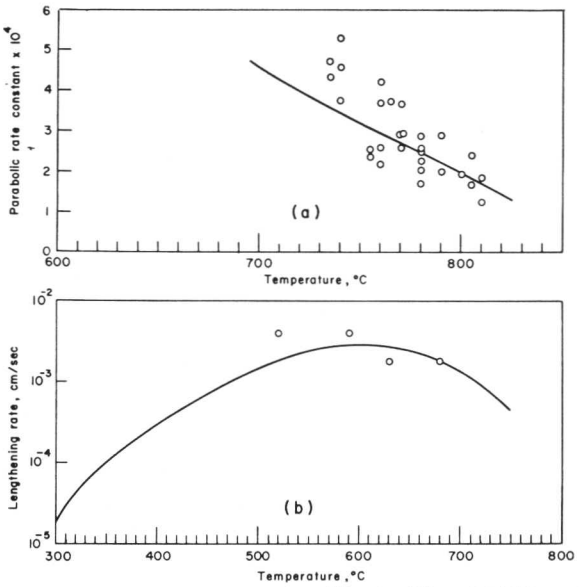

[*Courtesy Climax Molybdenum Co.*

Fig. 18 Experimental and calculated values of (a) *the parabolic rate constant α, for the thickening of grain-boundary allotriomorphs in Fe–0·11% C*[19] *and* (b) *the rate of lengthening of sideplates (data from Hillert*[52] *for Fe–0·21% C–0·36% Mn and calculated values from Trivedi and Pound*[54] *for Fe–0·24% C).*

A Limited-Nucleation, Limited-Growth Hypothesis

Although specific experimental data are not available, it is none the less plausible to consider the kinetic bainite phenomena in terms of limitations upon the rates of nucleation and growth of ferrite. Hehemann and Troiano[50] have proposed the following interpretations of these limitations. Nucleation of ferrite was proposed to be restricted by the inability of nuclei to form by statistical fluctuations at temperatures below the kinetic-B_s. The only nuclei available were taken to be ferrite embryos that were formed in the austenite region, retained during quenching, and promoted to nuclei at reaction temperatures determined by their size. Growth of ferrite was suggested to be limited by the loss of coherency between austenite and ferrite at the broad faces of ferrite plates. A suitable test for the nucleation component of this hypothesis is not yet available. However, the observation that transformation is incomplete at the temperature of the bay of the Fe–C–Mo alloy of Fig. 4 despite the fact that grain- and twin-boundary allotriomorphs, much the dominant morphologies present (Fig. 5(*b*)), usually exhibit (partial) coherency with austenite over only a small proportion of their interfacial area,[51] indicates that this explanation of limited growth between kinetic-B_s and B_f is unlikely to be generally applicable.

Kinetic Bainite as a Special Effect of Certain Alloying Elements upon Proeutectoid Ferrite Reaction Kinetics

This section summarizes and further develops the recent proposal[19] that the various phenomena encompassed by the kinetic definition of bainite are not characteristic of pure Fe–C alloys, but result instead from a special effect of certain of the substitutional alloying elements upon the kinetics of the proeutectoid ferrite reaction.

Considering first the kinetics of growth, data on Fe–C alloys will be employed as a standard of comparison. Fig. 18(*a*) gives data on the parabolic rate constant, α,* as a function of temperature in a high-purity Fe–0·11% C alloy.[19]

*The defining equation for α is $s = \alpha t^{1/2}$, where s is the distance which a planar boundary has moved in the direction normal to itself in time t.

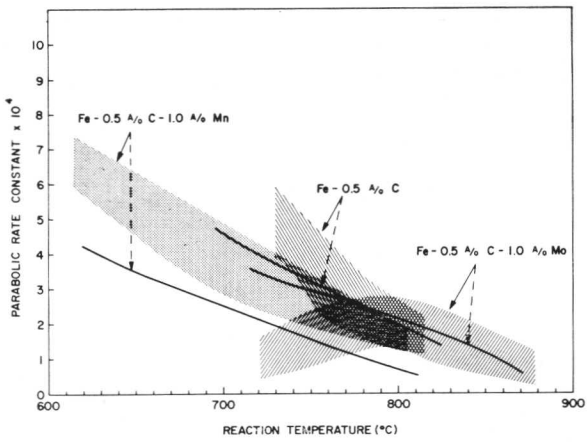

[*Courtesy Climax Molybdenum Co.*

Fig. 19 *Comparison of calculated values of the parabolic rate constant, α, for the thickening of grain-boundary allotriomorphs with the experimental scatterbands in Fe–0·11wt.-% C, Fe–0·11wt.-% C–1·01wt.-% Mn, and Fe–0·11wt.-% C–1·95wt.-% Mo.*[19]

Fig. 18(*b*) presents data on the rate of lengthening of side-plates in an Fe–0·21% C alloy containing 0·26% Mn and 0·02% Si.[52] The curve in Fig. 18(*a*) was calculated from the equation due to Dubé[34] and Zener[53] for the migration kinetics of a planar disordered interphase boundary. The curve in Fig. 18(*b*) was calculated by Trivedi and Pound[54] for Fe–0·24% C on the basis of an elaborate numerical solution of the differential equation expressing the diffusion process accompanying the lengthening of ferrite plates. In both examples, reasonable agreement is seen to have been obtained between the experimentally measured growth rates and those calculated on the assumption that growth is controlled by the diffusion of carbon in austenite.

Turning now to alloy steels, Fig. 19 compares calculated and measured values for α for the thickening of ferrite allotriomorphs in Fe–C, Fe–C–Mn, and Fe–C–Mo alloys having identical carbon contents and nearly equal atomic fractions of alloying element. Although α was decreased by Mn, its calculated values were brought into reasonable agreement with the experimental ones simply by taking account, in the application of the Dubé–Zener equation, of the displacement of the no-partition Ae 3 curve (calculated for the metastable equilibrium condition of no Mn partition between austenite and ferrite[44]) to lower carbon contents. This is taken to be the " normal " effect of an alloying element upon the growth kinetics of ferrite.[19] The Fe–C–Mo data in Fig. 19 illustrate both the normal and the special effects. At temperatures above the upper nose of the *TTT* curve (Fig. 4), i.e. 800° C, adequate agreement exists between the calculated and the experimental values of α. At lower temperatures, however, the calculated α continues to rise, whereas the experimental α decreases. This result is clearly anomalous, and constitutes the " special " effect that certain alloying elements exert upon growth kinetics.[19] The finding that the lengthening rates of plates at temperatures below the kinetic-B_s are significantly less than those allowed by the rate of diffusion of carbon in austenite[55,56] in some alloy steels, and the observation that overall rates of transformation at the temperature of the bay are markedly slower than at lower temperatures,[8] suggests that growth rates may pass through a minimum in the vicinity of the bay. The special effect upon growth kinetics may thus play a major role in the formation of the bay and in the evolution of the phenomena

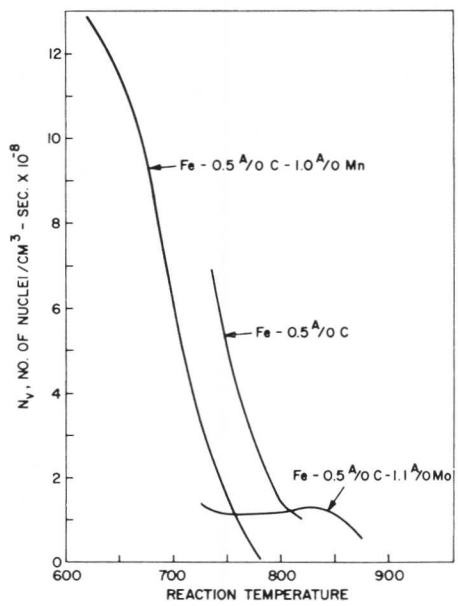

[*Courtesy Climax Molybdenum Co.*

Fig. 20 *Variation with temperature of the rate of nucleation of grain-boundary allotriomorphs per unit volume of austenite in Fe–0·11% C, Fe–0·11% C–1·01% Mn, and Fe–0·11% C–1·95%.*[19]

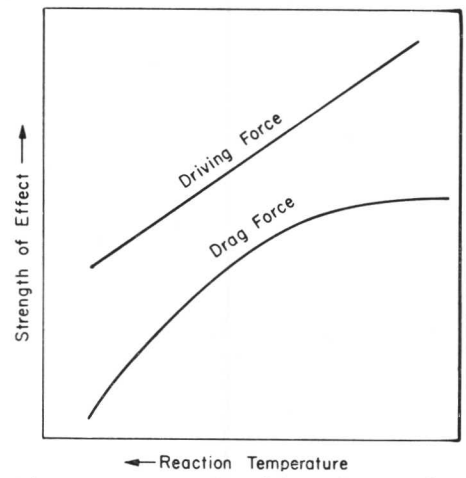

Fig. 21 *Schematic representation of the variation with temperature of the driving force for growth and the substitutional-solute drag effect.*

constituting kinetic bainite.

Fig. 20 shows the effects of temperature and alloy content upon the rate of nucleation of allotriomorphs.[19] The abnormally low nucleation rates in the Fe–C–Mo alloy indicate that the special effect upon nucleation kinetics may also make a contribution to the formation of the bay.[19]

The special effect of alloying elements upon growth kinetics has been interpreted in terms of a " drag effect " produced by the segregation of certain alloying elements to austenite/ferrite boundaries.[19] Alloying elements that reduce the activity of carbon in austenite should be particularly prone to such segregation. The tendency for segregation ought to increase with decreasing temperature, partly because of the declining importance of the entropy factor, but especially because of the rapid rise of the carbon concentration in austenite at austenite/ferrite boundaries. As indicated schematically in Fig. 21, the special effect should begin to appear when the drag effect

becomes sufficiently large relative to the driving force. If the drag is sufficiently large, an " upper nose " will develop in the *TTT* diagram high above the temperature of the single nose normally formed (Fig. 4). Conversely, as the drag effect approaches saturation in such a steel, a bay will begin to develop in the *TTT* diagram as the driving force for growth begins to overcome this effect. The successively smaller reductions in the activity of carbon in austenite produced by Cr,[57] Mn,[58] and Ni[59] are consistent with the declining effectiveness of a given proportion of these elements in producing a bay in the *TTT* diagram.[13,60–62] Conversely, Si[58] and Co[63] raise the activity of carbon in austenite, should not give rise to the kinetic-bainite phenomena, and probably do not do so in high-purity Fe–C–*X* alloys.[20]

At temperatures appreciably above or below that of the bay, where the available measurements showing the special effect upon growth kinetics have been made,[19,55,56] the amount of the retardation is orders of magnitude too small to be explained by volume diffusion of the alloying elements. It was accordingly proposed that the mechanism of the drag effect in this type of situation is that atoms of these elements are constrained by their binding energy to the austenite/ferrite boundaries to make a number of jumps within the boundaries before " escaping " to the ferrite phase.[19] In the vicinity of the bay or kinetic-B_s, however, it seems plausible that after the initial stage of growth (when the thickening rates of both allotriomorphs[19] and plates[64] have declined appreciably) a transition could be made into the conventional volume-diffusion-controlled drag mechanism familiar from studies of grain growth and recrystallization in single-phase alloys.[65,66] At the temperatures involved, the volume diffusivities of the substitutional alloying elements are so low that this would halt completely the observable movement of austenite/ferrite boundaries, thus giving rise to the incompleteness of transformation found near the kinetic-B_s.

These drag effects may similarly interfere with the evolution of ferrite embryos into stable nuclei, producing parallel effects upon the kinetics of nucleation.

Since kinetic bainite does not appear to be a characteristic of high-purity Fe–C alloys, and is evidently associated with a special effect of certain alloying elements upon the proeutectoid ferrite reaction, it is recommended that the kinetic definition of bainite be dropped, and that the phenomena involved be reclassified as part of the characteristics of the proeutectoid ferrite reaction in Fe–C–*X* alloys.

The Surface-Relief Definition

The significance currently attached to the appearance of a martensitic relief effect in association with a ferrite plate formed at a free surface has been succinctly stated by Christian.[67,68] This type of relief is taken to be macroscopic evidence of a correspondence between the austenite and the ferrite lattices. Such a relationship is permissible only if the iron atoms undergo the displacement necessary for the f.c.c. $\rightarrow$ b.c.c. transformation by a shear mechanism. The shear is accomplished by the gliding of arrays of misfit or " transformation " dislocations at the austenite/ferrite boundaries. Any further displacement required of the iron atoms takes place by sub-diffusional " shuffles ". Diffusion of carbon atoms during the transformation affects the kinetics of the process but not the mechanism.

Clearly, the basic concern of the surface-relief definition is with the growth mechanism of plates, and the first mechanism that must be considered is that of shear.

Shear Mechanisms for the Growth of Ferrite or Bainite Plates

The proposals that ferrite or bainite plates form by one long, continuous, high-velocity* shear[1] has been disproved by hot-stage microscopy observations that these plates actually grow slowly,[16,55,69–71] at rates approximating to those permitted by the diffusion of carbon in austenite.[46,51,72] The concept of growth by many short (a few μm), high-velocity shears, separated by prolonged intervals of quiescence,[73] has been disposed of at high temperatures by the finding that the W_s temperature lies well above the T_0 temperature over an appreciable range of carbon content (Fig. 12).[46,51] Formation of individual plates within sheaves of plates by high-velocity shear at temperatures below T_0 is a mechanism that must be evaluated experimentally by some form of elevated-temperature microscopy offering better resolution than the optical technique.[37] However, it is difficult to see how any of the high-velocity shear mechanisms differs from conventional near-sonic[74] martensitic growth, and thus why they should be able to take place above the M_s temperature, particularly since bainite grows slowly below the M_d temperature[75] and almost certainly also below the M_s temperature.[76]

The concept of diffusion-controlled (" slow ") shear is currently widely accepted. Essentially following Ko and Cottrell,[16] if the broad faces of ferrite plates are displaced by shear they should move at rates determined by the diffusion of carbon in austenite when the reaction temperature is above T_0. Fig. 22 shows that this is not so in an Fe–C alloy. The overall rates are slower, and there are repeated

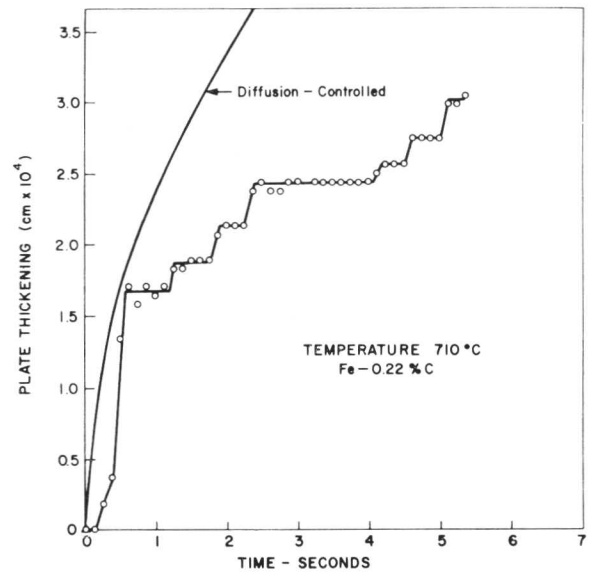

Fig. 22 Thickness vs. time for a ferrite sideplate in Fe–0·22% C as measured by thermionic emission microscopy and as calculated assuming volume diffusion control.[71]

arrests in the growth process. It has been proposed that the shear displacement of the broad faces, which must be accomplished through the agency of glissile dislocations, can be retarded by carbon atmospheres or by phonon scattering.[55] However, the slope of the measured thickness vs. time plot in Fig. 22 is either zero or (usually) greater than that of the

* The term high velocity is used here to include all rates higher than those allowed by carbon diffusion control under the condition of near-equilibrium compositions at the γ/α boundary

calculated plot at a given growth time; slopes markedly less than those calculated are not observed. If movement of the glissile dislocations is periodically halted through " jamming "[77] by forest dislocations, a shear-based explanation is provided for the arrests in Fig. 22 but, again, not for the steep slopes of the risers. Equivalent results were obtained at temperatures above T_0, where such rapid movement of the broad faces is thermodynamically not permissible.

If plates thicken by a ledge mechanism, it is possible that the edges of the ledges have a glissile dislocation structure and that the ledges lengthen by shear. However, it is difficult to understand how such a structure can be stable against thermal fluctuations in view of the poor lattice matching[78] across the austenite/ferrite boundary at orientations other than that of the broad faces.

Growth of Ferrite or Bainite Plates without Shear

Mechanism of Diffusional Growth

On a general theory of precipitate morphology,[51] the structure of the boundary between a precipitate crystal and the matrix grain in which it nucleated varies with the orientation of the boundary when the two lattices have different structures. At most orientations, lattice matching across the boundary is poor, and a disordered or incoherent structure results. At one or a very few orientations, however, matching is appreciably better and the structure can then be of either the fully coherent or the misfit dislocation type. When the precipitate has a composition different from that of the matrix, the requirement of long-range volume diffusion toward or away from the growing precipitate provides ample time in which to ensure that the equilibrium type of interfacial structure is continuously maintained by short-range diffusion within the boundary.

During growth, orientations of the boundary with a disordered structure are normally able to grow at the rates allowed by the kinetics of long-range mass transport.* This is because the total energy of the bonds broken when an atom leaves the " surface " of the matrix crystal differs sufficiently little from that of the energy of the bonds formed when the atom enters the " surface " of the precipitate at such a boundary that the decrease in free energy accompanying growth is adequate to yield a relatively high average probability that this atom will not return to the matrix crystal. Although substitutional as well as interstitial atoms are required to make this transfer in an interstitial alloy, it is readily shown (for example in the proeutectoid ferrite reaction) that the time required for iron atoms to do so is small compared with that needed for the long-range diffusion of carbon in austenite.

Both fully coherent and misfit dislocation boundaries, on the other hand, should be entirely immobile in the direction normal to themselves because the coherent areas have no practicable mechanism of migration. In such areas, the probability that a substitutional atom in the " surface " of the matrix will become attached to the " surface " of the precipitate is very small, because the total bond energy of this atom is sharply reduced when it leaves the matrix " surface ". Such a jump will almost invariably be reversed. It was accordingly proposed, by analogy with equivalent situations in evaporation, condensation, solidification, and the migration of coherent twin boundaries, that such boundaries are displaced by the formation and lateral movement of ledges. One would expect the edges of the ledges to have a disordered structure, thus allowing the ledges to lengthen freely. Should these edges have a dislocation structure, however, achievement of a finite migration rate usually requires that jogs with disordered edges be formed on them.[80] On this view, the basic atomic mechanism through which boundary migration actually takes place in a diffusional transformation is thus one of diffusional jumps across disordered regions of the interphase boundary.

When the ledges on a dislocation interphase boundary are spaced far enough apart and the driving force for growth is sufficiently high, the *overall* rate of migration of this boundary, i.e. in the direction normal to the dislocation facets, is less than that of a boundary which is disordered along its entire length under given conditions of temperature and composition.[51,81] Should a dislocation structure be present at only one orientation of the interphase boundary under these conditions, the precipitate crystal will become a plate. Even if the edges of a plate also have a misfit dislocation structure, e.g. θ' plates in Al–Cu[82,83] and γ plates in α Al–Ag,[84] a smaller spacing between the ledges on the plate edges can furnish the necessary orientation-dependence of the growth kinetics.

It should be noted that the basic predictions of this theory have been experimentally confirmed for θ' and γ plates: the broad faces of γ plates have an immobilized misfit dislocation structure,[84] while those of θ' have a basically coherent structure;[83] both γ[85] and θ'[81] plates thicken at rates less than those allowed by volume diffusion-control. In the case of γ, lengthening and thickening by the ledge mechanism and arrests in both processes equivalent to those in Fig. 22 were observed directly by high-temperature transmission electron microscopy.[85] The theory not only predicts the arrests of Fig. 22 but also explains, in most simple fashion, the steep slopes of the risers between them as the consequence of the passage of a ledge across the line of measurement.

Origin and Significance of Surface Relief

When a grain-boundary allotriomorph grows to a free surface, the absence of coherency between the austenite and ferrite lattices allows the increase in volume accompanying its formation to be released " amorphously " at the surface, leading to the familiar non-crystallographic surface-rumpling effect.[17] However, when a plate grows to the surface, the volume increase is constrained to occur in a manner that allows partial coherency to be retained at the broad faces of the plate.[84] This requirement forces the relief to occur in a well-defined geometrical pattern. As ledges moving in a given direction successively reach the surface, each increment of relief effect will be slightly displaced relative to its predecessor and will continue the pattern initially established. It is thus not unexpected that the resultant macroscopic relief is formally similar to that produced by a martensite plate, and that an attempt to analyse it on this basis might prove at least partially successful, as Srinivasan and Wayman[86] have reported. The simpler $\alpha \rightarrow \gamma$ reaction in Al–Ag produces surface reliefs that were explained in equivalent fashion,[84,85] and are being quantitatively analysed as if they had been produced martensitically.[87]

* The " special effect " of certain alloying elements discussed earlier represents an essentially non-structural mechanism through which the migration of a disordered boundary can be impeded. Conversely, a disordered interphase boundary can sometimes serve as a short-circuit through which mass transport can be accelerated.[79] The latter effect accentuates the superior mobility of a disordered boundary. The former, however, can diminish the difference in the mobility of disordered and dislocation boundaries if the special effect is exerted preferentially upon disordered boundaries, as suggested by simple considerations and supported by preliminary experimental results.[21]

From the discussions of the preceding sub-section, however, it is clear that the atomic mechanism of a transformation cannot be deduced solely from examination of the relief effect when this effect is of the martensitic type. Although such reliefs are currently taken to mean that the transformation mechanism is martensitic, i.e. an appropriately modified homogeneous shear accomplished by the movement of glissile dislocations, these discussions indicated that the actual mechanism of the thickening of a plate in a diffusional transformation is the migration of disordered boundaries located at the edges of ledges. The relief effect in such a transformation is thus not produced by the growth mechanism itself but rather by the geometrical constraint placed upon this mechanism by (partial) coherency of the broad faces of the ledges. In contradistinction to diffusional transformations, the fundamental mechanism of martensitic " growth " is the co-ordinated transport of atoms across the interphase boundary by dislocation glide.* The dislocation structures that make this possible would usually wholly prevent diffusional growth. Similarly, the position that an atom in the matrix will ultimately occupy in the product phase is predictable to within the radius of action of a sub-diffusional " shuffle " in a martensitic transformation, but is basically indeterminate in the diffusional case.

Applying these considerations to the surface-relief bainite problem, it is first noted that a Widmanstätten sideplate normally evolves from a grain-boundary allotriomorph.[88] Both are usually part of the same single crystal,[51] but only the sideplate portion of the crystal exhibits a martensitic surface relief.[17,51] The growth mechanism, and thus the morphology of the allotriomorph, differs from that of the sideplate only in that diffusional jumps can take place at nearly all sites on the interphase boundary of the allotriomorph, but only at the tip and at the edges of the ledges on the sideplate. Development of the sideplate from the allotriomorph is the direct result of the growth barrier at one orientation of the austenite/ferrite boundary produced by the presence of a misfit dislocation structure at this orientation. The surface-relief effect reflects only the presence of this barrier, not a fundamental change in the mechanism of the transformation. Terming the sideplate " bainite " and the grain-boundary allotriomorph from which it evolved " ferrite ",[17] which is customarily rationalized on the basis of such a change, is thus unjustified. Replacing the long-established term of Widmanstätten ferrite with that o bainite (which was itself originally applied to a different phenomenon, here recognized explicitly as a non-lamellar eutectoid reaction) seems particularly inappropriate. The recommendation is accordingly offered that the surface-relief definition of bainite be discarded.

Summary

There are currently three principal definitions of bainite.

(1) The *microstructural* definition: bainite is the composite structure produced when a dispersion of non-lamellar carbides is precipitated in association with Widmanstätten ferrite during the decomposition of austenite.

(2) The *kinetic* definition: the bainite reaction has its own C - curve (centred between the pearlite and the martensite ranges), and is increasingly incomplete as the upper limiting temperature of this curve (the kinetic-B_s) is approached.

(3) The *surface-relief* definition: any precipitate plate (or needle, rod, or lath) that differs in composition from its matrix phase and exhibits a martensite-like surface relief is bainite.

These definitions are in substantial mutual conflict. A more detailed examination gives the following principal conclusions.

The *microstructural* definition refers specifically to the non-lamellar mode of eutectoid decomposition. The customary restriction of the morphology of the ferritic component of microstructural bainite to the Widmanstätten form can and should be removed. Whether the non-lamellar (bainite) or the lamellar (pearlite) form of the eutectoid reaction occurs in a given steel at a given temperature below that of the eutectoid is a complex question of competitive reaction kinetics, rather than of thermodynamics. Particularly from a historical point of view, it is recommended that the generalized microstructural definition be adopted as the definition of bainite.

The phenomena encompassed by the *kinetic* definition appear to be the result of a special effect of certain alloying elements upon the kinetics of the proeutectoid ferrite reaction, and it is proposed that they be categorized in this manner, rather than as bainite. This effect reduces both the rates of nucleation and the rates of growth of ferrite to values lower than those allowed by the diffusion of carbon in austenite. It is evidently not present in high-purity Fe–C alloys. Since the effect appears to be more pronounced the more an element reduces the activity of carbon in austenite, it may be produced by the segregation of such elements to austenite/ferrite boundaries, causing a " drag effect " that inhibits both the nucleation and the growth processes.

The martensite-like reliefs characteristic of *surface-relief* bainite are currently taken to mean that this transformation product forms by a shear mechanism. Examination of a number of the proposed variants of this mechanism discloses that most of them can be dismissed as thermodynamically unfeasible or as kinetically implausible. It appears, instead, that when such reliefs develop in association with a precipitate plate formed by diffusional growth they reflect only the constraint on the shape change at a free surface imposed by the existence of partial coherency across the broad faces of the plate. The dislocation structure of these faces renders them immobile; their migration can be accomplished only by the formation and lateral movement of ledges with sufficient atomic disorder at their edges to make it likely that an atom jumping diffusionally across the edges will become attached to the " surface " of the precipitate crystal. Such a jump is the basic mechanism of a diffusional transformation, whereas in a truly martensitic transformation the basic mechanism is non-diffusional transport by dislocation glide. It is accordingly recommended that the surface-relief definition of bainite be discarded as mechanistically, and also historically, inappropriate.

Acknowledgements

Several of the experimental studies utilized in the microstructural bainite section were performed when the author was associated with the Carnegie Institute of Technology (now Carnegie–Mellon University) under the sponsorship of the U.S. Air Force (Wright–Patterson Air Force Base) and the U.S. Office of Naval Research. Appreciation is expressed to Mr. E. T. Kennedy for laboratory assistance, both at Carnegie and at Ford, to Dr. K. R. Kinsman for permission to use as yet unpublished results from several current investi-

* In the special case of f.c.c.→h.c.p. tranformations, e.g. $\alpha \rightarrow \gamma$ in Al–Ag, plate thickening *is* accomplished by "glide" of some of the misfit dislocations.[84,85] However, this glide is diffusion-controlled[85] and thus takes place atom by atom by means of individual uncoordinated *diffusional* jumps, in contrast to the homogeneous shear taking place by *non-diffusional* glide, characteristic of a truly martensitic transformation.

gations being jointly undertaken, to Dr. C. W. Spencer and Professor R. F. Hehemann for providing original prints of micrographs, to Drs. Kinsman, N. A. Gjostein, and C. L. Magee for their comments on the manuscript, and to Professor Bruce Chalmers for the encouragement that led to the preparation of this paper.

References

1. E. S. Davenport and E. C. Bain, *Trans. Amer. Inst. Min. Met. Eng.*, 1930, **90,** 117.
2. J. M. Robertson, *J. Iron Steel Inst.*, 1929, **119,** 391.
3. F. Wever and E. Lange, *Mitt. K.-W. Inst. Eisenforsch.*, 1932, **14,** 71.
4. F. Wever and W. Jellinghaus, *ibid.*, p. 85.
5. F. Wever and W. Jellinghaus, *ibid.*, p. 105.
6. F. Wever and W. Jellinghaus, *ibid.*, 1933, **15,** 167.
7. W. T. Griffiths, L. B. Pfeil, and N. P. Allen, " Second Report of the Alloy Steels Research Committee " (Special Rep. No. 24), p. 343. **1939:** London (Iron Steel Inst.).
8. N. P. Allen, L. B. Pfeil, and W. T. Griffiths, *ibid.*, p. 369.
9. S. Steinberg and V. Zyuzin, *Arch. Eisenhüttenwesen*, 1934, **7,** 537.
10. S. Steinberg and V. Zyuzin, *Rev. Mét.*, 1934, **31,** 554.
11. V. D. Sadovsky, *Trudy UFAN*, 1945, **(5)** and **(6)**; 1949, **(13).**
12. E. P. Klier and T. Lyman, *Trans. Amer. Inst. Min. Met. Eng.*, 1944, **158,** 394.
13. T. Lyman and A. R. Troiano, *Trans. Amer. Soc. Metals*, 1946, **37,** 402.
14. T. Lyman and A. R. Troiano, *Trans. Amer. Inst. Min. Met. Eng.*, 1945, **162,** 196.
15. R. F. Hehemann and A. R. Troiano, *Metal Progress*, 1956, **70,** (2), 97.
16. T. Ko and S. A. Cottrell, *J. Iron Steel Inst.*, 1952, **172,** 307.
17. T. Ko, *ibid.*, 1953, **175,** 16.
18. C. A. Dubé, H. I. Aaronson, and R. F. Mehl, *Rev. Mét.*, 1958, **55,** 201.
19. K. R. Kinsman and H. I. Aaronson, " Transformation and Hardenability in Steels ", p. 39. **1967:** Ann Arbor, Mich. (Climax Molybdenum Co.).
20. H. I. Aaronson and H. A. Domian, *Trans. Met. Soc. A.I.M.E.*, 1966, **236,** 781.
21. H. I. Aaronson and K. R. Kinsman, unpublished research.
22. E. S. Davenport, *Trans. Amer. Soc. Metals*, 1939, **27,** 837.
23. J. R. Cruciger and J. R. Vilella, *ibid.*, 1944, **32,** 195.
24. A. Schrader and F. Wever, *Arch. Eisenhüttenwesen*, 1952, **23,** 489.
25. H. I. Aaronson and C. Wells, *Trans. Amer. Inst. Min. Met. Eng.*, 1955, **203,** 1002.
26. S. M. Kaufman, G. M. Pound, and H. I. Aaronson, *ibid.*, 1957, **209,** 855.
27. S. Modin, *Jernkontorets Ann.*, 1958, **142,** 37.
28. A. Hultgren, *Trans. Amer. Soc. Metals*, 1947, **39,** 915.
29. A. Hultgren, *Jerkontorets Ann.*, 1951, **135,** 403; *Kgl. Svenska Vetenskapsakad. Handl.*, 1953, **4,** Ser. 4.
30. C. W. Spencer and D. J. Mack, " Decomposition of Austenite by Diffusional Processes ", p. 549. **1962:** New York and London (John Wiley).
31. H. I. Aaronson, W. B. Triplett, and G. M. Andes, *Trans. Met. Soc. A.I.M.E.*, 1960, **218,** 331.
32. C. J. Kubit and H. I. Aaronson, unpublished research.
33. H. I. Aaronson, H. A. Domian, and G. M. Pound, *Trans. Met. Soc. A.I.M.E.*, 1966, **236,** 753.
34. C. A. Dubé, Ph.D. Thesis, Carnegie Inst. Technol., **1948.**
35. H. I. Aaronson, *Trans. Met. Soc. A.I.M.E.*, 1958, **212,** 212.
36. M. Hillert, Ref. 30, p. 197.
37. J. M. Oblak and R. F. Hehemann, Ref. 19, p. 15.
38. H. I. Aaronson, *Trans. Met. Soc. A.I.M.E.*, 1962, **224,** 870.
39. C. Zener, *Trans. Amer. Inst. Min. Met. Eng.*, 1946, **167,** 550.
40. J. R. Lacher, *Proc. Camb. Phil. Soc.*, 1937, **33,** 518.
41. R. H. Fowler and E. A. Guggenheim, " Statistical Thermodynamics ", p. 442. **1939:** London (Cambridge University Press).
42. C. Zener, *Trans. Amer. Inst. Min. Met. Eng.*, 1955, **203,** 619.
43. K. R. Kinsman and H. I. Aaronson, Ref. 19, p. 33 (discussion).
44. H. I. Aaronson, H. A. Domian, and G. M. Pound, *Trans. Met. Soc. A.I.M.E.*, 1966, **236,** 768.
45. R. P. Smith, *J. Amer. Chem. Soc.*, 1946, **68,** 1163.
46. L. Kaufman, S. V. Radcliffe, and M. Cohen, Ref, 30, p. 313.
47. R. B. McLellan, *Trans. Met. Soc. A.I.M.E.*, 1965, **233,** 1664.
48. T. Bell and W. S. Owen, *ibid.*, 1967, **239,** 1940.
49. J. R. Blanchard, R. M. Park, and A. J. Herzig, *Trans. Amer. Soc. Metals*, 1941, **29,** 317.
50. R. F. Hehemann and A. R. Troiano, *Trans. Amer. Inst. Min. Met. Eng.*, 1954, **200,** 1272.
51. H. I. Aaronson, Ref. 30, p. 387.
52. M. Hillert, unpublished research; see also Ref. 30, p. 313.
53. C. Zener, *J. Appl. Physics*, 1949, **20,** 950.
54. R. Trivedi and G. M. Pound, *ibid.*, 1967, **38,** 3569.
55. R. H. Goodenow, S. J. Matas, and R. F. Hehemann, *Trans. Met. Soc. A.I.M.E.*, 1963, **227,** 651.
56. M. M. Rao and P. G. Winchell, *ibid.*, 1967, **239,** 956.
57. R. J. Brigham and J. S. Kirkaldy, *ibid.*, 1963, **227,** 538.
58. R. P. Smith, *J. Amer. Chem. Soc.*, 1948, **70,** 2724.
59. A. J. Heckler and P. G. Winchell, *Trans. Met. Soc. A.I.M.E.*, 1963, **227,** 732.
60. J. V. Russell and F. T. McGuire, *Trans. Amer. Soc. Metals*, 1944, **33,** 103.
61. J. P. Sheehan, C. A. Julien, and A. R. Troiano, *ibid.*, 1949, **41,** 1165.
62. D. A. Scott, W. M. Armstrong, and F. A. Forward, *ibid.*, p. 1145.
63. L. C. Brown and J. S. Kirkaldy, *Trans. Met. Soc. A.I.M.E.*, 1963, **227,** 1461.
64. K. R. Kinsman, E. Eichen, and H. I. Aaronson, to be published.
65. J. W. Cahn, *Acta Met.*, 1962, **10,** 789.
66. P. Gordon and R. A. Vandermeer, " Recrystallization, Grain Growth, and Textures ", p. 205. **1965:** Metals Park, Ohio (Amer. Soc. Metals).
67. J. W. Christian, Ref. 30, p. 371.
68. J. W. Christian, " Physical Properties of Martensite and Bainite " (Special Rep. No. 93), p. 1. **1965:** London (Iron Steel Inst.).
69. K. Tsuya, *J. Mech. Lab. Japan*, 1956, **2,** 20.
70. G. R. Speich and M. Cohen, *Trans. Met. Soc. A.I.M.E.*, 1960, **218,** 1050.
71. G. R. Speich, Ref. 30, p. 353.
72. R. Trivedi, Ph.D. Thesis, Carnegie–Mellon Univ., **1966.**
73. E. Eichen and J. W. Spretnak, *Trans. Amer. Soc. Metals*, 1959, **51,** 454.
74. R. F. Bunshah and R. F. Mehl, *Trans. Amer. Inst. Min. Met. Eng.*, 1953, **197,** 1251.
75. M. F. Smith, G. R. Speich, and M. Cohen, *Trans. Met. Soc. A.I.M.E.*, 1959, **215,** 528.
76. R. T. Howard and M. Cohen, *Trans. Amer. Inst. Min. Met. Eng.*, 1948, **176,** 384.
77. L. Kaufman and M. Cohen, *Progress Metal Physics*, 1958, **7,** 165.
78. R. F. Mehl, C. S. Barrett, and D. W. Smith, *Trans. Amer. Inst. Min. Met. Eng.*, 1933, **105,** 215.
79. H. B. Aaron and H. I. Aaronson, *Acta Met.*, 1968, **16,** 789.
80. H. I. Aaronson and C. Laird, unpublished research.
81. H. I. Aaronson and C. Laird, *Trans. Met. Soc. A.I.M.E.*, in the press.
82. K. Matsuura and S. Koda, *J. Phys. Soc. Japan*, 1963, **18,** Suppl. 1, 50.
83. C. Laird and H. I. Aaronson, *Trans. Met. Soc. A.I.M.E.*, in the press.
84. C. Laird and H. I. Aaronson, *Acta Met.*, 1967, **15,** 73.
85. C. Laird and H. I. Aaronson, unpublished research.
86. G. R. Srinivasan and C. M. Wayman, *Acta Met.*, 1968, **16,** 621.
87. Y. C. Liu, private communication.
88. H. M. Howe, *Proc. Amer. Soc. Test. Mat.*, 1911, **11,** 262.

The Isothermal Decomposition of Nitrogen Austenite to Bainite

T. Bell and B. C. Farnell

Iron–nitrogen austenite decomposes directly to ferrite and Fe_4N at all temperatures below the eutectoid (591° C) and above the M_s. The kinetics of the isothermal decomposition has been examined in the range 200–350° C by an electrical-resistivity technique for compositions between 1·1 and 2·6 wt.-% N. The kinetics has been related to the morphology of the transformation products, which changes from an orientation-dependent grain-boundary-nucleated structure to a predominantly intragranular structure when the nitrogen content is increased to > 1·9 wt.-% N. The overall activation energy for growth of these transformation products rises uniformly from 20 kcal . mole^{-1} at 1·1 wt.-% N to 30 kcal . mole^{-1} at 2·6 wt.-% N.

Nitrogen, like carbon, forms an interstitial solid solution with γ-iron which undergoes a eutectoid reaction to ferrite and Fe_4N.[1] However, unlike the isothermal decomposition of iron–carbon austenite, the isothermal decomposition of nitrogen austenite has received little attention. Bose and Hawkes[2] have reported the presence of granular and lamellar nitrogen pearlites in a single alloy of near-eutectoid composition (2·35 wt.-% N) reacted at 580° C, and of nodular aggregates of ferrite and nitride at temperatures down to 400° C. These structures had been observed previously and were termed braunite by Fry.[3] No reports of bainitic structures in the iron–nitrogen system have been published. In the present investigation the isothermal decomposition of nitrogen austenite has been investigated by an electrical-resistometric technique below 591° C, the eutectoid temperature, and above the M_s temperature.[4] The morphology of nitrogen pearlite or braunite is very briefly discussed and the kinetics of formation of nitrogen bainite over a wide range of concentration is discussed in relation to the observed morphologies.

Experimental Details

A series of homogeneous austenitic alloys containing up to 2·7 wt.-% N were produced from Johnson Matthey pure-iron strip, 0·010 in. thick, and wire, 0·008 in. dia., by nitriding between 640 and 740° C with ammonia–hydrogen mixtures of predetermined nitriding potential.[5] Specimens for X-ray diffraction and optical and electron metallography were quenched to the required isothermal reaction temperature and transformed for various times. They were then quenched into brine to suppress further transformation of the austenite. Wire specimens for electrical-resistivity studies were quenched directly into brine from the nitriding temperature.

Debye–Scherrer X-ray diffraction patterns of wire specimens in the partially and fully transformed conditions were taken at 20° C. Isothermally reacted strip specimens were prepared for optical metallographic examination in the usual manner and for thin-film electron microscopy by the techniques described in an earlier paper.[6] Two-stage carbon replicas were used where necessary to supplement the thin-film work.

Wire specimens, in the form of loops for the resistivity experiments, were re-austenitized in a vacuum by self-resistance heating. They were then quenched by a blast of argon to the reaction temperature maintained by an environmental furnace. Resistivity changes during the decomposition of the austenite were monitored continuously by recording the potential drop over the specimen when a small constant current was flowing. The temperature was generally maintained to ± 1 degC. All measurement leads were of 0·002 in. dia. platinum or platinum–13% rhodium to minimize thermal gradients. The reaction took place in the argon atmosphere provided by the quench gas.

Iron–nitrogen alloys are unstable in a vacuum or inert-gas atmosphere.[7] To establish the extent of the instability in relation to the resistivity experiments, samples of each alloy were resistance-heated in a vacuum of better than 1×10^{-4} mm Hg from room temperature to their individual formation temperatures, for a range of times, and then quenched to room temperature. Chemical analysis of these specimens showed no significant loss of nitrogen when alloys were austenitized for times up to ~ 3 min. Chemical analysis of alloys fully reacted in the argon atmosphere showed that they remained stable during the complete transformation up to 400° C. At higher temperatures up to 570° C there was no detectable nitrogen loss for times up to 2 h.

Results and Discussion

X-Ray Diffraction

X-ray diffraction studies of a wide range of alloys in the partially and fully transformed condition have shown that at all temperatures below the eutectoid temperature, the f.c.c. nitrogen austenite decomposes directly to ferrite of very low nitrogen content and the f.c.c. nitride, Fe_4N. As the nitrogen content of the initial austenite is raised, the intensity of the

Manuscript received 1 April 1968. T. Bell, B.Eng., Ph.D., A.I.M., and B. C. Farnell, B.Eng., are in the Department of Metallurgy, University of Liverpool.

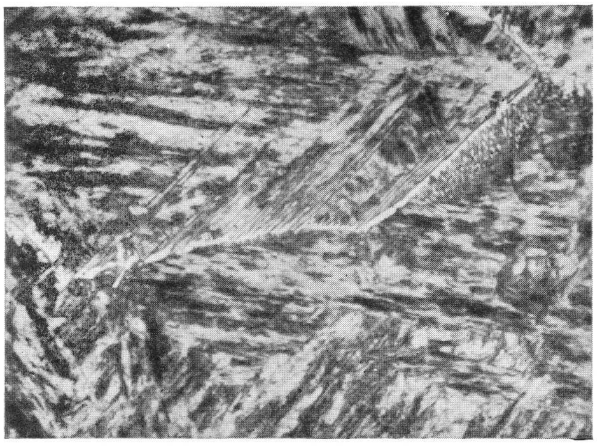

Fig 1 *Fe–0·7% N alloy reacted at* 360° *C. Nital etch.* × 550.

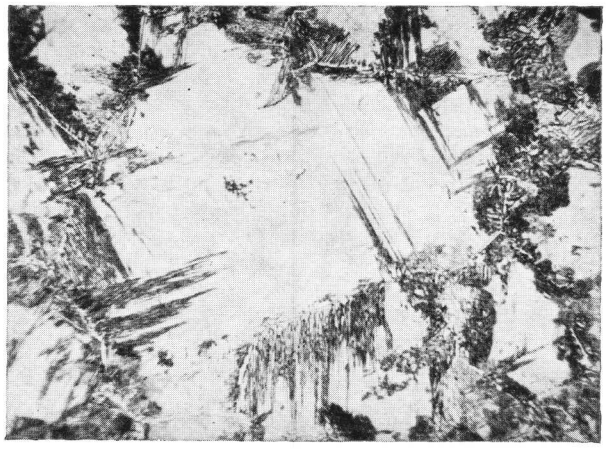

Fig 2 *Fe–1·1% N alloy partially transformed at* 365° *C. Nital etch.* × 320.

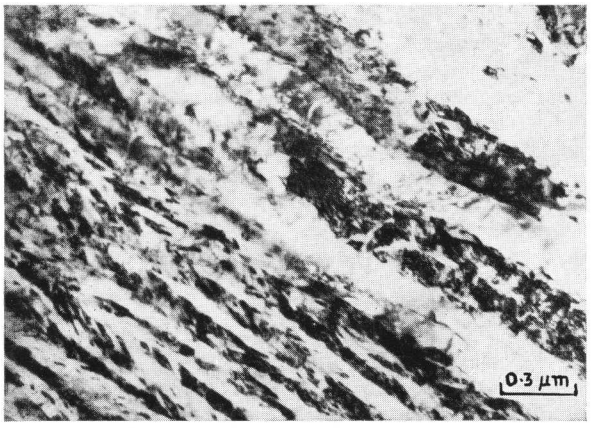

Fig. 3 *Thin-film electron micrograph of Fe–1·1% N alloy fully reacted at* 310° *C.*

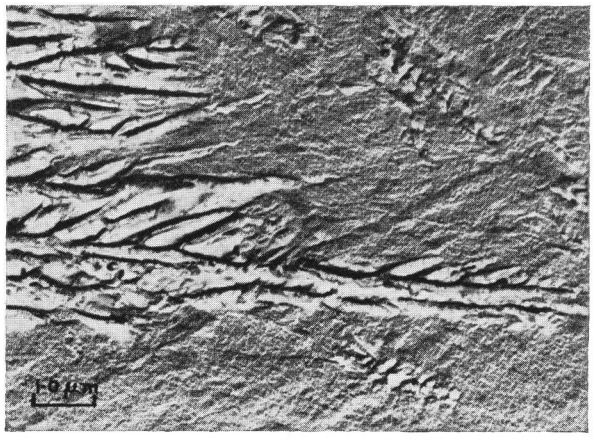

Fig. 4 *Carbon replica of Fe–1·1% N alloy partially reacted at* 310° *C.*

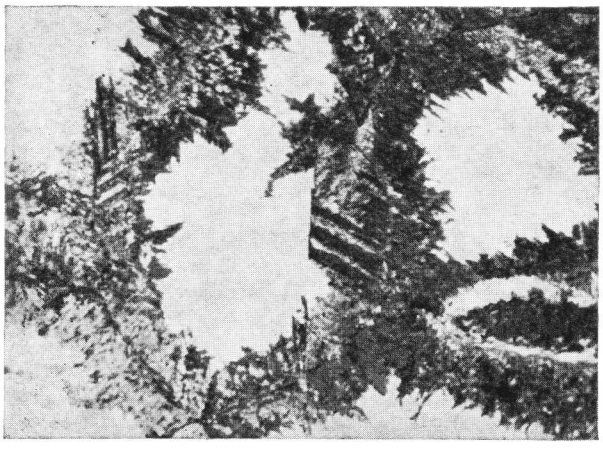

Fig. 5 *Fe–1·8% N alloy partially transformed at* 350° *C. Nital etch.* × 560.

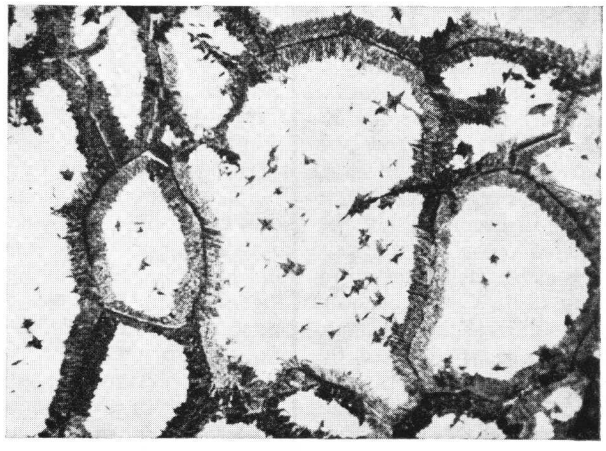

Fig. 6 *Fe–2·0% N alloy partially transformed at* 310° *C. Nital etch.* × 320.

nitride lines relative to the ferrite lines increases, indicating the expected increase in proportion of Fe_4N. A detailed investigation was made of 1·5 and 2·6 wt.-% N alloys after partial transformation at 50 degC temperature intervals from 300 to 575° C. This revealed no change in the lattice parameters of the retained austenite or the body-centred tetragonal martensite for both alloys at all temperatures up to 400° C. These results indicate that the austenite is decomposing directly to ferrite and Fe_4N in an apparently discontinuous fashion. At higher temperatures a slight increase in the austenite and martensite lattice parameters was detected for the 1·5% N alloy owing to nitrogen enrichment of the matrix austenite, but no observable change was found for the 2·6% N alloy.

Morphology

The lowest nitrogen content to be examined was 0·7% and Fig. 1 shows this alloy after partial reaction at 360° C. It consists of a mixture of tempered martensite[6] and a grain-boundary-nucleated product. Electron-diffraction studies have shown that the latter phase is ferrite. Later in the transformation, secondary Widmanstätten side plates or needles have grown from the grain-boundary allotriomorphs. From Fig. 2 it can be seen that for an iron–1·1% N alloy, the Widmanstätten ferrite plates grow into the austenite in only a small number of preferred directions. It is probable that this low-index habit plane is $(111)_\gamma$, as found for Widmanstätten ferrite in the iron–carbon system. The mode of decomposition in Fig. 2 persists at all temperatures up to 450° C. Above 350° C the nodular aggregates of nitride and ferrite reported by Bose and Hawkes[2] are also observed. In the 1·1% N alloy, as with the 0·7% N alloy, the individual ferrite needles grow long and deep into the austenite grains and a diffuse lamellar structure of ferrite and Fe_4N is apparent (Fig. 3). Carbon-replica studies have shown that the ferrite needles growing from the austenite grain boundary taper gradually to a sharp tip and that when the degree of tapering is appreciable side branching is often seen. This is illustrated in Fig. 4 for an iron–1·1% N alloy reacted at 310° C. At 1·8% N, single-phase nucleation is no longer visible by optical metallography. The transformation product, as seen in Fig. 5, covers both sides of the grain boundary and that structure is typical of this composition over the full temperature range 200–400° C. Growth in preferred directions still persists but on a smaller scale, to give the reaction product a ragged appearance. The structures discussed so far are very similar to iron–carbon upper bainites.[8] As with iron–carbon bainite[9] the transformation products are stopped by austenite twin boundaries indicating further that the growth is orientation-dependent. When the nitrogen content is increased to 2·0% growth occurs uniformly on both sides of the grain boundaries (Fig. 6). This structure may be resolved (Fig. 7) by replica electron microscopy, which shows that side branching of the ferrite still takes place. At this nitrogen concentration some transformation occurs within the grains which appears to have preferred overall directions of growth, similar to the intragranular bainites observed by Brooks and Stansbury in high-purity steels.[10] Comparison of Figs. 7 and 8 shows that the substructure of these intragranular star shapes is identical to the branched regions of the grain-boundary product. At 2·4% N, a further form of intragranular precipitation takes place as well as an increase in the number of intragranular stars. At 2·6% N, after the onset of a small amount of preferred nucleation and growth on grain boundaries, sub-boundaries, and twin interfaces, the majority of the transformation occurs by general matrix precipitation; this is illustrated in Fig. 9. Early in the transformation this fine-scale precipitate takes the form of ill-defined " cuboids ", the substructure of which has not been resolved (Fig. 10). At later stages in the transformation, the precipitates grow to form an intimate aggregate of very fine ferrite and nitride platelets. Alloys containing 2·6% N fully transformed in the range 200–400 °C have the structure shown in Fig. 11, where the overall appearance of the original austenite grains and annealing twins is relatively unaltered.

Kinetics

The changes in electrical resistivity accompanying the isothermal decomposition of austenite to ferrite and Fe_4N were measured at intervals of ~ 20 degC in the range 200–575° C for a series of alloys containing 0·8, 1·1, 1·3, 1·5, 1·9, 2·4, and 2·6% N. These changes amounted to a decrease in resistance of between 30 and 50% of the initial value and they came to a definite end-point. It is therefore possible to express the reaction in terms of the volume fraction of austenite transformed, assuming that the fractional change in electrical resistance is proportional to the volume fraction of the austenite undergoing decomposition. This assumption was checked in several instances by quantitative metallography and found to be valid. *TTT* diagrams derived from such data are of the classical C-curve form found for numerous reactions. Fig. 11 is a typical example for a 1·9% N alloy. At temperatures above the nose of the C-curve where the rate of reaction is increasing with decreasing temperature, meaningful activation energies cannot be found and the kinetics is necessarily complicated by the separation of proeutectoid constituents before the formation of braunite. Therefore, the following kinetic analysis has been applied only to the full range of nitrogen alloys at temperatures in the region of the nose of the C curves and below, where the overall transformation rate is decreasing.

The 0·8% N alloy began to transform during the quench, so no kinetic data are available. The reaction kinetics of alloys containing between 1·1 and 2·4% N was typical of heterogeneous nucleation-and-growth processes in which the fraction transformed has a sigmoidal time-dependence. After an incubation period the reaction proceeded at an increasing rate up to ~ 15% transformation. Thereafter the growth rate was approximately constant up to ~ 50% transformation; from thence the reaction slowed down and eventually stopped. In alloys with higher nitrogen contents the approximately constant reaction-rate range was narrower and a steady-state condition was not attained until after 35% transformation in the 2·6% N alloy.

The isothermal kinetics of such a nucleation-and-growth process may be described by the Burke modified form of the Avrami equation[11]

$$\frac{dx}{dt} = k^n t^{n-1} (1 - x) \qquad \ldots (1)$$

where x is the volume fraction transformed at time t, t is the time that has elapsed since the transformation began, k is a rate constant with dimensions $(\text{time})^{-1}$, and n is the rate index or time exponent.

Integration of equation (1) assuming k and n to be independent of x and thus of t and using the boundary condition $x = 0$ at $t = 0$ leads to

$$\ln \frac{1}{(1 - x)} = \frac{(kt)^n}{n} \qquad \ldots (2)$$

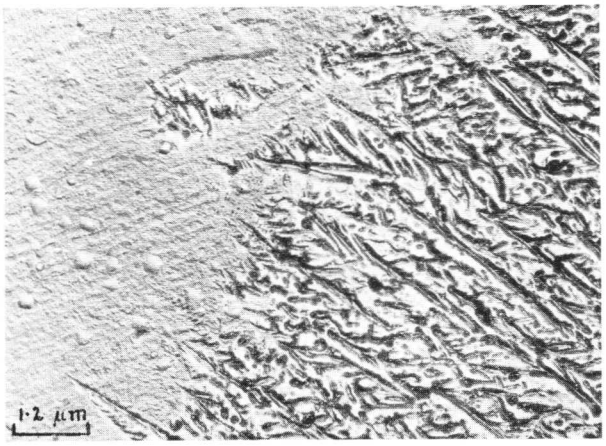

Fig. 7 *Carbon replica of Fe–2·0% N alloy partially transformed at 310° C, showing part of the reaction product growing from a grain boundary.*

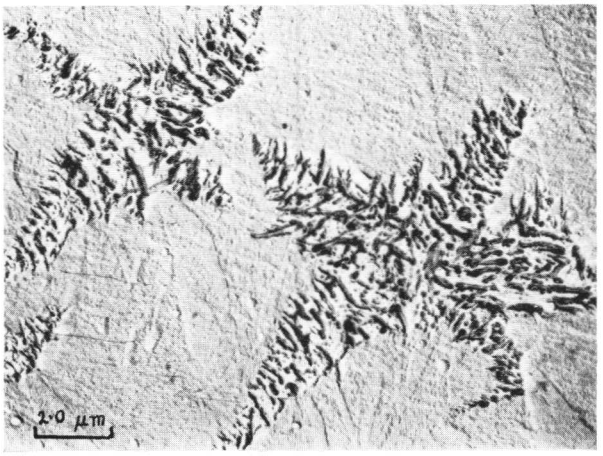

Fig. 8 *Same replica as Fig.* 7, *showing two intragranular precipitates.*

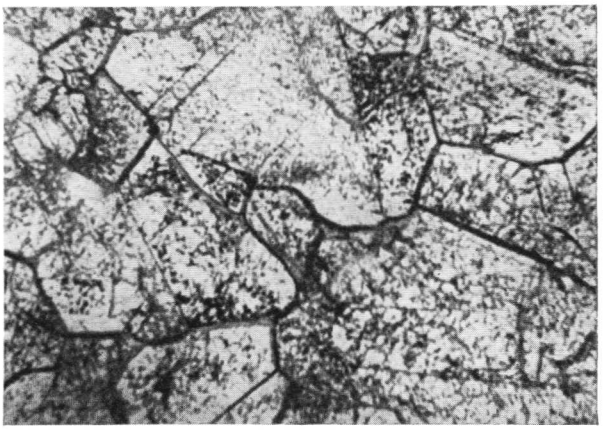

Fig. 9 *Fe–2·6% N alloy partially transformed at 310°. Nital etch.* × 560.

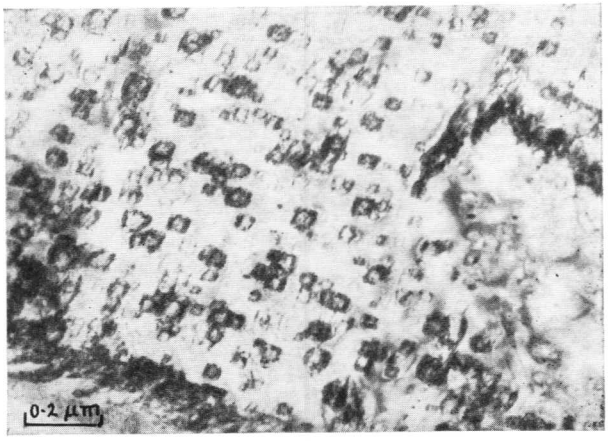

Fig. 10 *Thin-film electron micrograph of Fe–2·6% N alloy partially transformed at 250° C.*

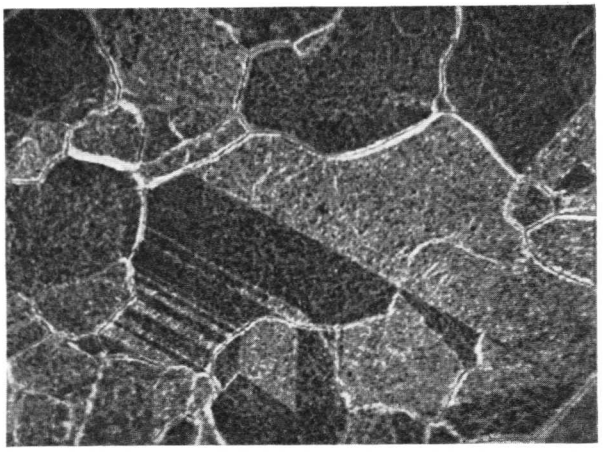

Fig. 11 *Fe–2·6% N alloy fully transformed at 310° C. Nital etch.* × 560.

Converting to base 10 logarithms and taking logarithms

$$\log \log \frac{1}{(1-x)} = n \log k + n \log t - \log 2{\cdot}3n \quad \ldots (3)$$

Hence for reaction data to fit equation (1) graphs relating log log $1/(1-x)$ to log t should be linear of slope n. In general these plots were linear for $0{\cdot}1 \leqslant x \leqslant 0{\cdot}7$ (the plot for the 2·6% N alloy was linear for $0{\cdot}35 \leqslant x \leqslant 0{\cdot}75$) and the values of n given in Fig. 13 for each composition were independent of temperature between 200 and 350° C. These results indicate an isokinetic reaction over the temperature range and degree of transformation specified above. Furthermore, within experimental error the rate index was independent of nitrogen concentration up to ~ 1·9% N. At 2·0% N, corresponding to the formation of the intragranular stars, there is an increase in the kinetic parameter n from $1{\cdot}65 \pm 0{\cdot}05$. This increase becomes more marked at 2·6% N, where there is a distinct change in growth geometry associated with the growth of the randomly distributed matrix precipitates.

It was stated earlier that curves relating the fraction of austenite transformed as a function of time were approximately linear over a certain restricted range of transformation.

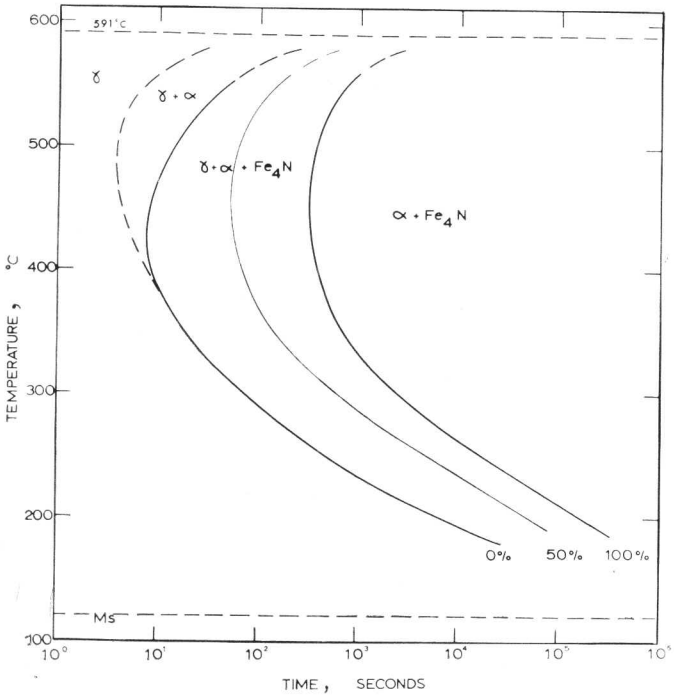

Fig. 12 Time/Temperature/Transformation diagram for Fe–1·9% N alloy, austenitized for 2 min at 700° C.

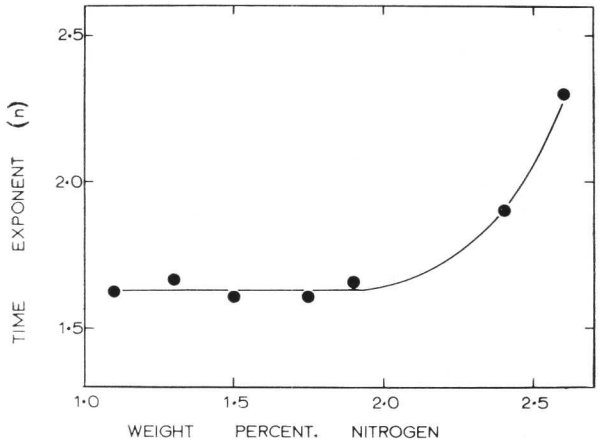

Fig. 13 Variation of time exponent with nitrogen content.

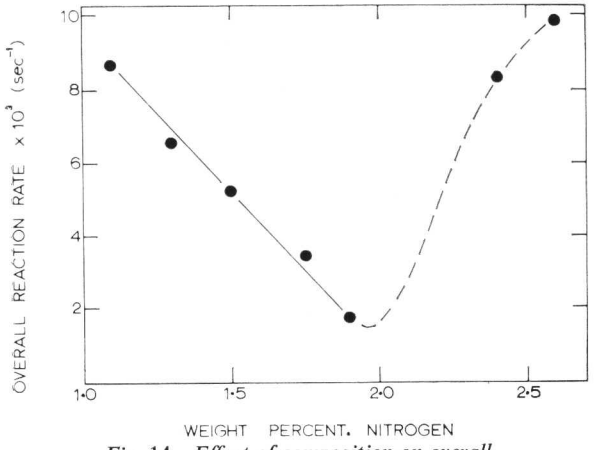

Fig. 14 Effect of composition on overall reaction rate at 310° C.

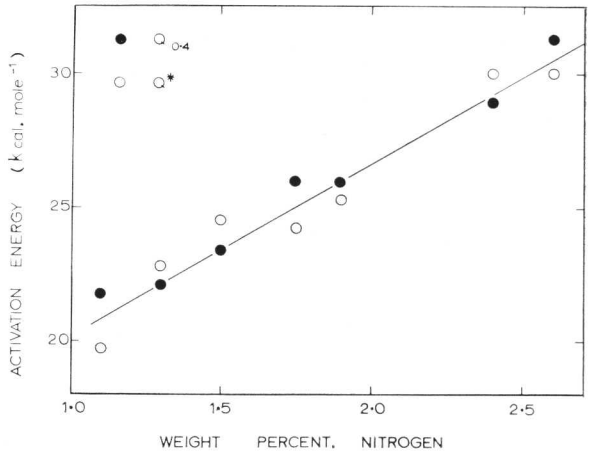

Fig. 15 Variation of average activation energy to 40% transformation (see equation (4)) and overall activation energy Q (see equation (5)) with nitrogen content.*

TABLE I

Variation with Composition of Average Activation Energy to 40% Transformation (see equation (4)) and of Overall Activation Energy (see equation (5))

Nitrogen Content, %	$Q_{0\cdot4}$, kcal/mole	Q^*, kcal/mole
1·1	21·8 ± 0·4	19·7 ± 1·0
1·3	22·1 ± 1·0	22·8 ± 1·1
1·5	23·2 ± 0·5	24·5 ± 0·6
1·7	26·0 ± 0·4	24·3 ± 0·3
1·9	25·9 ± 1·0	25·3 ± 1·0
2·4	28·9 ± 1·0	30·0 ± 1·6
2·6	31·3 ± 0·7	30·0 ± 0·3

However, measurement of the overall rate of transformation dx/dt directly from the resistivity curves at a fixed temperature shows that dx/dt is never really constant. At low degrees of transformation the rate is increasing; it reaches a maximum at ~ 40% transformation and then starts to decrease. The variation in the maximum reaction rate at 310° C as a function of composition is given in Fig. 14. When the nitrogen content is increased from 1·1 to 1·9% the overall rate of transformation dx/dt at a fixed temperature decreases. This decrease is overshadowed at nitrogen concentrations > 1·9%, where there is a rapid increase in the rate of transformation at all temperatures due to the increased degrees of freedom associated with the growth of intragranular Widmanstätten stars and, at very high nitrogen contents, random matrix precipitates.

Two independent techniques have been used to evaluate the overall activation energy for growth of the transformation products. The first is based on the equation

$$\frac{\partial(\log tx)}{\partial(1/T)} = \frac{Q}{2{\cdot}3\,R} \qquad \ldots (4)$$

where t_x is the time (sec) for volume fraction x of transformation product to form at temperature T, R is the universal gas constant, and Q is the overall activation energy. The equation was derived assuming n in equation (1) to be independent of x and T. When n and k do vary with x

between $x = 0$ and $x = x_1$, the average activation energy is calculated. The second technique is based on an equation due to Hillert[12]

$$\frac{\partial}{\partial(1/T)} \log \left(\frac{\partial x}{\partial t}\right)_{x_1} = \frac{-Q^*_{x_1}}{2{\cdot}3\,R} \qquad \ldots (5)$$

This technique does not assume n to be independent of temperature and fraction transformed and gives the activation energy for growth $Q^*_{x_1}$ at fraction transformed x_1.

Graphs relating $1/T$ to $\log t_{0{\cdot}4}$ and to $\log (\partial x/\partial t)_{0{\cdot}4}$, i.e. at the fraction transformed corresponding to the maximum overall growth rate, were plotted for each of the alloys studied. The activation-energy plots were linear at all temperatures up to $\sim$ 350° C; beyond this temperature the reaction ceased to be isokinetic. Activation energies calculated from the linear portions of both types of graph, at each alloy composition, were the same within experimental error and are presented in Table I and Fig. 15. The overall activation energy increases linearly from $\sim$ 20 kcal/mole at 1·1% N to $\sim$ 30 kcal mole at 2·6% N. As in all indirect measurements of reaction rates, there is some uncertainty in deciding the physical significance of experimentally determined overall activation energies. A single activation energy for the reaction under discussion is in theory related directly to the specific activation energy of the rate-controlling process. This event controls the velocity with which the interface between parent and product phases moves. Consequently, the experimentally determined overall activation energies for combined edgewise and sideways growth presented in Fig. 15 are not expected to represent the true activation energy for either form of growth. It may therefore be fortuitous that the activation energy determined indirectly varies, over the full range of nitrogen content studied, between the activation energies for diffusion of nitrogen in ferrite[13] and in austenite.[14,15] The measured activation energy at 2·6% N is $\sim$ 31 kcal/mole, which agrees well with the known activation energy for the diffusion of nitrogen in austenite. Possibly at this composition, where there are discrete " cuboid " matrix precipitates, normal volume diffusion of nitrogen in austenite is rate-controlling.

Summary and Conclusions

(1) At temperatures below $\sim$ 350° C and above the M_s temperature iron–nitrogen austenite decomposes to ferrite and Fe_4N in an apparently discontinuous fashion.

(2) Over the temperature range 200–350° C there is an isokinetic reaction mechanism for alloys containing between 0·7 and 2·6% N.

(3) There is a transition from a completely grain-boundary-nucleated product at compositions up to 1·9% N to a predominantly intragranular-nucleated product at 2·6% N. This is reflected by a marked increase in the overall rate of transformation.

(4) The variation of the kinetic parameter n with composition reflects a change in the nucleation and growth geometry of the reaction products at nitrogen concentrations > 1·9% N.

(5) Ferrite is the leading phase in the edgewise growth direction of the grain boundary and intragranular bainitic products.

(6) After the initial stages of transformation, at nitrogen concentrations up to $\sim$ 2·4% N, growth of bainite is by branching of ferrite in preferred directions.

(7) At 2·6% N the majority of the transformation takes place by the growth of ill-defined " cuboids ".

(8) There is a uniform increase in the overall activation energy for growth of the ferrite and Fe_4N aggregate from 20 kcal/mole at 1·1% N to 30 kcal/mole at 2·6% N.

Acknowledgements

The authors wish to thank their colleague Mr. V. M. Thomas for many helpful discussions. The financial support received from B.I.S.R.A. is gratefully acknowledged.

References

1. V. G. Paranjpe, M. Cohen, M. B. Bever, and C. F. Floe, *Trans. Amer. Inst. Min. Met. Eng.*, 1950, **188,** 261.
2. B. N. Bose and M. F. Hawkes, *ibid.*, p. 307.
3. A. Fry, *Krupp Monats.*, 1923, **4,** 138.
4. T. Bell, *J. Iron Steel Inst.*, to be published.
5. D. Atkinson, T. Bell, and D. Brough, *ibid.*, 1965, **203,** 836.
6. T. Bell and W. S. Owen, *ibid.*, 1967, **205,** 428.
7. M. Okamoto, R. Tanaka, T. Naito, and R. Fujimoto, *Tetsu-to-Hagane*, 1961, **2,** 25.
8. A. Hultgren, *Trans. Amer. Soc. Metals*, 1947, **39,** 915.
9. M. Hillert, " Decomposition of Austenite by Diffusional Processes " (edited by V. F. Zackay and H. I. Aaronson), Chap. 4, p. 230. **1962:** New York and London (Interscience Publishers).
10. C. R. Brooks and E. E. Stansbury, *J. Iron Steel Inst.*, 1965, **203,** 514.
11. J. Burke, " The Kinetics of Phase Transformation in Metals ". **1965:** Oxford, &c. (Pergamon Press).
12. M. Hillert, *Acta Met.*, 1959, **7,** 653.
13. J. D. Fast and M. B. Verijpe, *J. Iron Steel Inst.*, 1954, **176,** 24.
14. A. Bramley and G. Turner, *ibid.*, 1928, **17,** 23.
15. L. S. Darken, R. P. Smith, and R. W. Filer, *Trans. Amer. Inst. Min. Met. Eng.*, 1951, **191,** 1174.

The Isothermal Decomposition of Alloy Austenite

F. G. Berry, A. T. Davenport, and R. W. K. Honeycombe

The isothermal decomposition of austenite containing iron–4 wt.-% Mo–0·2% carbon and iron–2 wt.-% V–0·2% carbon has been studied in the range 600–800° C, when aggregates of ferrite and alloy carbide are formed. The carbide can occur in a fibrous form in which the individual fibres, 200–300 Å in dia., grow to several microns in length approximately normal to the original austenite boundaries. Alternatively, the carbide is precipitated as very fine particles at the α/γ phase boundary (interphase precipitation), which as it moves leaves closely spaced walls of precipitate within the ferrite. The crystallographic relationships of the carbide fibres and particles with the ferrite and austenite have been investigated and are used to explain the mechanisms by which the transformation takes place.

When a plain carbon austenite is decomposed eutectoidally in the range 550–700° C to form ferrite and cementite, the pearlite reaction commences primarily at the austenite grain boundaries.[1] This transformation is a very familiar example of a discontinuous reaction in which the growth of the two phases is closely interrelated. However, if a strong carbide-forming element is added to form a ternary iron–carbon alloy, cementite can be replaced by one of a number of alloy carbides. The present work deals with the structural changes in high-purity iron-base alloys where the carbide phase is either vanadium carbide (V_4C_3 f.c.c.) or molybdenum carbide (Mo_2C h.c.p.). These carbides possess simpler crystal structures than cementite, and thus facilitate a detailed crystallographic study of the eutectoid reaction as well as more closely reflecting the behaviour of commercial alloy steels.

Morphology of the Eutectoid Reaction in Alloy Austenites

We have investigated in detail two alloys:

(1) Iron–4 wt.-% molybdenum–0·2% carbon (~ 2 at.-% Mo, 1 at.-% C)

(2) Iron–2 wt.-% vanadium–0·2% carbon (~ 2 at.-% V, 1 at.-% C)

Both of these form homogeneous austenite when annealed for several hours between 1150 and 1300° C. On quenching into a fused-salt or lead bath held between 600 and 800° C, the eutectoid reaction proceeds inwards from the austenite boundaries as in the pearlite reaction. The reaction product is not predominantly nodular, but the α/γ interphase boundary is frequently approximately parallel to the original austenite boundary (Fig. 1). The product is an aggregate of ferrite and alloy carbide (V_4C_3 or Mo_2C), but thin-foil electron microscopy reveals major differences in morphology from pearlite. In the molybdenum alloy, the Mo_2C exists primarily as very fine monocrystalline fibres ~ 200–300 Å in dia., and several μm in length (Fig. 2). The spacing of the fibres is ~ 500 Å, which is at least an order of magnitude finer than that of the lamellae in cementite–pearlite aggregates formed under comparable conditions.

In the vanadium-containing alloy, the V_4C_3 precipitate was not primarily fibrous, but occurred as closely spaced (~ 100 Å) bands of extremely fine particles, initially less than 50 Å in dia. These bands are predominantly parallel to the α/γ transformation interface and follow its changes in direction (Fig. 3). Detailed metallographic examination has shown that the particles are formed at the α/γ interface,[2] which moves in a series of short steps allowing repeated nucleation of the carbide phase. We have termed this phenomenon " interphase precipitation ". This mode of carbide precipitation is strikingly different from the growth of long carbide fibres in the molybdenum alloy, though it takes place in the same temperature range.

Further work has shown that the two basic modes of carbide growth during the eutectoid reaction are not mutually exclusive. In some circumstances, V_4C_3 fibres grow in Fe–V–C alloys, while in Fe–Mo–C alloys both fibre growth and interphase precipitation of Mo_2C can occur in the same specimen—indeed in the same grain and associated with the same transformation front (Fig. 4).

Crystallography of Mo_2C in Ferrite

The crystallographic features of Mo_2C precipitation in tempered martensite are well documented.[3,4] The particles are small rods whose axes lie along the three cube directions in ferrite; the orientation relationship is of the Pitsch–Schrader[4,5] type, originally found between ε-iron carbide and ferrite (ε-iron carbide and Mo_2C are isostructural):

$$(011)_\alpha \parallel (0001)_{Mo_2C}$$
$$(100)_\alpha \parallel (2\bar{1}\bar{1}0)_{Mo_2C}$$
$$[100]_\alpha \parallel [2\bar{1}\bar{1}0]_{Mo_2C} \quad \text{(growth direction)}$$

The acicular morphology is explained in terms of a low atomic mismatch (< 5%) which can only be achieved along the $[100]_\alpha$ when the direction in the carbide along which growth occurs is $[2\bar{1}\bar{1}0]$. The orientation relationship arises from the fact that the atomic arrangement on the $(011)_\alpha$ plane closely resembles that on the $(0001)_{Mo_2C}$ plane and near-registry of atoms can be achieved by a slight expansion normal to the $[100]_\alpha$ growth direction, which lies in the $(011)_\alpha$ plane.[4]

Electron-diffraction studies of the Mo_2C fibres reveals that they do not obey the above relationship. Instead we find that

$$(011)_\alpha \parallel (0001)_{Mo_2C}$$
$$(101)_\alpha \parallel (1\bar{1}01)_{Mo_2C}$$
$$[1\bar{1}1]_\alpha \parallel [1\bar{2}10]_{Mo_2C}$$

which is a relationship of the type first described for ε-iron carbide in tempered martensite by Jack.[6] The difference

Manuscript received 3 July 1968. F. G. Berry, B.Eng., A. T. Davenport, M.Met., and Professor R. W. K. Honeycombe, D.Sc., Ph.D., F.I.M., are in the Department of Metallurgy, University of Cambridge.

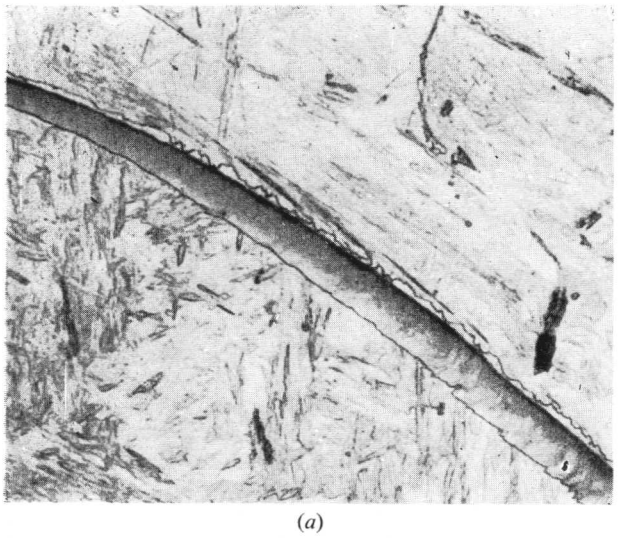

(*a*)

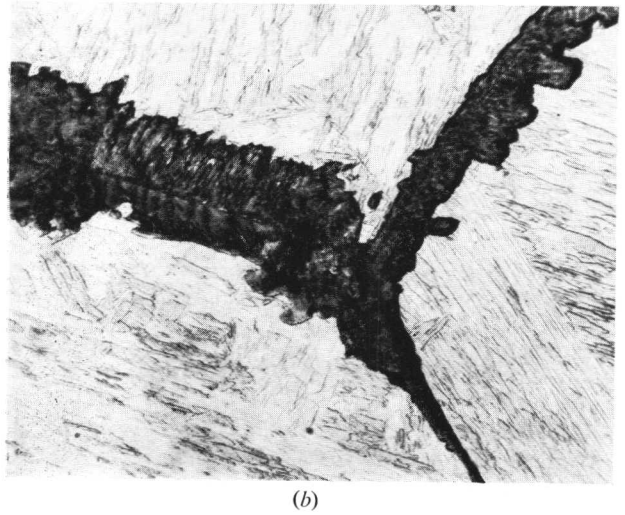

(*b*)

Fig. 1 (a) *Fe–2V–0·2C alloy isothermally transformed for* 20 *sec at* 650° *C. Optical micrograph. Etchant:* 2% *nital.* × 400. (b) *Fe–4Mo–0·2C alloy isothermally transformed for* 4 *h at* 650° *C. Optical micrograph. Etchant:* 2% *nital.* × 320.

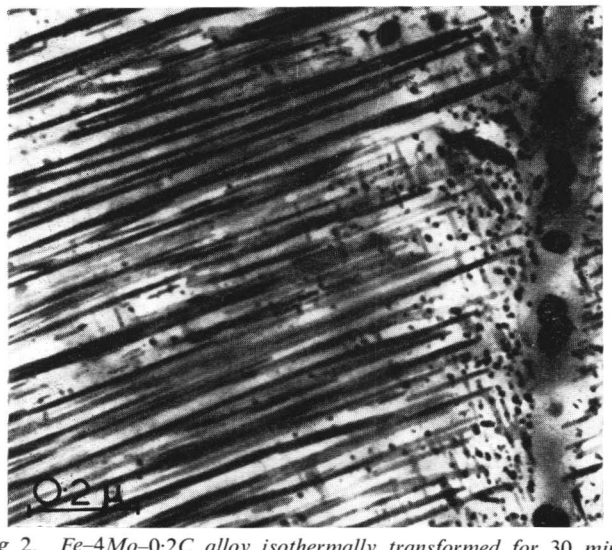

Fig 2. *Fe–4Mo–0·2C alloy isothermally transformed for* 30 *min at* 700° *C. Thin-foil electron micrograph.* × 68,000.

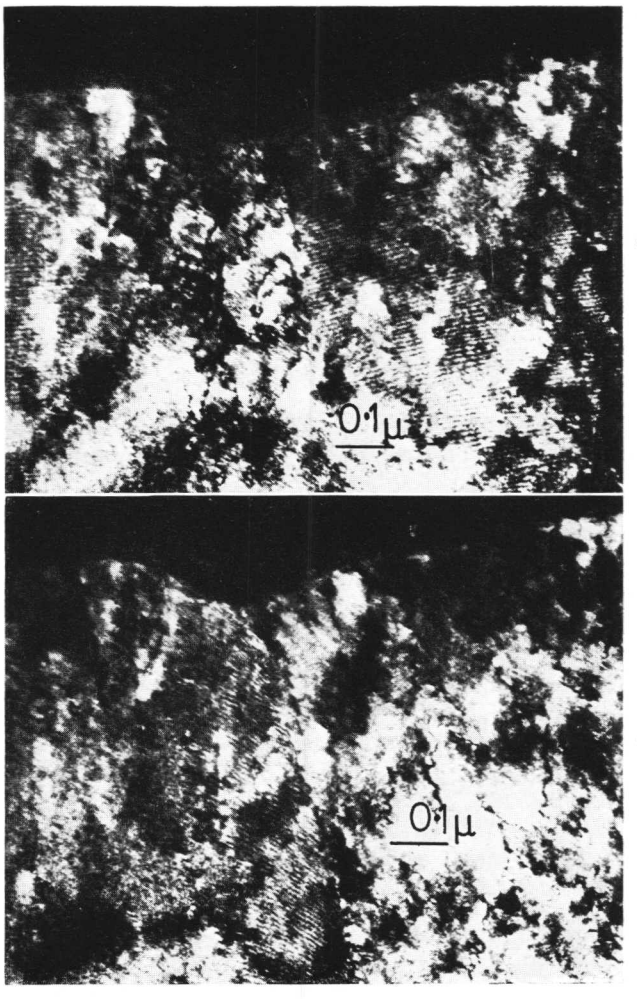

(*a*)

(*b*)

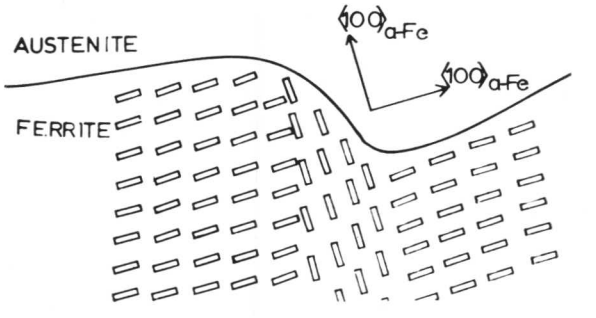

(*c*)

Fig. 3 *Fe–2V–0·2C alloy partially transformed for* 10 *sec at* 600° *C.* (a) *is a thin-foil micrograph of an* α/γ *interface where the ferrite side is observed in dark field. Fine lines of* V_4C_3 *can be seen lying parallel to the horizontal part of the interface. In* (b) *the contrast conditions have been altered by tilting and it can be seen that the lines also lie parallel to the kink in the interface. Electron-diffraction analysis reveals that the* V_4C_3 *lies on the ferrite cube plane most nearly parallel to the plane of the interface and that a change in the habit plane occurs in regions near the kink. This is illustrated schematically in* (c).

between the above two relationships is a 5° rotation in the basal plane, which can readily be differentiated in suitably orientated specimens (see Fig. 5). Moreover, the growth direction of the fibres is not a well-defined crystallographic direction in ferrite.

We believe that the different orientation relationships reflect a basic difference in growth mechanisms. Whereas the Widmanstätten rods of Mo_2C nucleate and grow in ferrite, a detailed examination of structures and orientation relationships suggests that the fibres form on the γ side of the α/γ interface. One could expect the orientation relationship of the Mo_2C in austenite to be the familiar

$$(111)_\gamma \parallel (0001)_{Mo_2C}$$
$$[1\bar{1}0]_\gamma \parallel [1\bar{2}10]_{Mo_2C}$$

but unfortunately it was not possible to retain sufficient austenite to verify this assumption. If the austenite then transforms to ferrite, obeying the Kurdjumov–Sachs[7] relationship

$$(111)_\gamma \parallel (011)_\alpha$$
$$[1\bar{1}0]_\gamma \parallel [1\bar{1}1]_\alpha$$

This leads to the α/Mo_2C fibre relationship of the Jack type described above.

Crystallography of V_4C_3 in Ferrite

The precipitation of f.c.c. V_4C_3 in tempered martensite obeys the relationship proposed by Baker and Nutting:[8]

$$(100)_\alpha \parallel (100)_{V_4C_3}$$
$$[011]_\alpha \parallel [010]_{V_4C_3}$$

The carbide forms as very small platelets, initially $\sim$ 20 Å wide and a few Å thick, on the cube planes of the ferrite matrix, mainly in association with dislocations inherited from the martensite.

When the Fe–V–C steel is isothermally transformed direct from austenite in the range 600–700° C, the product appears to be entirely ferritic. There is little evidence of the growth of V_4C_3 fibres, though these are sometimes observed.[9] Instead, bands of very fine V_4C_3 particles are formed parallel to the α/γ interface but, unlike the same precipitate in tempered martensite, there is little evidence of nucleation on dislocations. Another important difference is revealed by dark-field studies, namely that the V_4C_3 is present on only one cube plane of the matrix in a given region of the transformation product (Fig. 6). These platelets still obey the Baker–Nutting orientation relationship which implies that the V_4C_3 has nucleated in the ferrite. However, the restriction of the possible habit planes to a single one arises from the fact that the particles nucleate at the α/γ interface.

Fibre growth occasionally occurred in the vanadium alloy and the carbide was again shown to be V_4C_3, but it did not possess the Baker–Nutting orientation relationship with the ferrite matrix. Indeed, the evidence so far indicates that there is a Kurdjumov–Sachs relation between this fibrous V_4C_3 and ferrite, i.e.

$$(111)_{V_4C_3} \parallel (110)_\alpha$$
$$[1\bar{1}0]_{V_4C_3} \parallel [1\bar{1}1]_\alpha$$

It is already known[10] that when V_4C_3 precipitates in austenitic steels the following relationship is observed:

$$(100)_{V_4C_3} \parallel (100)_\gamma$$
$$[011]_{V_4C_3} \parallel [011]_\gamma$$

Consequently, when the austenite is replaced by the ferrite, the vanadium carbide would be related to the ferrite by the Kurdjumov–Sachs relationship. We thus deduce that the V_4C_3 fibres grow in association with the austenite in an analogous way to the Mo_2C fibres.

Nucleation and Growth of Carbide Fibres

The nucleation and growth of α-Mo_2C fibre aggregates has very similar features to the nucleation and growth of pearlite, except that the fibres within one particular colony are more precisely aligned with each other. However, crystallographic analysis shows that the fibre growth axis is not a rational direction in the ferrite. If the fibres had nucleated and grown in ferrite, there is no reason to believe that they would have formed in other than the Pitsch–Schrader orientation relationship with a $\langle 100 \rangle_\alpha$ growth direction. The crystallographic observations thus suggest that the fibres form not in ferrite but in contact with austenite. We envisage that the first stage of the eutectoid reaction is the formation of idiomorphic grain-boundary carbide precipitates, which lower the carbon content of the adjacent austenite and allow a series of ferrite nuclei to form along the boundary. The spontaneous formation of ferrite nuclei in the grain boundary can also occur in alloys of proeutectoid composition. The metallographic evidence indicates that the ferrite develops in two ways:

(1) Nucleation on either side of the austenite grain boundary followed by growth into the grain in which the ferrite was nucleated, probably with the Kurdjumov–Sachs relationship.[11] These may be referred to as " related-orientation " grains.

(2) Nucleation on one side of the austenite grain boundary followed by growth into both adjoining grains. This results in the ferrite grain being orientation-related to one austenite grain, and randomly related to the other. The crystallographic data indicate that both the fibres and the adjacent ferrite are uniquely related to the austenite; consequently it is very likely that the fibre colony nucleates in association with " related-orientation " grains of ferrite, i.e. ferrite grains that have the Kurdjumov–Sachs orientation relationship with the austenite into which they are growing. The colony is nucleated at the α/γ interface which presents the most favourable sites for nucleation, and grows always with the tips of the fibres in contact with the γ. We have not observed a ferrite gap between the ends of the fibres and the austenite (Fig. 7).

Nucleation and subsequent growth of fibre colonies on α/γ interfaces, across which the ferrite is unrelated to the austenite, is not expected to occur as it would be impossible for the fibre to possess, at the same time, an orientation relationship with the austenite into which it is growing and the ferrite with which it is associated.

In the first of the two cases of initial grain-boundary ferrite nucleation referred to above, fibre nucleation and growth can occur from both sides of the austenite grain boundary, while in the second case fibre nucleation and growth will occur only on the side where the ferrite is related to the austenite by the Kurdjumov–Sachs orientation relationship. Both these types of morphology have been observed in the Fe–Mo–C alloy.

Interphase Precipitation

The formation of discrete fine particles of carbide repeatedly at the advancing α/γ interface is clearly an alternative form of eutectoid decomposition to that of fibrous growth. In the Fe–V–C alloy, interphase precipitation predominates but

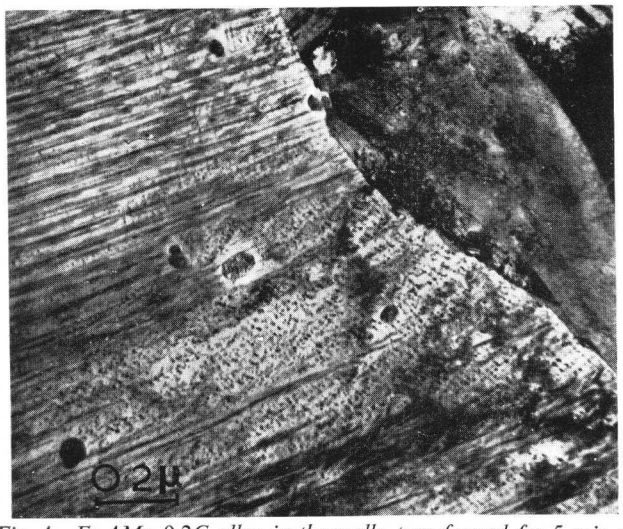

Fig. 4 Fe–4Mo–0·2C alloy isothermally transformed for 5 min at 700° C. Thin-foil electron micrograph. × 48,000.

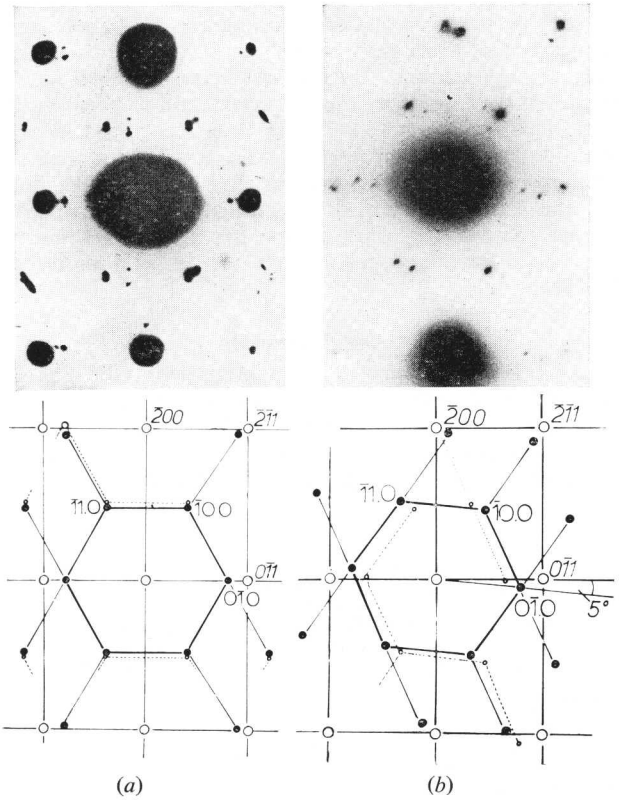

(*a*) (*b*)

Fig. 5 (a) *shows a typical diffraction pattern of Widmanstätten rods of Mo_2C as observed in tempered martensite and its indexed interpretation. The zones present are the $(011)_\alpha$ and $(0001)_{Mo_2C}$ and are related according to the Pitsch and Schrader orientation relationship.* (b) *is a diffraction pattern of Mo_2C fibre precipitate formed during isothermal transformation. Corresponding zones to those in* (a) *are present, but there is a 5° rotation of the Mo_2C zone about the $[011]_\alpha$. (The reflections joined by the broken lines arise from double diffraction.)*

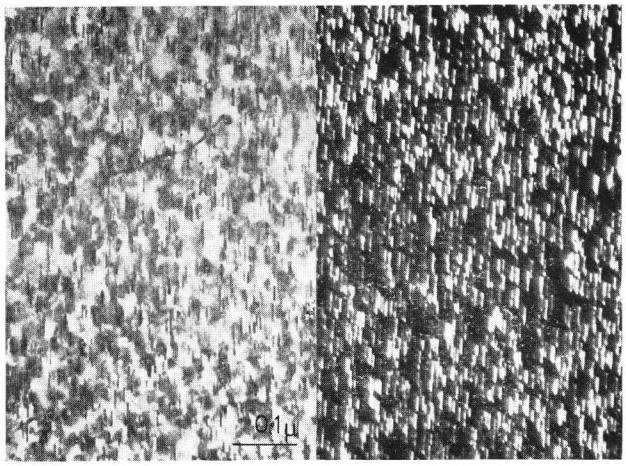

Fig. 6 Fe–2V–0·2C alloy isothermally transformed for 3 h at 700° C. Thin-foil bright and dark fields showing V_4C_3 platelets lying on only one cube plane.

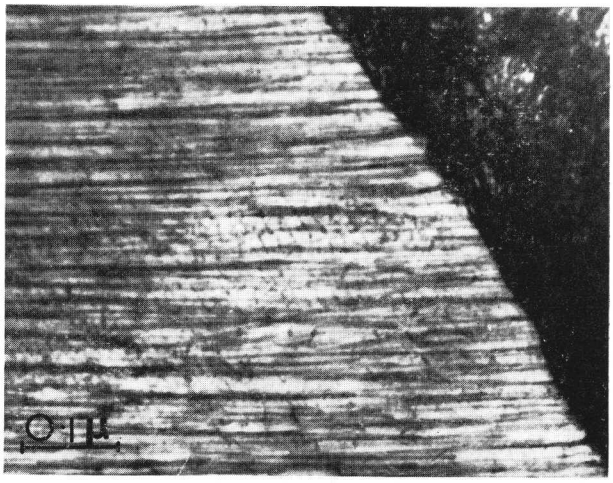

Fig. 7 Fe–4Mo–0·2C alloy isothermally transformed for 20 min at 650° C. Transformation front. Thin-foil electron micrograph. × 120,000.

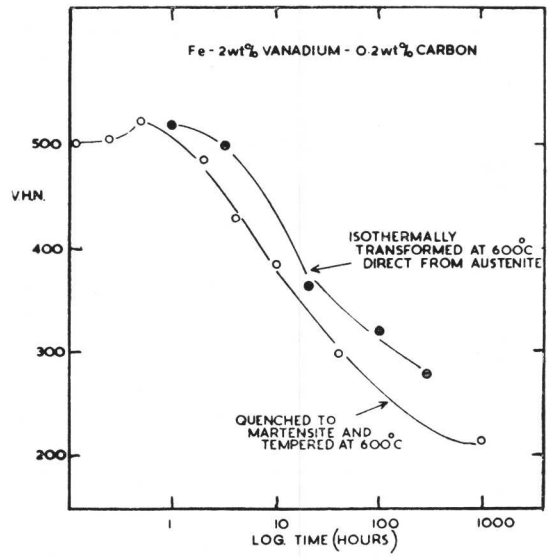

Fig. 8 Isothermal hardness curves from an Fe–2V–0·2C alloy that has been (○) quenched to martensite and subsequently tempered and (●) isothermally transformed direct to ferrite at the same tempering temperature.

fibres are sometimes observed. In the Fe–Mo–C alloy, on the other hand, fibre growth accounted for much of the carbide formation but this was associated in many cases with interphase precipitation of the same carbide, Mo_2C, in a finely divided form (Fig. 4). Crystallographic investigation of the Fe–V–C alloy revealed that interphase precipitation nucleated and grew in the ferrite, and had no relationship with the austenite. Hence this product differs from the fibre colonies in that it can nucleate at any one of the α/γ interfaces, and does not require the associated ferrite grain to be related to the austenite.

The reaction starts with the formation of a layer of ferrite at the austenite grain boundaries, as described in the previous section. However, in order for the growth of ferrite to continue, carbon depletion in the austenite in its immediate vicinity must take place. This is achieved by the nucleation of a row of V_4C_3 particles along the α/γ interface, which adopt only one of the three α-iron {100} habit planes, i.e. the one most nearly parallel to the interface (Fig. 3). This choice of habit plane could arise from one of two causes:

(1) The diffusion path from the interface for the vanadium atoms to form plates on this {100} habit plane is the shortest.

(2) The coherency strains are minimized.

While the fibre growth process approximates to an equilibrium structure, it is very likely that the interphase precipitation initially does not. First, the particles are coherent, and secondly, the matrix is not depleted of vanadium to the equilibrium concentration at the transformation temperature. Prolonged treatment at this temperature results in slow growth of the interphase precipitate, initially by further depletion of the matrix in vanadium and later by coarsening.

Mechanical Properties Resulting from the Transformations

The fineness of the initial interphase precipitation of V_4C_3 indicates that the mechanical properties are likely to be interesting. In fact, it has been found that the hardness of the alloy after isothermal transformation at 600° C is higher than that of the identical alloy quenched and then tempered for similar times at the same temperature (Fig. 8). The interphase precipitate has been shown to over-age less rapidly than the tempered martensite.

One possible advantage of the fibrous structure is its thermal stability, experiments having shown that the fibres are unaltered by prolonged annealing in the range 600–700° C, in striking contrast with the behaviour of Mo_2C in tempered martensite.

Discussion and Conclusions

The main problem posed by this work is to determine the conditions that lead on the one hand to the growth of fibre colonies and on the other to the formation of the ultra-fine interphase precipitation.

In the case of the vanadium alloy, fibres have been observed at high temperatures (800–900° C),[9] while interphase precipitation predominates between 600 and 700° C. It is envisaged that the fibrous reaction product has a lower free energy than the interphase precipitation, and at high temperatures where adequate diffusion can take place it will thus tend to be the dominant reaction. However, at lower temperatures, where the thermodynamic driving force is higher, the reaction takes place more rapidly but the diffusivity is inadequate for the growth of the fibre colonies. Very fine carbide fibres do not form because the increased energy needed for the fibre/matrix interface would affect the driving force for the reaction. Consequently, interphase precipitation would be expected at lower temperatures because it provides:

(1) A much shorter diffusion path between nuclei.

(2) Minimum interfacial energy as a result of coherent precipitation.

It is likely that the bainite reaction at still lower temperatures incorporates interphase precipitation, and indeed Ohmori[12] has recently found interphase precipitation of cementite in bainite formed at 450° C in a 0·8% plain carbon steel. Recent work by Srinivasan and Wayman[13] has also shown that in lower bainite formed at 285° C in Fe–Cr–C alloys, carbide particles are lined up in bands along one growth axis of the bainite.

The molybdenum-containing alloy exhibits both fibres and interphase precipitation in the one specimen and even in association with the same interface. We have indicated that two types of α/γ boundary exist, the orientation-related and the random types. While fibres must be associated with orientation-related boundaries, it is likely that interphase precipitate occurs at random α/γ boundaries which possess higher energies and provide better sites for nucleation. This would explain the observed cases where fibre growth occurs on one side of an austenite boundary and interphase precipitation on the other. There remains the case where both types of precipitation are associated with a single interface. The boundary between orientation-related grains is likely to have large regions of order (low energy) connected by disordered or high-energy sections. Interphase precipitation will not be expected in the former regions but could tend to occur in the latter. This type of boundary has been recognized in proeutectoid ferrite by Aaronson,[11] who emphasizes that the boundary comprises highly ordered and disordered regions. That the local character of the boundary can markedly influence the mode of precipitation has also been found in recent grain-boundary-precipitation studies in non-ferrous alloys.[14]

Acknowledgements

The work was supported by a grant from the Science Research Council, which the authors gratefully acknowledge. They are also much indebted to the British Iron and Steel Research Association (now the Inter-Group Laboratories of the British Steel Corporation) for the provision of bursaries to F.G.B. and A.T.D.

References

1. V. F. Zackay, " Decomposition of Austenite by Diffusional Processes " (edited by H. I. Aaronson). **1962:** New York and London (Interscience Publishers).
2. A. T. Davenport, F. G. Berry, and R. W. K. Honeycombe, *Metal Sci. J.*, 1968, **2**, 104.
3. D. Raynor, J. A. Whiteman, and R. W. K. Honeycombe, *J. Iron Steel Inst.*, 1966, **204**, 349.
4. D. J. Dyson, S. R. Keown, D. Raynor, and J. A. Whiteman, *Acta Met.*, 1966, **14**, 867.
5. W. Pitsch and A. Schrader, *Arch. Eisenhüttenwesen*, 1958, **29**, 715.
6. K. M. Jack, *J. Iron Steel Inst.*, 1951, **169**, 26.
7. G. Kurdjumov and G. Sachs, *Z. Physik*, 1930, **64**, 325.
8. R. G. Baker and J. Nutting, " Precipitation Processes in Steels " (Special Rep. No. 64), p. 1. **1959:** London (Iron Steel Inst.)
9. H. C. Sutton, unpublished work.
10. H. J. Harding, Ph.D. Thesis, Univ. Sheffield, **1963.**
11. H. I. Aaronson, " Proeutectoid Ferrite and Cementite Reactions ", in Ref. (1).
12. Y. Ohmori, unpublished work.
13. G. R. Srinivasan and C. M. Wayman, *Acta Met.*, 1968, **16**, 609.
14. P. N. T. Unwin, unpublished work.

Research Note

The Effect of Manganese on Pearlite Degeneracy in Iron–Nitrogen Alloys

J. Williams, R. C. Cochrane, L. G. T. Davy, and S. G. Glover

The isothermal decomposition of Fe–N austenites of eutectoid composition was first studied by Bose and Hawkes.[1] They reported that at reaction temperatures between 550° C and T_e (the eutectoid, 591° C) the kinetically favourable lamellar morphology constituted only a small fraction of the eutectoid product. The remainder consisted of a granular mixture of ferrite and nitride (Fe_4N). These observations have been confirmed in the present investigation (Fig. 1), and we find that the proportion of lamellar constituent increases with increasing undercooling. In addition, a careful study of the morphology of the product at early reaction times showed that:

(1) The smallest nodule was duplex.

(2) The duplex structure was often lamellar in form and could be considered as embryonic pearlite.

(3) In many cases the nitride constituent tended to be completely surrounded by ferrite and thus further development as lamellar pearlite was obstructed.

Typical examples of these microstructures are shown in Fig. 2.

Now the lamellar morphology, because of the small and constant diffusion distance at the duplex growth front, favours rapid growth. However, because a portion of the available free energy is utilized in forming new interphase boundary, this does not lead to the greatest free-energy decrease. The free energy of the new interfaces is then the driving force for concurrent and subsequent spheroidization of the lamellae. We are thus led to the conclusion that minimization of interfacial energy is a dominant characteristic of the transformation in these alloys.

Hillert[2] has suggested that pearlite growth depends on co-operation between the two phases. Since these two phases influence each other only at their interface, we liberally interpret this to suggest that the surface terms $\sigma^{\alpha X}$, $\sigma^{\alpha\gamma}$, and $\sigma^{\gamma X}$ (Fig. 2(*c*)) are the factors that would determine the difference in eutectoid morphology between alloys where the total free-energy change and the diffusivity are similar.

Davy and Glover[3] have shown that small additions of Mn to hypoeutectoid Fe–C alloys alter the interfacial terms and their temperature-dependence in a manner that reduces the probability of the cementite forming a continuous film over proeutectoid ferrite. A development of this argument appears also to explain the occurrence of degenerate pearlite in Fe–N alloys.

In the Fe–C system it is impossible to study pearlite morphology in conditions where the total free-energy change and the diffusivity are similar because of the large changes in T_e brought about by Mn additions. In the Fe–N alloys, however, we find experimentally that T_e is little changed by the addition of 0·25 or 0·5 wt.-% Mn (Table I).

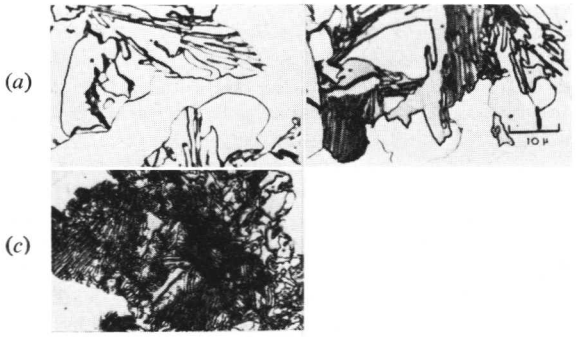

Fig. 1 Showing increasing tendency for co-operative growth with increasing undercooling: (a) 581° *C, 90 min;* (b) 574° *C, 40 min;* (c) 556° *C, 8 min (partially transformed specimens of Fe–2·3N).*

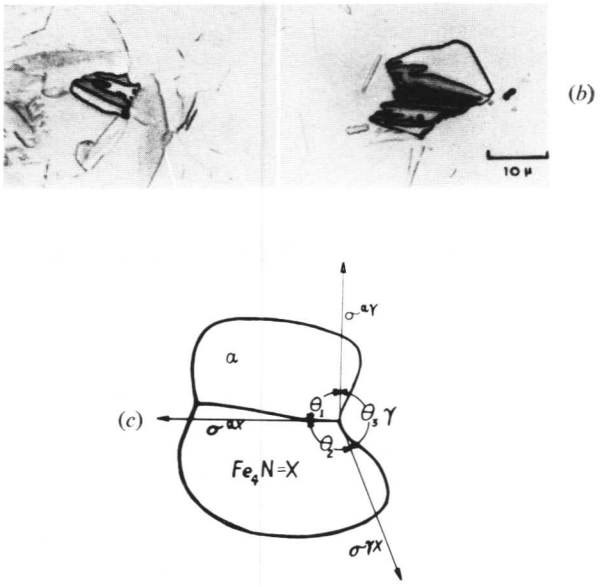

Fig. 2 Duplex nodules in Fe–2·3N alloy reacted at 574° *C for:* (a) 10 *min and* (b) 20 *min;* (c) *schematic nodule showing interfacial-energy balance at a three-phase junction as deduced from* (a) *and* (b). *Since* $\theta_3 > \theta_2 > \theta_1$, *from the sine rule* $\sigma^{\alpha X}/\sin\theta_3 = \sigma^{\alpha\gamma}/\sin\theta_2 = \sigma^{\alpha\gamma}/\sin\theta_1$; *hence* $\sigma^{\alpha X} < \sigma^{\alpha\gamma} < \sigma^{\gamma X}$ *and the ferrite phase will tend to overgrow (wet) the nitride phase.*

Manuscript received 3 July 1968. J. Williams, B.Sc., R. C. Cochrane, B.Sc., Ph.D., L. G. T. Davy, A.I.M., and S. G. Glover, B.Sc., Ph.D., are in the Department of Physical Metallurgy, University of Birmingham.

TABLE I

Composition	Eutectoid Temp. (T_e), °C
Fe–2·3 wt.-%N*	586·5 ± 0·5
Fe–0·23 wt.-% Mn–2·1 wt.-% N†	588·0 ± 1·0
Fe–0·55 wt.-% Mn–2·1 wt.-% N†	590·0 ± 1·0

* Nitrided BISRA " AH " iron.
† Detailed analysis, before nitriding, given in Ref. 3.

Isothermal transformation studies reveal a very striking change in the morphology of the transformation products both at constant temperature of reaction and at constant undercooling (Fig. 3), which we consider lends considerable support to our capillarity arguments.

The microstructures shown in Fig. 2 suggest that in the binary alloy the free energies of the γ/α and γ/X interfaces are unequal, so that during growth the ferrite tends to overgrow (wet) the nitride. It would appear that for the development of lamellar pearlite one requires the following conditions:

(1) The interfacial energy between the product phases and the parent phase should be about equal, so that there is little tendency for preferential surface growth of one of the phases.

(2) The values of the specific energies for all interfaces should be low, so that the tendency to spheroidization is reduced and interfacial instability develops,[4,5] leading to pearlite formation in the manner suggested by Davy and Glover.[3]

Growth rates in Fe–N alloys are being studied but it is impossible to define an interlamellar spacing because of the degenerate nature of the structure. However, preliminary analysis of reaction kinetics suggests that the establishment of co-operative growth leads to an increase in the isothermal transformation rate. Successive additions of Mn increasingly retard the transformation and, though a systematic study of the relationship between growth rate and interlamellar spacing has yet to be completed, it would appear that Mn interferes with the interface transport mechanism through its surface activity.

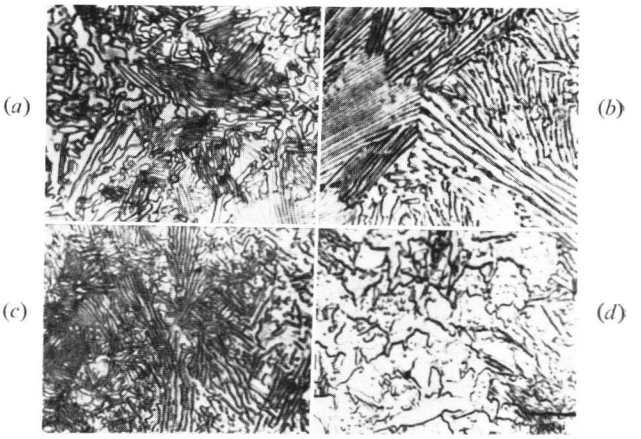

Fig. 3 Comparison of: (a) *Fe–0·23 Mn–2·1 N and* (b) *Fe–0·55 Mn–2·1N fully transformed at 577° C; also of* (c) *Fe–0·23 Mn–2·1 N and* (d) *Fe–2·3 N fully transformed at* 571 *and* 568° *C, respectively, i.e. an identical amount of undercooling.*

References

1. B. N. Bose and N. F. Hawkes, *Trans. Met. Soc. A.I.M.E.*, 1950, **188**, 307.
2. M. Hillert, " Decomposition of Austenite by Diffusional Processes ", p. 197. **1960:** New York and London (Interscience Publishers).
3. L. G. T. Davy and S. G. Glover, *J. Australian Inst. Metals*, 1968, **13**, (2), 71.
4. W. W. Mullins and R. F. Sekerka, *J. Appl. Physics*, 1963, **34**, 381.
5. P. G. Shewmon, *Trans. Met. Soc. A.I.M.E.*, 1965, **233**, 736.

Research Note

The Decomposition of the γ Phase of a Cu–27 wt.-% Sn Alloy

W. Vandermeulen and A. Deruyttere

The aim of the present study was to examine further the decomposition of the γ phase of a Cu–27 wt.-% Sn alloy during different ageing treatments below 350° C.[1,2] The ageing was preceded by direct quenching from the γ region to the decomposition temperature, by water-quenching, or by splat-cooling, i.e. quenching from the liquid state. Two splat-cooling techniques were used.[3,4] With the first of these the droplet falls apart into numerous small particles which cool with extreme rapidity, whereas with the second method the droplet remains intact and therefore the cooling should be somewhat less rapid. The specimens obtained by both splat-cooling techniques consist mainly of the γ phase. An interesting property is that some parts of the specimens are transparent in the electron microscope without any preparation.

Manuscript received 3 July 1968. W. Vandermeulen, b.mt.ir., and A. Deruyttere, b.mt.ir., Ph.D., are at the Instituut voor Metaalkunde, Universiteit te Leuven, Heverlee, Belgium.

To obtain the γ phase at room temperature by quenching from the γ region the cooling rate has to be very high; it was thus impossible with a plate specimen of 3 mm thickness to avoid partial decomposition.[1] The experiments were therefore carried out on specimens of 0·5 and 0·05 mm thickness.

Fig. 1 gives a survey of the different heat-treatments and results. If a plate (0·05 mm thick) is quenched from the γ region in water the γ phase is retained since X-ray diffraction gives no indication of another phase. After ageing for a few seconds at 300° C the δ phase forms, almost immediately followed by α′, a copper-rich transition phase between γ and the α solid solution. The equilibrium phases α and ε form only after longer annealing periods.[1,2] Alternatively, if a 0·05-mm-thick plate is directly quenched from the γ region to 300° C the ζ phase forms instead of δ. The rest of the decomposition follows the same scheme as for the water-quenched specimens. A thicker specimen (0·5 mm) directly

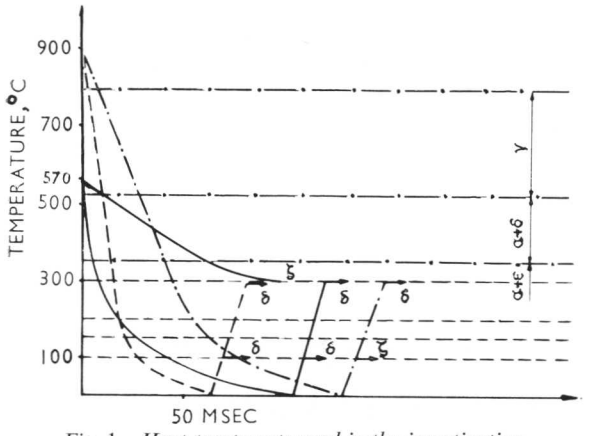

Fig. 1 Heat-treatments used in the investigation
——— *0·05 mm plate*
— — — *Rapid splat-cooling*
—·—·— *Slower splat-cooling*

quenched to 300° C gives a mixture of δ and ζ.[1] If the isothermal ageing temperature is lowered from 300° C, there is a transition from ζ to δ formation at ~ 150° C for the directly quenched specimens. The water-quenched specimens form δ at any ageing temperature between 100 and 300° C.

With the specimens quenched from the liquid state the situation is reversed to a certain extent. The method where numerous small particles impact on a copper plate gives the γ phase, the decomposition of which starts with the formation of δ at all ageing temperatures. The other technique gives a disc which probably consists of already partially decomposed γ. X-ray-diffraction patterns taken from such specimens show diffuse bands at places where ζ lines are expected. On ageing these specimens at 100° C, the ζ phase forms after < 15 min, in contrast with the more rapidly quenched specimens where δ appears only after ageing for 1 h. The ability of the relatively slowly splat-cooled specimens to form ζ disappears at higher temperatures, e.g. the transformation at 300° C is the same as for the rapidly splat-cooled or water-quenched specimens.

While the formation of δ as a transition phase can be considered as normal, the occurrence of ζ is less expected because this phase is stable only at much higher temperatures. As X-ray examinations provided no clue as to why ζ should form instead of δ it was decided to seek further information by means of electron microscopy. It seemed appropriate to compare the transformation of specimens prepared by the two different splat-cooling methods, since the δ phase was obtained in the more rapidly cooled specimens and the ζ phase in those less rapidly cooled.

Fig. 2(*a*) shows a thin region of a specimen obtained by the rapid splat-cooling technique. Besides the lamellae, which may be martensite needles, several dislocations can be seen. Moreover, numerous particles of < 50 Å dia. are visible. Selected-area diffraction patterns show that besides the γ reflections, there are other spots that can be indexed in accord with the δ phase. Dark-field images show that these reflections come from the small particles. Fig. 2(*b*) shows the same part of the foil after ageing for 2 h at 100° C; new precipitates have formed. In this grain they nucleated primarily on the dislocations and grain boundaries; in others they nucleated in places that contained no visible defects. Probably these new precipitates consist also of the δ phase because their appearance coincides with the δ lines becoming visible on the X-ray patterns. After ageing for 2 h the small particles have grown while their number decreased.

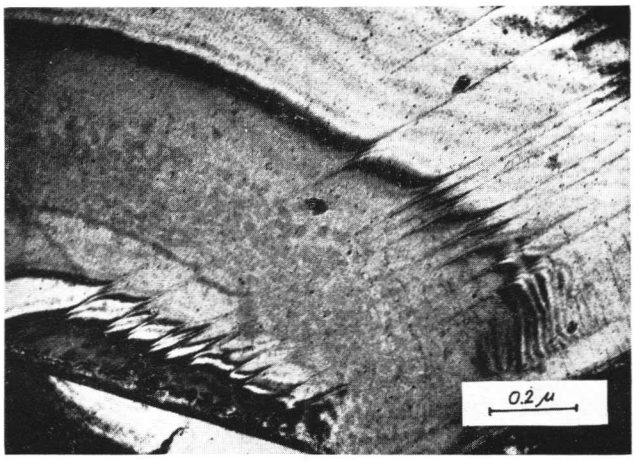

(*a*)

(*b*)

Fig. 2(a) Rapidly splat-cooled specimen showing plates (possibly martensite), dislocations (lower right corner), and very small precipitate (mottled background); (b) as (a) but aged for 2h at 100° C.

The transformation at thin places in specimens prepared by the slower splat-cooling method did not differ from the transformation at thin places in specimens prepared by the preceding method. This can be explained by supposing that the thin regions are cooled at a comparable rate. A splat-cooled disc was therefore thinned electrolytically to obtain an image of the bulk material. From contrast effects one could see that again there were many small particles. These particles also give reflections which could be indexed in terms of the δ phase. After ageing the foil for 30 min at 100° C there was no appreciable change, though X-ray diffraction revealed the existence of ζ precipitates. Thus, it is possible that the ζ precipitate forms but remains very small because of the low annealing temperature. Selected-area diffraction is not very useful in this case because of the great similarity of the ζ and δ structures and also because the structure of the ζ phase is not yet thoroughly known. Moreover, because of the lack of a tilting stage good diffraction patterns could not be obtained.

The conclusion that can be drawn from these experiments is that the conditions to obtain ζ are rather critical. The quenching rate has to be high enough to prevent the formation

of δ on passing through the (δ + α) region. On the other hand, the time spent in the higher-temperature range has to be sufficiently long to allow the formation of ζ nuclei. This would explain why no ζ occurs on ageing the most rapidly quenched specimens.

References

1. A. Deruyttere, *Mém. Sci. Rev. Mét.*, 1963, **60**, 359.
2. M. De Bondt and A. Deruyttere, *Acta Met.*, 1967, **15**, 993.
3. P. Predecky, A. W. Mullendore, and N. J. Grant, *Trans. Met. Soc. A.I.M.E.*, 1965, **233**, 1581.
4. P. Pietrokowsky, *Rev. Sci. Instruments*, 1963, **34**, 445.

Research Note

A Study of $\alpha \rightarrow (\alpha+\gamma) \rightarrow \gamma$ Transformations by Heating or Quenching for Binary Fe–Cr Alloys with Compositions in the γ Loop

A. M. Huntz, P. Guiraldenq, M. Aucouturier, and P. Lacombe

The Fe–Cr phase diagram exhibits a " gamma loop " for compositions between 0 and ~ 15 wt.-% Cr. Small amounts of Cr (≤ 7·5 wt.-%) lower the α → γ transformation temperature and large amounts raise this temperature. The morphology and properties of Fe–Cr alloys quenched from the δ temperature range have been studied by Lacoude and Goux.[1]

This paper attempts to classify the different structures obtained either by cooling Fe–Cr alloys from the γ range (1200° C) and tempering at different temperatures in the α range, or by heating a stable α structure in the (α + γ) range and quenching. Radioisotopes and micrographic techniques have been used in this study.

If the alloys are water-quenched from 1200° C, a martensite-type structure is obtained. The alloy content has an influence on this transformation; the higher the Cr content the slower is the quenching rate necessary to obtain this type of structure. On the contrary, with a slow cooling rate from 1200° C (furnace-cooling) a classical, nearly stabilized, ferritic structure is obtained. If the cooling rate is between those two limits, e.g. air-cooling or oil-quenching, or if the martensite structure is tempered in the α temperature range, one can observe different morphologies, intermediate between those usually called massive martensite[2] and equiaxed ferrite.

The usual classification of the cooling structures of Fe alloys into ferrite, equiaxed ferrite, massive martensite, and martensite is based on crystallographic, diffusional, or deformation criteria, but it is sometimes difficult to allocate a given structure to one or other of these classes. Following an idea initially proposed by Smith,[3] we have investigated the structure of the interfaces present in the alloys in greater detail.

A study of radioactive-tracer diffusion in Fe–Cr alloys has shown that preferential diffusion can occur at these interfaces and that this preferential diffusion is a function of the degree of coherency of the interfaces. Fig. 1 reveals that the nature of preferential diffusion can be totally different, depending on the cooling rate and the tempering temperature and time. Fig. 1(*b*) exhibits considerable preferential diffusion in the interfaces of a martensite structure, compared with the ordinary grain-boundary diffusion in a ferritic structure (Fig. 1(*a*)). Fig. 2(*a*) shows more precisely that the structure is strongly orientated, but Fig. 2(*b*) gives evidence that the interfaces are not completely coherent, since preferential diffusion is not so marked as in ordinary grain boundaries (but is also not negligible). The differences in preferential diffusion when the structure is a mixture of martensite-type grains and ferrite-type grains are clearly seen in Fig. 3. Fig. 4 is an example of diffusion in a structure obtained by air-cooling a 9% Cr alloy. When the chromium content of the alloy is low and after long annealing in the α temperature range, the structure (Fig. 5) is that of an equiaxed ferrite with some orientated interfaces. The autoradiograph (Fig. 5(*b*)) shows preferential diffusion in some of these interfaces and can be used to determine their degree of coherency.

In conclusion, the comparison between micrographic and autoradiographic examinations proves that when a phase is developed with strong preferential orientations it does not mean that the boundaries in such phases are coherent. The coherent nature of the interfaces can be strongly modified by tempering. The Fe–Cr alloys used in this study can show a martensitic-type transformation by rapid cooling from the γ phase. However, observations of autoradiographs show that this martensitic phase is unstable and that the structure of the interfaces can be modified even by a short tempering.

The transformation on heating of previously ferritic Fe–Cr alloys has also been studied by micrographic and autoradiographic techniques. The γ crystals developed during annealing in the (α + γ) range are identified after rapid quenching by their martensitic nature. They can also be identified by the fact that the radioisotope ^{59}Fe diffuses much more rapidly in the α phase than in the γ phase.[4,5] After annealing in the (α + γ) range, the γ crystals, where diffusion is slow, are present on the autoradiograph as white fields on the black background of the α matrix. The 14·6% Cr alloy is the most interesting alloy for this study, because of the very large temperature range for coexistence of α and γ phases, with a nearly constant equilibrium α/γ ratio.

The autoradiograph of Fig. 6 shows that the γ crystals (in white on the photograph) appear preferentially at the former α grain boundaries, but some γ crystals can be nucleated inside the grains. For a very short anneal in the (α + γ) range, the γ crystals nucleated first at the grain boundaries of the α matrix are strongly orientated (Fig. 7).

Manuscript received 3 July 1968. Mme A. M. Huntz, Doct. 3e Cycle, M. Aucouturier, Doct. ès Sc., and Professor P. Lacombe, Doct. ès Sc., are at the Centre de Recherches Métallurgiques de l'Ecole des Mines de Paris. P. Guiraldenq, Doct. ès Sc., was with the Compagnie des Ateliers et Forges de la Loire, France, and is now at the Ecole Centrale Lyonnaise, France.

(*a*)

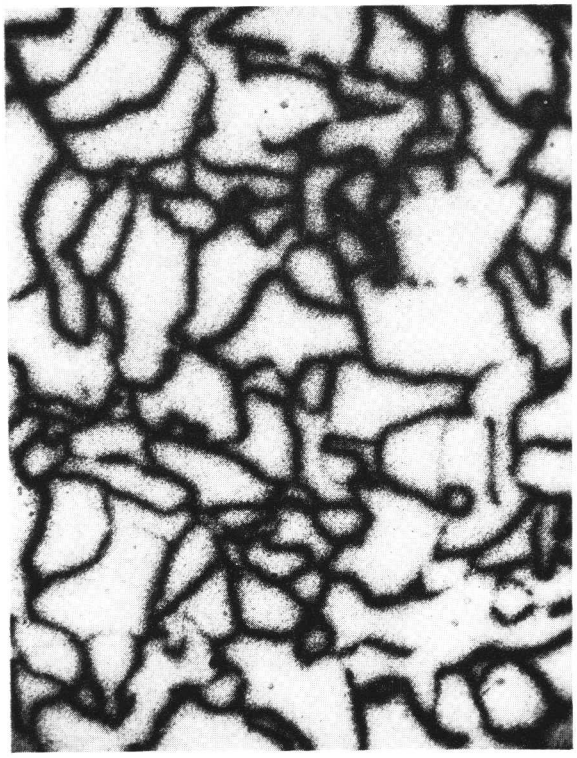

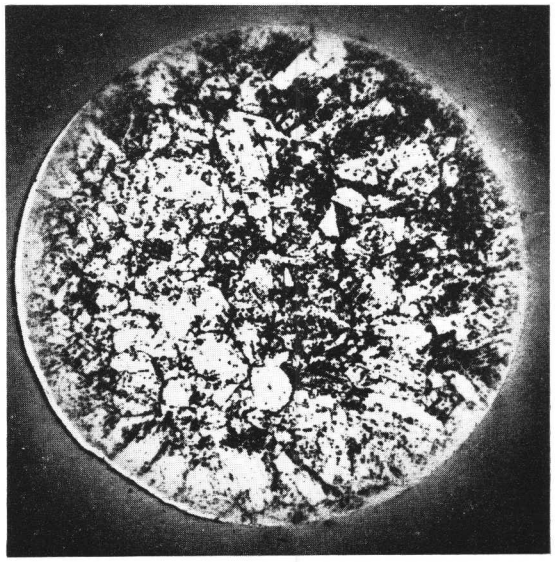

(*b*)

Fig. 1 *Autoradiographs of:* (a) 9% *Cr alloy. Thermal treatment:* 1200° *C, slow cool; diffusion-anneal* 7 *days at* 725° *C.* × 50. (b) 7·8% *Cr alloy. Thermal treatment:* 1200° *C, water-quench; diffusion-anneal* 8 *days at* 700° *C.* × 20.

(*a*)

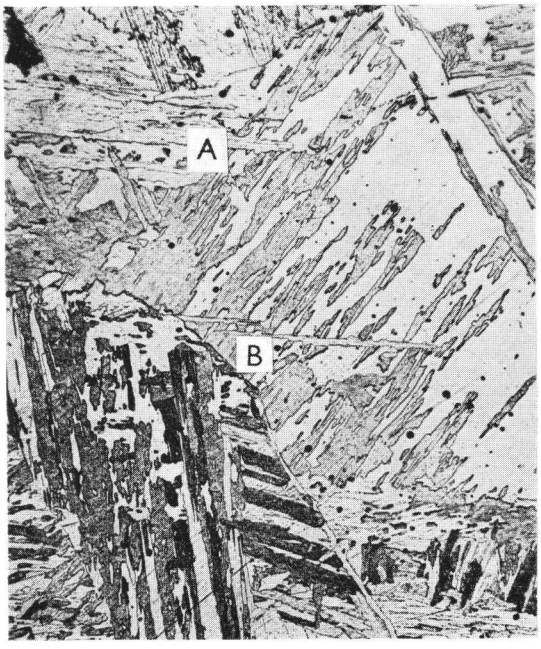

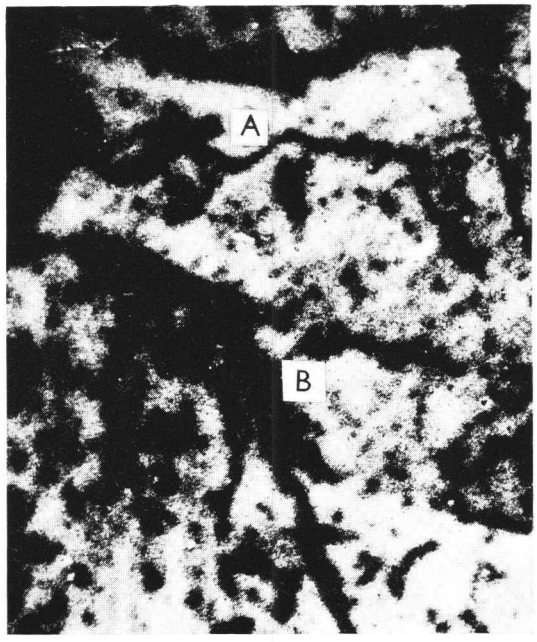

(*b*)

Fig. 2 (a) *Micrograph and* (b) *autoradiograph of a* 7·8% *Cr alloy. Thermal treatment:* 1200° *C, water-quench; diffusion-anneal* 80 *h at* 750° *C.* × 60.

(*a*)

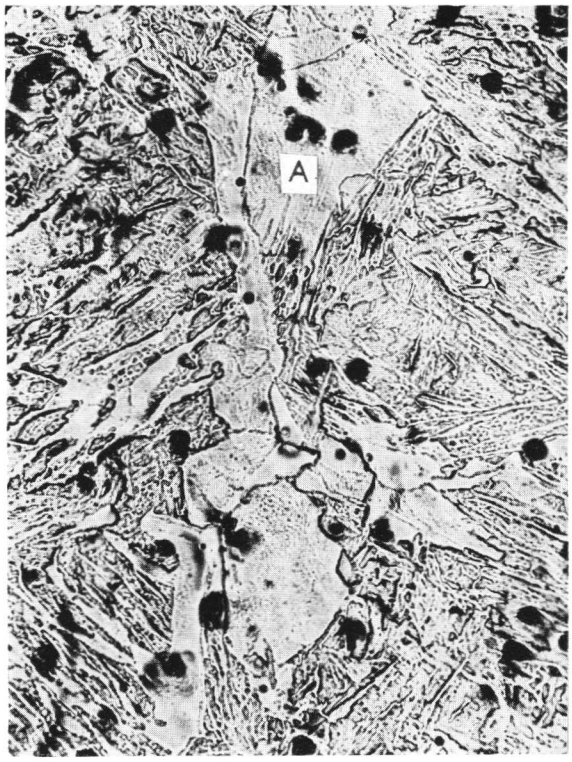

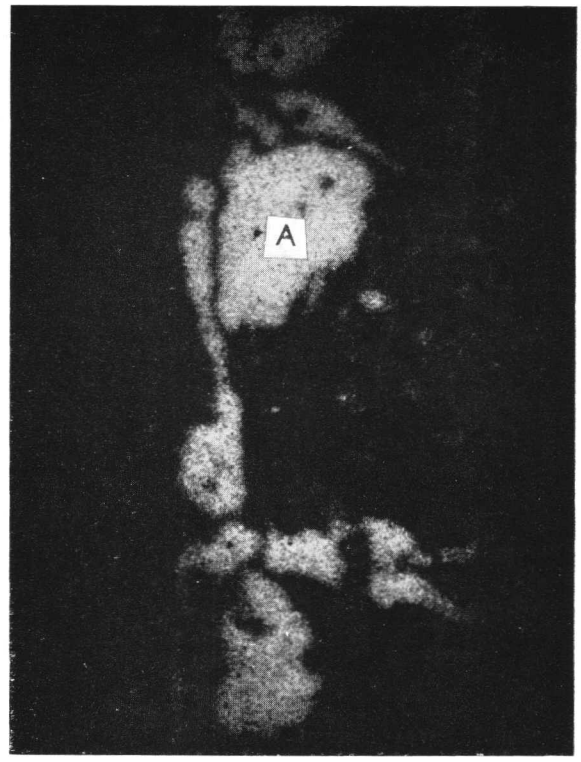

(*b*)

Fig. 3 (a) *Micrograph and* (b) *autoradiograph of a* 7·8% *Cr alloy. Thermal treatment:* 1200° *C, water-quench,* + 24 *h at* 700° *C* + 1 *h at* 1200° *C, furnace-cool; diffusion-anneal* 6 *h at* 740° *C.* × 100.

(*a*)

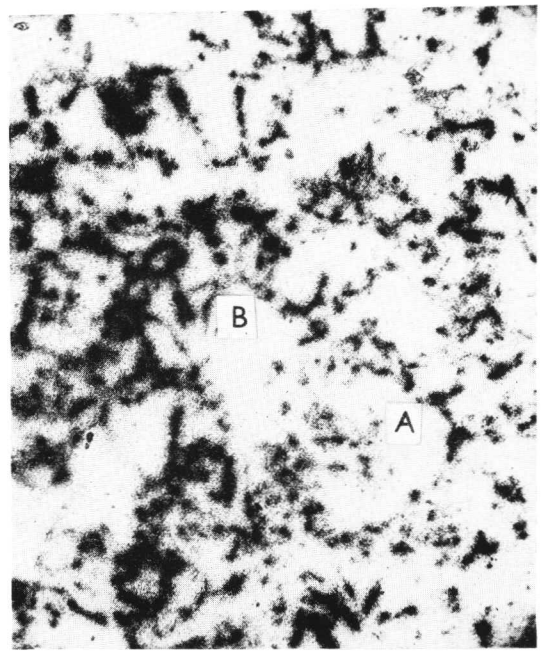

(*b*)

Fig. 4 (a) *Micrograph and* (b) *autoradiograph of a* 9% *Cr alloy. Thermal treatment:* 1200° *C, air-cool; diffusion-anneal* 1·5 *day at* 640° *C.* × 50.

(*a*)

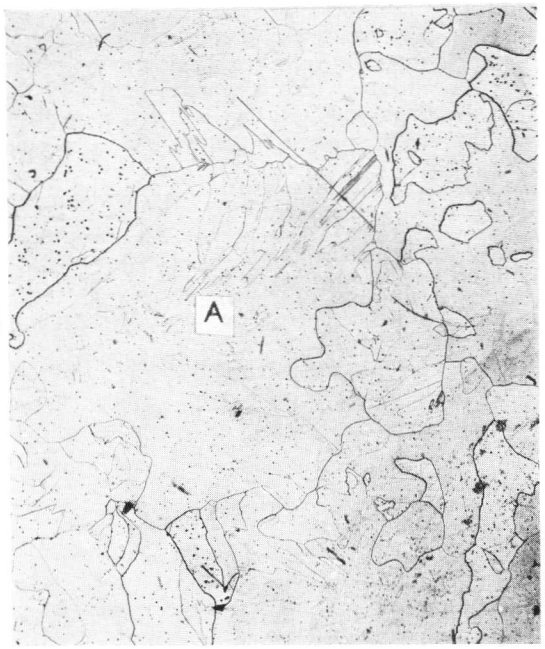

(*b*)

Fig. 5 (a) *Micrograph and* (b) *autoradiograph of a* 3% *Cr alloy. Thermal treatment:* 1400° *C, air-cool; diffusion-treatment* 15 *days at* 652° *C.* × 25.

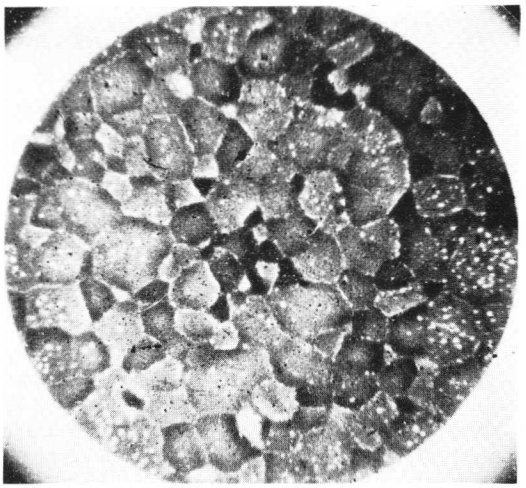

Fig. 6 *Autoradiograph of a* 14·6% *Cr alloy. Initial structure ferrite. Diffusion-anneal* 2 *days at* 1010° *C* ($(\alpha + \gamma)$ *range*). × 8.

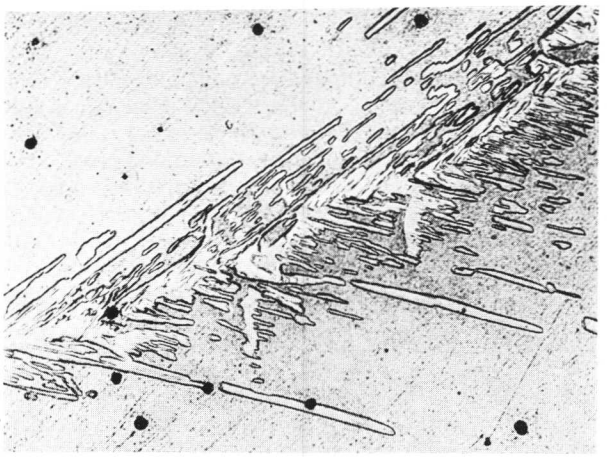

Fig. 7 *Micrograph of a* 14·6% *Cr alloy. Initial structure ferrite. Anneal* 30 *min at* 950° *C* ($(\alpha + \gamma)$ *range*), *water-quench. Orientated nucleation of* γ *crystals.* × 320.

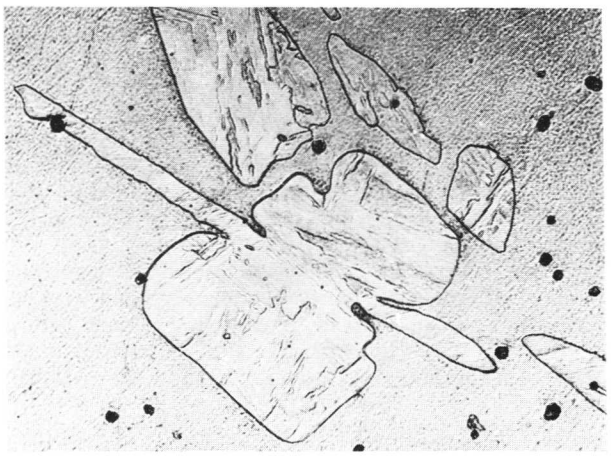

Fig. 8 *Micrograph of a* 14·6% *Cr alloy. Initial structure ferrite. Anneal* 2 *h at* 950° *C* ($(\alpha + \gamma)$ *range*), *water-quench.* × 320.

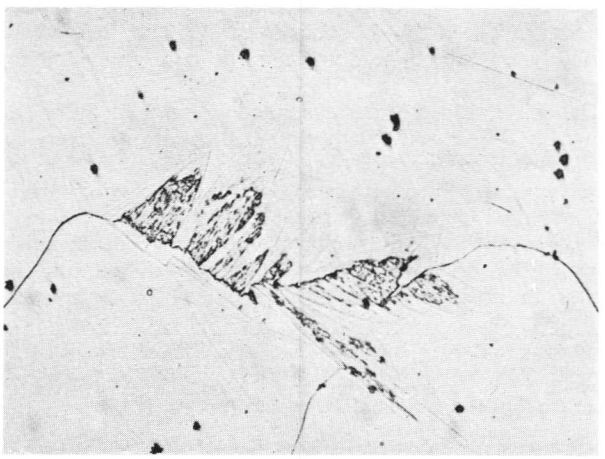

Fig. 9 *Micrograph of a* 3% *Cr alloy. Initial structure ferrite. Anneal* 20 *min at* 866° *C* ($(\alpha + \gamma)$ *range*), *water-quench.* × 320.

Some orientated γ crystals also appear inside the α grains. When annealing is prolonged, the growth of γ crystals tends to become isotropic (Fig. 8).

The kinetics of this phenomenon evidently depends on the α/γ equilibrium ratio, but the successive occurrence of orientated nucleation and growth, then of isotropic growth, is still observed at all temperatures. For lower chromium content, the same phenomena are observed (Fig. 9), but the experimental conditions are much more difficult to optimize.

In Fig. 9 the presence of a ferrite border surrounding the martensite is observed, *inside* the former γ crystals. This phenomenon is related to the carbon content of the alloys and will be described in another study.[6]

In summary, this investigation has shown the martensitic nature of the transformation of Fe–Cr alloys by quenching as well as by heating. The coherent interfaces developed during the quench transformation are not stable and, even after short tempering times, can become quite incoherent. The heating transformation seems to develop in two stages: first a coherent nucleation with a strong orientation relationship between the α and γ phases; then a diffusion-controlled growth with the interfaces between the two phases becoming incoherent.

References

1. M. Lacoude and G. Goux, *Mém. Sci. Rev. Mét.*, 1966, **63**, 805.
2. W. S. Owen, 2nd International Materials Symposium (Univ. California), 1964. J. W. Christian, this vol., p. 129.
3. C. S. Smith, *Trans. Amer. Soc. Metals*, 1953, **45**, 533.
4. P. Guiraldenq, M. Aucouturier, and P. Lacombe, *Mém. Sci. Rev. Mét.*, 1963, **60**, 681.
5. M. Aucouturier, O. P. Ribeiro de Castro, and P. Lacombe, *ibid.*, 1964, **61**, 543.
6. A. M. Huntz, P. Guiraldenq, M. Aucouturier, and P. Lacombe, *ibid.*, to be published.

Research Note

Electron Microscopy of the Massive Cu–Zn α_m Phase

L. Delaey, B. Hawbolt, and T. B. Massalki

The massive transformation in metals and alloys has recently received much attention. In the Cu–Zn system a detailed study of the kinetics of the $\beta \rightarrow \alpha_m$ reaction has been attempted and some criteria for nucleation and growth have been proposed.[1] Certain aspects of the morphology were also described by Hull and Garwood.[2] In this research note we report some details of the " fine " structure of the α_m product as revealed by transmission electron microscopy.

An alloy of composition Cu–37·6 at.-% Zn was prepared by techniques that have been previously described.[3] Spark-machined slices 0·020 in. thick were heat-treated for 4 min at 875° C and quenched into a solution of 16% NaOH maintained at 10° C. This produced a complete transformation to the α_m structure. Thin specimens for transmission microscopy were obtained, the preparation details being reported elsewhere.[3]

Fig. 1 shows the optical microstructure of the quenched alloy. Some " equilibrium α ", which precipitated on cooling through the $(\alpha + \beta)$ two-phase field, outlines the original β boundary. The α_m/α_m boundaries exhibit both faceted and smoothly contoured sections, and the α_m grains contain numerous twins.

The dense dislocation arrays noted within the α_m phase are shown in Fig. 2. Although a high dislocation density has previously been reported for some Cu–Ga[4] and Fe–Ni[5] massive phases, these have been described as random arrays. The observed characteristic alignment of the dislocations is not consistent with a specific direction. The dislocations seem to lie on certain crystallographic planes and are similar in appearance to those reported by Swann and Nutting[6] for a Cu–37% Zn alloy deformed 5%. While the high dislocation density may have been generated during the transformation to assist transformation volume strains, the alignment could be a consequence of a specific ledge-growth mechanism.[7]

In accordance with the optical metallography, twinning is also a pronounced feature of the internal structure of the massive product. Fig. 3 shows a large twin exhibiting small boundary steps, each step being associated with micro-twinning. The presence of parallel fringe patterns in the α_m phase is not related to the existence of single stacking faults. Although the fringe patterns produced by single stacking faults and by fine twins are similar in appearance, a careful analysis of the observed fringe patterns has established that they are related to the presence of micro-twins; the detailed arguments have been reported in several recent publications.[8,9]

Fig. 4 shows faceted and smoothly curving boundaries between two massive grains. Changes in boundary direction are often associated with the presence of fine twins (A). Aligned dislocations are visible in the dark area of (B) and isolated dislocations are present at the boundary.

Those boundaries that exhibit smooth curvature are thought to be associated with the interaction of two randomly growing, independent growth fronts, whereas the faceted interfaces may have resulted from the interaction of regions growing by a directional ledge-growth mechanism as proposed for some Cu–Ga alloys.[5,6]

Currently, efforts are being concentrated on explaining both the high density and the directional alignment of the dislocation arrays observed in the α_m phase. Investigations have also been initiated to examine the morphology of the α_m/retained-β interfaces by means of transmission electron microscopy.

Manuscript received 3 July 1968. L. Delaey, Dr.rer.nat., is at the Instituut voor Metaalkunde, Universiteit te Leuven, Belgium, B. Hawbolt, Ph.D., and Professor T. B. Massalski, D.Sc., F.Inst.P., are at the Carnegie-Mellon University, Pittsburgh, U.S.A.

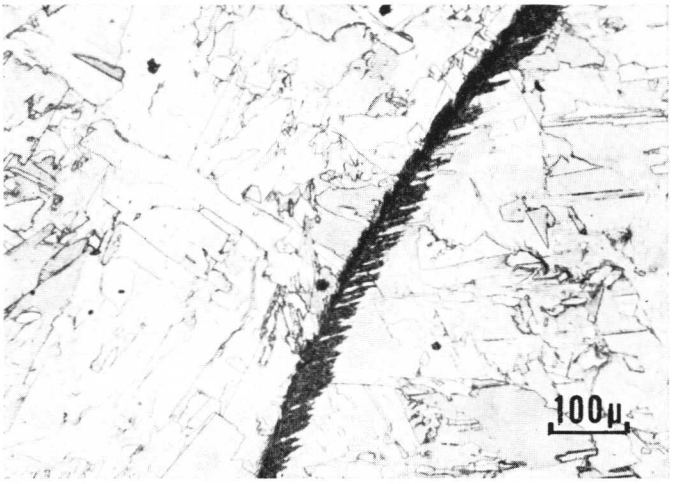

Fig. 1 *Optical microstructure of the quenched Cu–37·6 at.-% Zn alloy showing* α_m *grains and "equilibrium* α*" outlining the prior* β *boundary.*

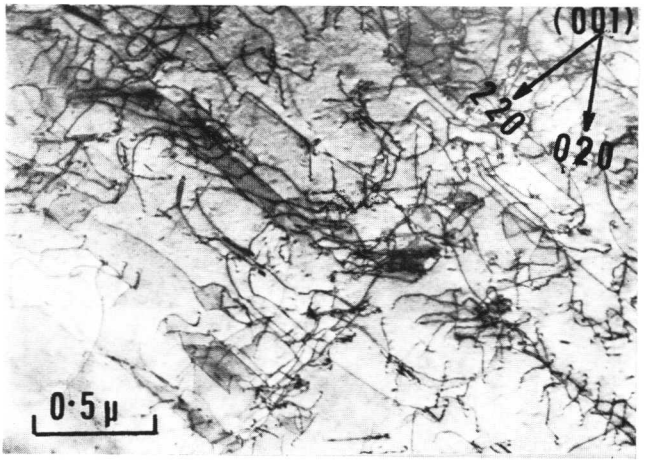

Fig. 2 *Internal structure of the* α_m *phase showing a high dislocation density and a marked alignment of the dislocation arrays.*

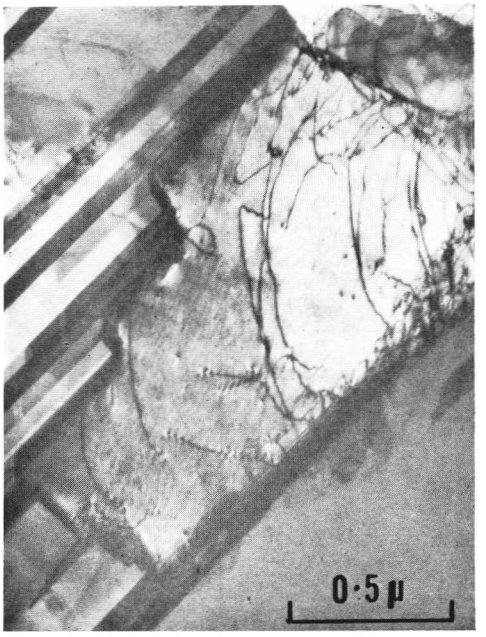

Fig. 3 *Twinned areas in the* α_m *phase showing micro-twins associated with the steps on the boundary of the larger twin.*

References

1. D. A. Karlyn, J. W. Cahn, and M. Cohen, Abstract Bulletin, Institute of Metals Division of Met. Soc. of A.I.M.E., 1967.
2. D. Hull and R. D. Garwood, "The Mechanism of Phase Transformations in Metals" (Monograph and Rep. Series No. 18), p. 219. **1956:** London (Inst. Metals).
3. G. A. Sargent, L. Delaey, and T. B. Massalski, *Acta Met.*, 1968, **16**, 723.
4. K. H. G. Ashbee, L. F. Vassamillet, and T. B. Massalski, *ibid.*, 1967, **15**, 181.
5. W. S. Owen, E. A. Wilson, and T. Bell, "High-Strength Materials" (edited by V. F. Zackay), p. 167. **1965:** New York and London (John Wiley).
6. P. R. Swann and J. Nutting, *J. Inst. Metals*, 1961–62, **50**, 133.
7. H. I. Aaronson, C. Laird, and K. R. Kinsman, *Scripta Met.*, 1968, **2**, 259.
8. L. Delaey, *Physica Status Solidi*, 1968, **25**, 697.
9. L. Delaey, G. A. Sargent, and T. B. Massalski, *Phil. Mag.*, 1968, **17**, 983.

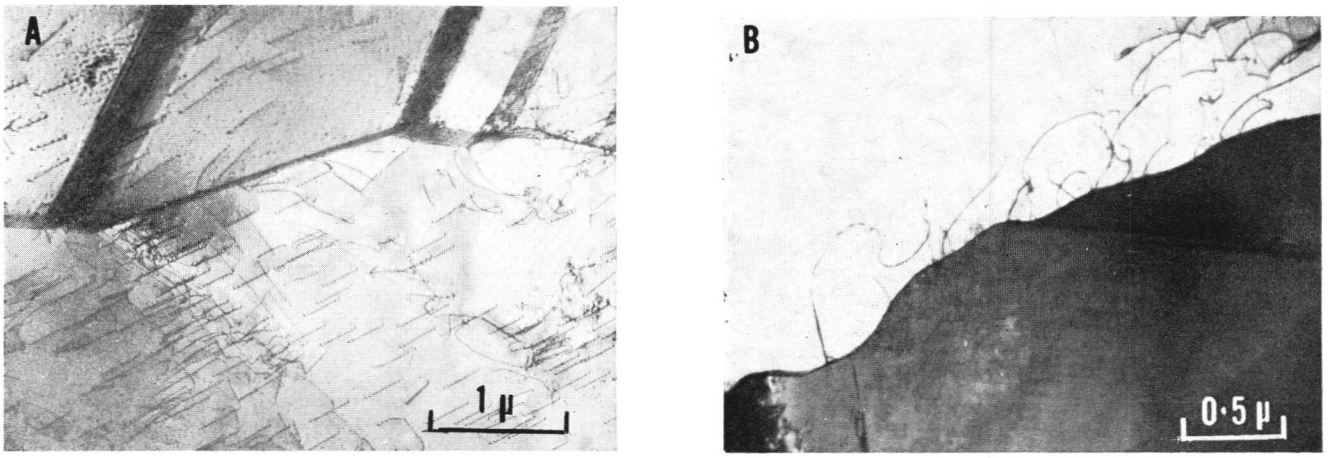

Fig. 4 *Internal structure of the* α_m *phase showing* α_m/α_m *faceted* (A) *and smoothly curving* (B) *boundaries.*

Morphological Studies of the $\beta \rightarrow \zeta^\circ$ and $\beta' \rightarrow \zeta^\circ$ Transformations in Equiatomic AgZn

H. McI. Clark, E. A. Merriman, and C. M. Wayman

The b.c.c. β phase existing above 275° C in the Ag–Zn alloy system undergoes transformation to a complex trigonal phase designated ζ° on slow cooling, and orders to a CsCl structure designated β' on quenching.[1] On upquenching β' to temperatures below 275° C, transformation to ζ° takes place.

Controversy exists at present as to the $\beta \rightarrow \beta'$ ordering temperature, which has not been measured directly.[2–4] This question has been fully discussed,[5] and it is concluded that $T_c(\beta \rightarrow \beta')$ is $\sim$ 240° C. Accordingly, the formation range for ζ° has been divided arbitrarily into a " high-temperature " region, above 240° C, corresponding to the nose of the C curve,[6] and a " low-temperature " region, below 225° C. The ζ° phase is known to have a unique orientation relationship with its parent cubic matrix:[7]

$$[0001]_{\zeta^\circ} \| [111]_{\beta/\beta'} \text{ and } (10\bar{1}0)_{\zeta^\circ} \| (1\bar{1}0)_{\beta/\beta'}$$

Thus, only four crystallographically distinct ζ° variants exist.

The structure of the ζ° phase may be derived from β' by a rearrangement of atoms along the $\langle 111 \rangle_{\beta'}$ direction which is parallel to the ζ° trigonal axis. Atom movements over distances greater than nearest-neighbour interchange are not required, since no composition change is involved in the transformation. The ζ° unit cell contains 9 atoms.[8] The lattice parameters (Å) of the β' and ζ° phases have been reported as:[8]

	β'		ζ°
a	7·7299	$(\sqrt{6}\, a_0)$	7·6360
c	2·7329	$\left(\frac{\sqrt{3}}{2} a_0\right)$	2·8197

$$\frac{V_{\zeta^\circ} - V_{\beta'}}{V_{\beta'}} = +0{\cdot}68\% \qquad \frac{c_{\zeta^\circ} - c_{\beta'}}{c_{\beta'}} = +3{\cdot}1\%$$

$$\frac{a_{\zeta^\circ} - a_{\beta'}}{a_{\beta'}} = -1{\cdot}21\%$$

Thus, the lattice transformation from β' to ζ° (at 20° C) involves an increase in length along $[111]_{\beta'}$ (parallel to $[0001]_{\zeta^\circ}$) and a contraction normal to this direction. Measurements of the length change along $[111]_{\beta'} \| [0001]_{\zeta^\circ}$ have been made, and compared with the length change expected theoretically.[9] For ζ° particles formed in the bulk, the dimensional changes associated with the lattice transformation must be accommodated by elastic and plastic deformation.[9]

Single-crystal disc specimens from a rod of composition 49·5 at.-% Zn were cut by spark-machining to expose faces with orientations (100), (110), and $(111)_{\beta'}$. These specimens were quenched from a salt bath at 350° C, mechanically polished, and then electropolished in reagent-grade phosphoric acid. The C-curve data of Zirinsky[6] indicate that at 140° C nucleation occurs after $\sim$ 10 min; the transformation is complete after $\sim$ 200 min. A partially transformed specimen of orientation $(001)_{\beta'}$ is shown in Fig. 1. Regular star-shaped particles of the type described earlier by Weerts[7] are seen. Each particle typically contains more than one ζ° variant, and shows four-fold morphological symmetry. The c axis of each variant is equally inclined to the specimen

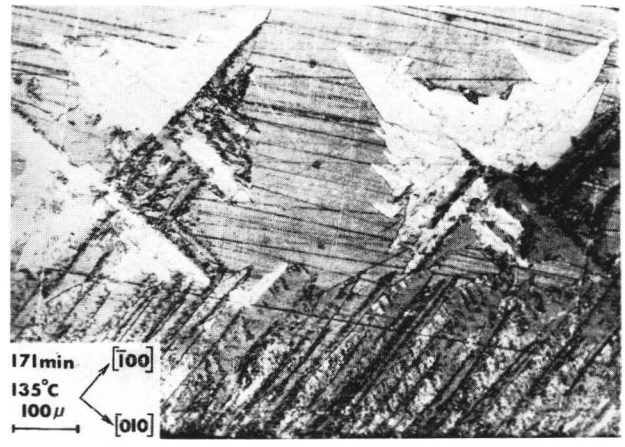

Fig. 1 $(001)_{\beta'}$ *section showing interior* ζ° *particles and preferential surface growth of* ζ° *along* $[\bar{1}00]_{\beta'}$.

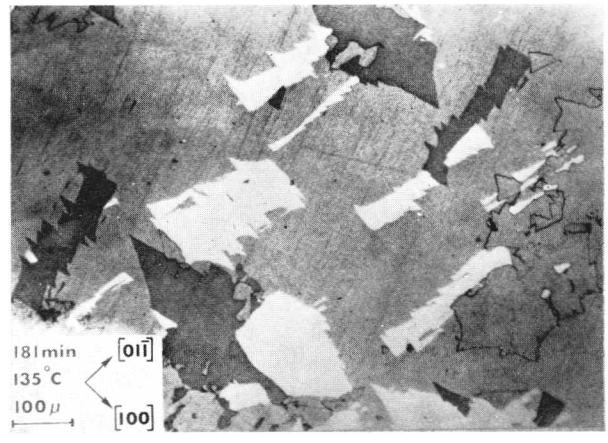

Fig. 2 $(011)_{\beta'}$ *section showing* ζ° *of two different morphologies.*

Manuscript received 3 July 1968. E. A. Merriman and C. M. Wayman are at the University of Illinois, Urbana, Ill., U.S.A., where the work was carried out. H. McI. Clark, B.Sc., Ph.D., is now at the University of Connecticut.

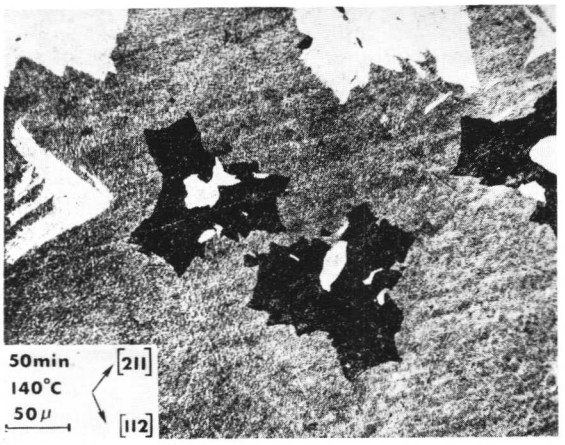

Fig. 3 $(111)_{\beta'}$ *section showing* 3*-fold and chevron-shaped* ζ° *variants.*

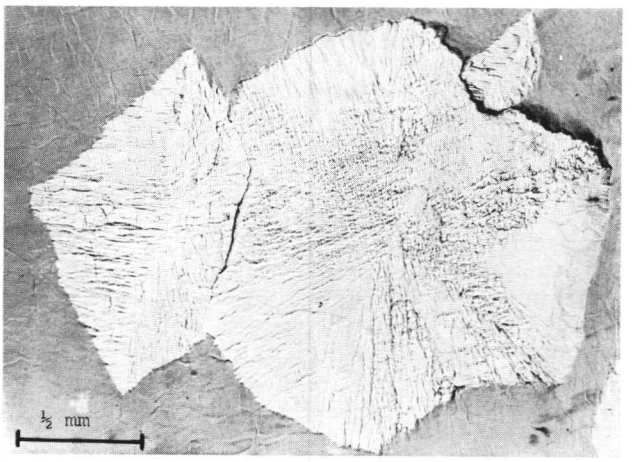

Fig. 5 ζ° *particles grown at* 265° *C on* $(111)_{\beta}$ *surface. Unetched.*

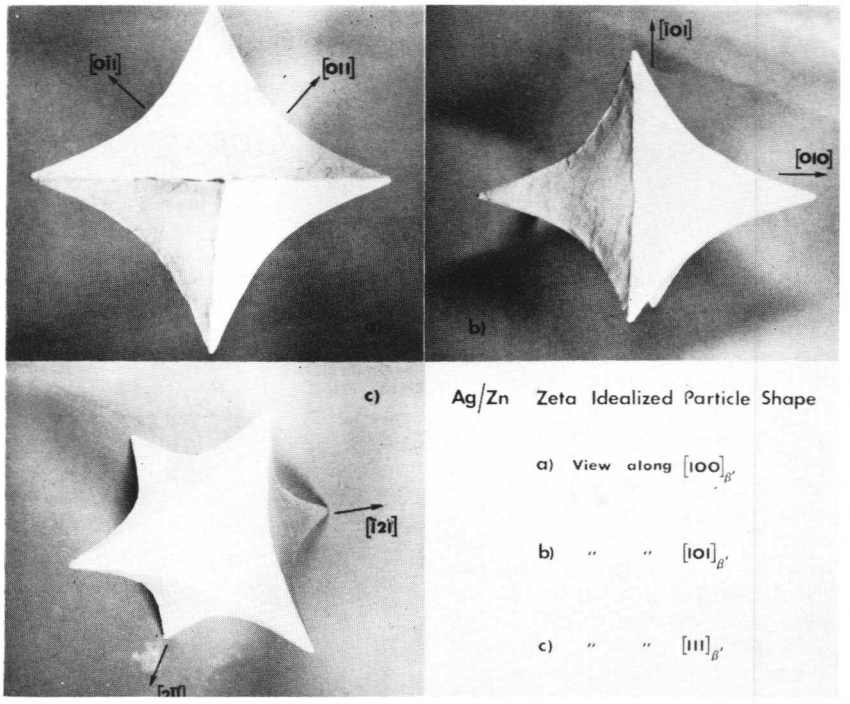

Fig. 4 *Idealized morphology of* ζ° *particles formed from* β′.

surface normal in the $(001)_{\beta'}$ orientation. The lower part of the micrograph shows ζ° nucleated at the free surface growing along $[\bar{1}00]_{\beta'}$. Such surface nucleation always occurred before nucleation in the bulk, independent of the manner of surface preparation. A $(011)_{\beta'}$ surface is shown in Fig. 2. Particles having the *c* axis in the surface are light and dark and show four-fold symmetry; particles with the *c* axis at 35·2° to the specimen surface normal are grey. Particles formed on a $(111)_{\beta'}$ surface are of two shapes; those particles with the *c*-axis normal to the surface appear darkly etched (Fig. 3), and show three-fold symmetry, while the remaining three variants all exhibit the same chevron shape. The appearance of ζ° particles in various sections is rationalized in terms of the idealized form shown in Fig. 4. This is a simplified model of the ζ° morphology at low temperatures. The asymmetry observed in the $(110)_{\beta'}$ sections is accounted for by the fact that the particle dimension parallel to the *c* axis is the smallest, and outgrowths from the faces form along $\langle 100\rangle_{\beta'}$ directions (Fig. 1). It is clear that this shape can be derived from a cube by making $\langle 100\rangle$ and $\langle 111\rangle$, respectively, the largest and smallest dimensions.

Particles formed at high temperature on a $(111)_{\beta}$ surface (i.e., from a disordered matrix) are shown in Fig. 5. The large particle has its *c* axis normal to the surface (the smaller diamond-shaped particles have their *c* axes inclined at 70·5° to the surface normal). These particles have the form of two obtuse-angle circular cones joined at the base, i.e., on the $(0001)_{\zeta}$° plane. Further, these particles always grow as single variants during the " high-temperature " transformation.

The ζ° morphology clearly depends on its formation temperature. The transition region between one morphology and

the other has been shown to be at ~ 230° C.[5] At this temperature the cubic matrix should have a long range-order parameter of ~ 0·5. Above this temperature, accommodation of the shape change involved in the lattice transformation should be relatively easy, since cross-slip either in a b.c.c. matrix or in a CsCl matrix with a small degree of long-range order is relatively easy. However, as the degree of long-range order increases it is to be expected that accommodation of length changes in arbitrary directions in the matrix will become more and more difficult. But growth in the $\langle 100 \rangle_{\beta'}$ directions at low temperature can be accommodated most easily because of the symmetrical arrangement of $(110)_{\beta'}$ slip planes about $[100]_{\beta'}$. The shape changes involved at low temperature can be made more symmetrical by the growth of more than one $\zeta°$ variant in a given particle, as observed.

It is concluded therefore that a primary influence on the morphology of $\zeta°$ is the ability of the matrix to accommodate the length changes associated with the lattice transformation. Of secondary importance, and leading to small asymmetries in growth direction, is the trigonal structure of the $\zeta°$ phase. These conclusions are also supported by work on the effect of compressive stress on the transformation.[9]

References

1. M. Hansen and K. Anderko, " Constitution of Binary Alloys ". **1958:** New York and London (McGraw-Hill).
2. L. Muldawer, *J. Appl. Physics,* 1951, **22,** 663.
3. J. P. Abriata, A. Cabo, and J. Kittl, *Scripta Met.,* 1968, **1,** 41.
4. M. E. Brookes and R. W. Smith, *Trans. Met. Soc. A.I.M.E.,* 1968, **242,** 31.
5. H. McI. Clark, E. A. Merriman, and C. M. Wayman, *Acta Met.,* to be published.
6. S. Zirinsky, M.S.Thesis, Columbia Univ., **1949.**
7. J. Weerts, *Z. Metallkunde,* 1932, **11,** 265.
8. I. G. Edmunds and M. M. Qurashi, *Acta Cryst.,* 1951, **4,** 417.
9. A. Chaudhuri, H. McI. Clark, and C. M. Wayman, *Acta Met.,* to be published.

Research Note

A Phase-Interface Reaction during the Interdiffusion of Chromium and Tungsten

F. J. A. den Broeder

The phase diagram of the b.c.c. Cr–W system shows a simple miscibility gap[1] (Fig. 1). In view of the limited mutual solubility below ~ 1500°C and the great difference between the melting points of the components (and hence in their atomic mobility), it seemed interesting to investigate the way in which interdiffusion between chromium and tungsten leads to a homogeneous alloy in the stable region of the phase diagram, starting from appropriate amounts of both metals.

This was done by heating at 1250°C a diffusion couple consisting of a 0·6-mm-thick single-crystal W rod electroplated with a thin Cr layer. The Cr deposit was so thin (~ 10 μm) that a beam of Cr K_α X-rays penetrated the layer and part of the underlying W, so that the whole diffusion zone gave rise to diffraction and became "visible" in one diffraction pattern. The interdiffusion process was thus followed in its consecutive stages by Straumanis exposures, the rod being rotated perpendicular to the beam. Because the 211 reflections are the most sensitive to changes in lattice spacing, only these are shown in Fig. 2.

Fig. 2(*a*) was obtained after a low-temperature treatment to relieve the stress and to recrystallize the Cr, and shows, before the beginning of the interdiffusion, diffraction spots from the W single crystal and a diffraction ring from the polycrystalline Cr. After 11 h diffusion, Fig. 2(*b*) demonstrates that W has diffused into the Cr, while no Cr has diffused into W, and also that a secondary recrystallization of the Cr has occurred to form a crystal that is in parallel orientation to the W crystal. The former effect can be explained by the large difference in the concentration and mobility of vacancies in Cr (low melting point) and in W (high melting point).

It must be emphasized that W atoms do not diffuse intrinsically faster than Cr atoms,[2] since Kirkendall-effect[3] experiments have shown the opposite to be the case.[4]

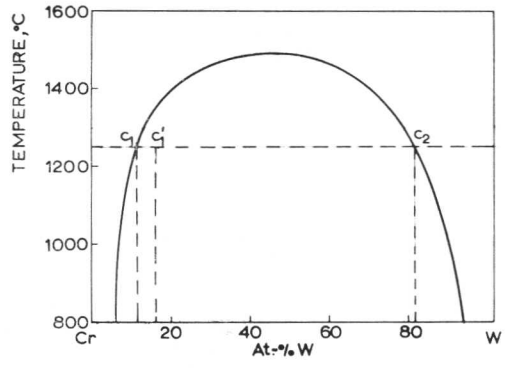

Fig. 1 Miscibility gap in the Cr–W system; c_1 and c^2 are equilibrium compositions at 1250°C.

After 20 h diffusion (Fig. 2(*c*)) the couple consists of pure W and a Cr–W alloy, saturated with W (composition c_1 in Fig. 1), between which a small amount of a W-rich equilibrium phase (composition c_2 in Fig. 1) has just been formed (see solid arrow*), epitaxially to the W. This phase has grown after 25 h (Fig. 2(*d*)) and it is noticeable that its reflections are separated from those of pure W. This fact and the observation that the time necessary to develop this phase increased very much with the thickness of the initial Cr layer, suggest that the phase has developed "discontinuously" by an interface reaction between the saturated Cr-rich phase and pure W. After 38 h the reaction has been completed at the total expense of the Cr-rich phase (Fig. 2(*e*)). From this stage on the couple merely consists of pure W and a W-rich phase, between which

Manuscript received 3 July 1968. F. J. A. den Broeder, Ir., is working for the Dutch Foundation for Fundamental Research on Matter at the Laboratory for Physical Chemistry of the Solid State, Technological University, Delft, The Netherlands.

* The broken arrow points to an irrelevant Cr K_β 220_W reflection.

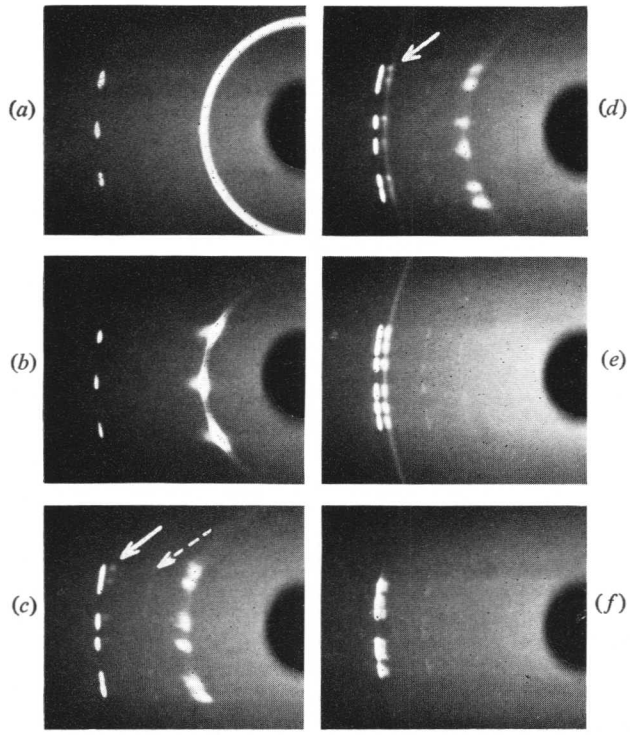

Fig. 2 Cr K$_\alpha$ X-ray diffraction patterns, showing the 211 reflections from a Cr–W diffusion couple after heating at 1250°C for: (a) *0 h;* (b) *11 h;* (c) *20 h;* (d) *25 h;* (e) *38 h;* (f) *60 h.*

the ultimate W-rich alloy is formed by normal diffusion (Fig. 2(*f*)).

Bearing in mind that the gradient of the chemical potential of a component is the driving force for its diffusion,[2] Fig. 3 represents the variation of this quantity with composition for both components at 1250°C in a regular binary system *A–B*, having a miscibility gap with a critical point at 1500°C.

When *A* and *B* dissolve into each other at the same rate, then μ^B rises in the *A*-rich part (μ^A falls), and falls in the *B*-rich part of the couple (where μ^A rises) until equilibrium between the two phases occurs when $\mu_1^B = \mu_2^B$ and $\mu_1^A = \mu_2^A$ at compositions c_1 and c_2.

However, when *B* is tungsten and *A* is chromium, the X-ray pattern Fig. 2(*b*) indicates that only W dissolves in Cr, the W itself remaining pure (though there is a solubility for Cr in W). So μ^W rises in the Cr-rich part of the couple but remains constant in pure W. When so much W has dissolved in the Cr-rich alloy that the equilibrium composition c_1 has been attained, there still exists a gradient of μ^W from pure W to this alloy. Thus, more W may diffuse into this phase, making an interface layer supersaturated with respect to W (composition

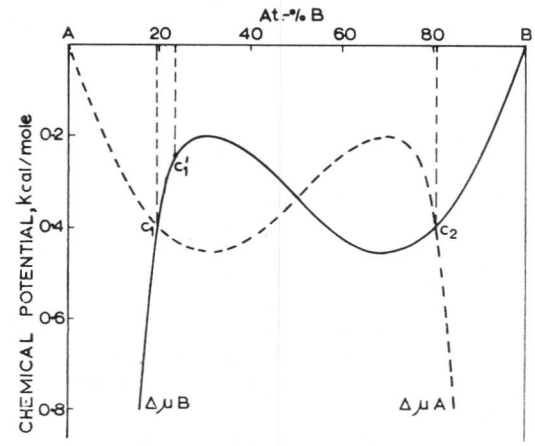

Fig. 3 Calculated variation of the (relative) chemical potential of both components at 1250°C in a regular system A-B with a critical point of the miscibility gap at 1500°C.

c_1'; cf. also Fig. 1). This supersaturation will arise when there exist nucleation difficulties in precipitating the W-rich phase (composition c_2). Actually the presence of a supersaturated Cr-rich phase was visible on an X-ray pattern taken in the course of a similar diffusion experiment (not shown here). After nucleation, decomposition into the two equilibrium phases will occur and this reaction goes on until the Cr-rich phase has been completely converted into the W-rich phase.

A close examination of Fig. 2(*c*) reveals striking support for the proposition that the W-rich phase has been formed after nucleation at the phase interface. This pattern has been obtained very shortly after the first formation of this phase. Its reflections are not of the same intensity above and below the equator. Evidently this phase has nucleated and grown a small amount on one side of the square W rod producing a 211 reflection above the equator, but has probably not yet nucleated on the opposite side of the rod, which accounts for the absence of the corresponding $\bar{2}\bar{1}\bar{1}$ reflection below the equator.

Acknowledgement

The author is much indebted to Professor Dr. W. G. Burgers, in whose laboratory this investigation was carried out, and to Professor Dr. J. L. Meijering for their constant interest in the work and for many useful discussions.

References

1. M. Hansen and K. Anderko, "Constitution of Binary Alloys", **1958:** New York and London (McGraw-Hill).
2. L. S. Darken, *Trans. Amer. Inst. Min. Met. Eng.*, 1948, **175**, 184.
3. A. D. Smigelskas and E. O. Kirkendall, *ibid.*, 1947, **171**, 130.
4. F. J. A. den Broeder, to be published.

Discussion

Dr. A. Bar-Or (Israel Atomic Energy Commission, Negev, Israel): I agree with Professor Hillert in his conclusion that volume diffusion is not rate-controlling for discontinuous precipitation, but I do not agree with him that it does not occur near the transformation temperature. We have results that disprove this.

Professor M. Hillert (Royal Institute of Technology, Stockholm, Sweden): I have to accept your experimental results. I should be interested to see how close to the solubility limit you have obtained discontinuous precipitation.

Dr. H. I. Aaronson (Ford Motor Co. Research Laboratories, Dearborn, U.S.A.): Would Professor Hillert please draw out the width of the interface boundary relative to the width of the concentration profile as a function of undercooling, for example?

Professor Hillert: This information is implicit in Fig. 31 of my paper, since a decrease in temperature has the same effect as an increase in growth rate.

Dr. Aaronson: Is the solute spike wholly contained within the grain boundary for the case of iron–carbon–X?

Professor HILLERT: There is one spike ahead of carbon wholly in the γ phase and there is one spike inside the boundary.

Dr. AARONSON: Under all conditions of undercooling?

Professor HILLERT: Yes, except during a martensitic or massive transformation. I have a comment to make on Professor Turnbull's paper. The microstructure shown in his Fig. 1 very much resembles the structure we obtained in the pearlite colony that we polished right through, finding that all the lamellae were interconnected. The similarity is really remarkable, so I am surprised to hear that he does not find that the lamellae are connected.

Professor D. TURNBULL (Harvard University, U.S.A.): We have not proved this by sectioning, but we do find, in the early stages, many widely separated plates in a particular habit lying on the boundary. Unless there is a connection along the boundary initially it seems to me that they could not be connected. We have been carrying out some work on dissolving the matrix away from the lamellae, which can easily be done with a hydrogen peroxide/acetic acid solution, and we get disintegration into separate plates. It is possible, of course, that in the dissolution process tenuous connections between the plates were actually broken, but the plates were not attacked chemically or even etched by the solution. A solidified Pb–Sn eutectic structure was not disintegrated by the solution, though almost all the lead was dissolved away. We conclude that the precipitated tin lamellae in a cell are not extensively connected but tenuous connections are not ruled out.

Dr. V. A. PHILLIPS (General Electric Research Laboratories Schenectady, U.S.A.): Regarding Professor Hillert's paper, I would like to say that discontinuous precipitation is extremely common in precipitation systems. In fact, I showed an example in my paper on Cu–Ni–Co, where it is competitive with coherent precipitation in the grains. In this case part of the driving force is the re-solution of these very fine precipitates to form coarse lamellae, with a consequent lowering of the total interfacial energy. It would be very interesting to consider this as an additional case.

Dr. AARONSON: As Professor Turnbull showed long ago, low-temperature growth in Pb–Sn can occur only by a cellular reaction. If an interfacial energy balance cannot be achieved around the particle, the grain boundary will be in contact with the particle only very briefly. However, if as a result of the crystallography of the particle relative to the boundary a balance can eventually be achieved, then growth will continue.

Dr. R. D. DOHERTY (University of Sussex): I am a little curious regarding the suggestion by Williams *et al.* that the condition for cementite spreading on the α/γ interface is that the interfacial energy of the α/Fe_3C interface should be less than that of α/γ. Surely, there should be three terms in the equation. There are three interfaces—α/Fe_3C, α/γ, and Fe_3C/γ. In order to spread, I should have thought that the energy of the α/γ interface had to be greater than the sum of the other two.

Professor J. W. CHRISTIAN (University of Oxford): It seems to me that Dr. Doherty is right. If you assume a virtual displacement of the boundary to one side you change all three interfacial areas.

Dr. S. G. GLOVER (University of Birmingham) (*written reply*): Dr. Doherty is, of course, quite correct in that there are three terms in the balance of interfacial energies when a particle of a new phase forms at the boundary between two existing ones. To explain the use of only two energies, we refer to Fig. D.VI.1 which is taken from Ref. (3) of our paper. This shows a particle of cementite forming at the interface of proeutectoid ferrite and austenite; this interface is assumed rigid, while that between the growing cementite and the austenite is mobile. In other words, we regard the cementite as a fluid drop on a rigid substrate. Our justification for this is quite simply that, in the Fe–C–Mn alloy studied, for $\varphi < 90°$ the cementite spread as a film, whereas for $\varphi > 90°$ it did not. Whether for a particular composition and temperature φ was $>$ or $< 90°$ was established in the following way: for $\varphi < 90°$ (spreading condition) $\sigma^{\alpha\gamma} > \sigma^{\alpha cem}$ and hence $\sigma^{\alpha\gamma}/\sigma^{\alpha\alpha} > \sigma^{\alpha cem}/\sigma^{\alpha\alpha}$. The ratios in the latter inequality were determined from dihedral-angle measurements on well-annealed specimens.

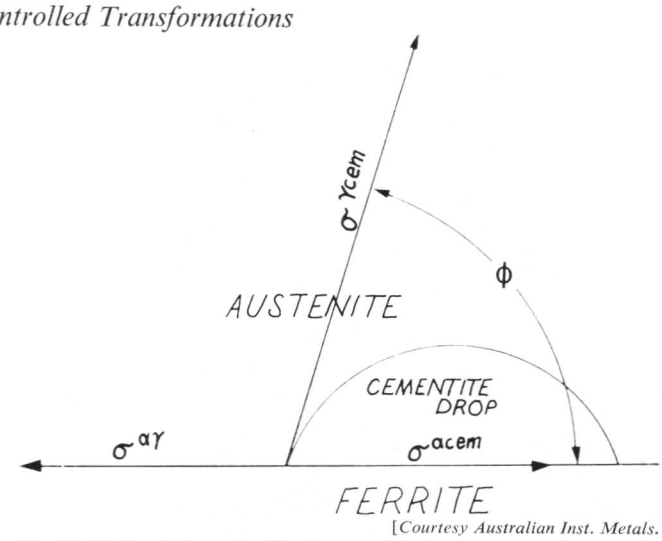

[*Courtesy Australian Inst. Metals.*

Fig. D.VI.1 *Schematic illustration of cementite forming at an* α/γ *interface in steel.* $\sigma^{\alpha\gamma}$, $\sigma^{\gamma cem}$, *and* $\sigma^{\alpha cem}$ *represent the interfacial energies.* (Glover.)

Professor HILLERT: I would like to raise a question. In Fe–Mn–C alloys you found that these granular structures were formed instead of the lamellar structures under conditions where the wetting effect existed. Was there any lamellar structure at all?

Dr. GLOVER: Yes, there was some.

Professor HILLERT: If that is the case, how can your point be valid?

Dr. GLOVER: The lamellar structure forms from a film that is already present. First of all, a film of cementite spreads across the α/γ interface; this interface becomes unstable and the pearlite grows from it. We have specimens where the intergranular film and the pearlite are connected right through the specimen. Thus, each colony of pearlite appears to be linked to all the other colonies in the specimen by the cementite film, where there is degeneracy and where the cementite can spread. So the fact that pearlite is present really does not come into the argument.

Mr. J. DARBYSHIRE (Central Electricity Research Laboratories, Leatherhead): I would like to ask Dr. Slattery what justification he has for using Ham's treatment of precipitation kinetics for the $\beta \rightarrow \alpha$ phase transformation. Surely Ham's treatment is applicable only to the growth of very small precipitate particles.

Dr. G. SLATTERY (U.K.A.E.A., Springfields): We were following the work of Burke* who comes to conclusions very similar to those of Ham. All we were setting out to show was that the curves that we had drawn were linear in a certain

* P. H. Dixon and J. Burke, *Atomic Energy Research Estab. Rep.* **(4431)**, 1964.

region. This, in fact, was the case, up to 50% of the transformation. I think it would be unwise, as you suggest, to apply the Ham theory too rigorously.

Dr. A. BAR-OR (*written discussion*): White* has determined n values in U–Cr alloys from dilatometric measurements and found $n = 4$ below 530° C, $n = 5$ above 580° C. The profound effect of molybdenum on n, as reported by Haberlin and Slattery, suggests that to rely on the values of n for the interpretation of the mechanism of this transformation is extremely difficult.

Professor J. BURKE (University of Swansea): Can I address two questions to Dr. Bar-Or? First, concerning his mechanism for the martensite plates, did he find any variation in the growth rates from plate to plate and within the same plate? We tried a similar experiment at Liverpool some years ago but we had to give it up because the results were so scattered. I should also like to ask about the bainite region. Does he not find any structure that resembles Haberlin and Slattery's Fig. 4? In other words, did he discover any evidence that there is a phase separation after the formation of the α crystal structure?

Dr. BAR-OR: The simple answer to the question about the growth of martensite is carbon. If you do not have carbon, the needles grow very nicely. If carbon is present, as in your experiments, they do not.

As regards the question about bainite, we did not possess an electron microscope until recently but we now intend to look into the structure of the bainite.

Mr. J. WOODHEAD (University of Sheffield): I am a little puzzled by Fig. 2(*a*) of Dr. Bar-Or's paper, when he says that the growth rate of pearlite remains constant even though the interlamellar spacing changes. I should like to know what evidence shows that the interlamellar spacing alters. You are looking at a two-dimensional section; it is quite conceivable that the spacing does not change.

Dr. BAR-OR: I am really more happy about Fig. 2(*b*) than about Fig. 2(*a*) and I think it is clear that you cannot section the lamellae in 2(*b*) in such a way that you will get the observed difference.

Dr. J. KITTL (Argentine Atomic Energy Commission, Buenos Aires, Argentine): I should like to raise another point. You are measuring the velocity of the advance and have assumed λ equal to the interatomic distance but this has nothing to do with it.

Dr. BAR-OR: I am measuring the velocity in one direction.

Dr. KITTL: Referring to Fig. D.VI.2, the value of λ should be taken as the distance x through which the interface advances as a result of atom movements such as y. The distance y is irrelevant.

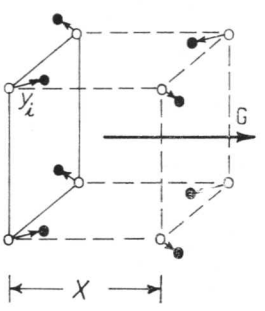

Fig. D.VI.2 *Showing the quantities* x *and* y *for a phase growing in the direction* G. (*Atoms in the initial positions* ○ *and atoms in the final positions* ●.) (Kittl.)

Dr. A. R. ENTWISLE (University of Sheffield): With reference to the paper by Huntz *et al.*, in alloys that have a chromium content corresponding to the minimum in the α–γ transformation temperature, one should be able to transform γ to α without changing the composition. Do you observe any special features of the transformation behaviour in the alloys at that particular composition?

Dr. M. AUCOUTURIER (Ecole Nationale Supérieure des Mines, Paris, France): We are now trying to make the alloy at the exact minimum of the curve. We studied the 7·8% Cr alloy and this already includes an (α + γ) range of ~ 10 degC. It is very difficult, especially in slightly impure alloys, to determine the minimum exactly. This 7·8% Cr alloy has abnormal values for the self-diffusion coefficients of Fe and Cr.

Dr. T. BROOM (Central Electricity Research Laboratories, Leatherhead): I think it would be interesting to know what were the time and temperature of typical radioactive diffusion-anneals.

Dr. AUCOUTURIER: An example is shown in Fig. 4 of our paper, where the diffusion-anneal was at 700° C for several days. Some structural change takes place during the anneal.

Mr. R. D. GARWOOD (University of Cardiff): I wonder whether Dr. Delaey would describe his twins as annealing twins or mechanical twins. When they form is there a change in shape?

Dr. L. DELAEY (University of Leuven, Belgium): No change in shape has been observed on the surface.

Professor J. W. CAHN (Massachusetts Institute of Technology, U.S.A.): One of our research students, Dr. Karlyn, looked for upheavals on the surface and did not find any. These twins therefore must be growth twins. May I summarize his finding briefly? The α′ region on the Cu–Zn phase diagram has a nose at 38·3% Zn. The massive α product does not form at all at any cooling rate if the zinc content exceeds 38·3%. If the zinc content is reduced to 37·5% the transformation occurs so rapidly that it cannot be suppressed by quenching. Karlyn studied 38·0% alloys by quenching β specimens to room temperature to retain the β and then pulse-heating to various temperatures and observing the rate of massive formation. He found that he could not get the massive transformation started at any temperature in the two-phase (α + β) region. It occurred only in the single-phase α region, and then only after a delay time that was longer at high and low temperatures near the two-phase region. Once the transformation commences, it proceeds very rapidly, at 1–3 cm sec^{-1} (Fig.D.VI.3). This rapid growth and delay time are illustrated in the sequence in Fig. D.VI.4(*a*)–(*c*). Note that the massive product has just begun to form at 8 msec, but that it grows rapidly thereafter.

The explanation of these results is really very simple. We believe that α nucleates quite readily at grain boundaries during the quench, but that this α rejects zinc into the surrounding β. Only while the specimen is in the single-phase α region can the α accommodate all the zinc and even assimilate the excess zinc previously rejected. Until the zinc excess is absorbed, the growth cannot be rapid. This accounts for the delay time, and we have here a case where a delay time is in no way attributable to the time to overcome a surface-energy nucleation barrier. Once the massive transformation has started, it is like a polymorphic transformation or

* D. W. White, *Trans. Amer. Inst. Min. Met. Eng.*, 1955, **203**, 1221.

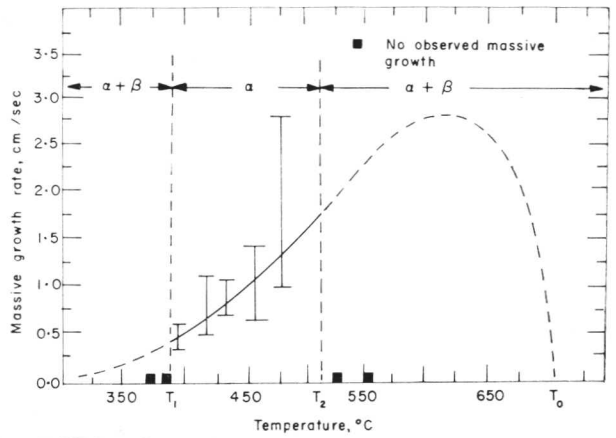

Fig. D.VI.3 *The isothermal growth rate of massive* α *from a Cu–38·0% Zn* β *alloy. The curve is calculated from absolute-reaction-rate theory using an activation free energy of* 15,000 *cal mole*$^{-1}$. *Massive* α *does not start in the two-phase region even though there is a thermodynamic driving force below* T_0. (Cahn.)

recrystallization in a pure metal. The high rate is quite reasonable when compared with experience in recrystallization, considering the temperature and the large driving force. We could fit our growth rate to a well-known rate expression, with the proper pre-exponential and an activation free energy of 15 kcal mole^{-1}.

Mr. GARWOOD: I wonder if any pulse-heating experiments were carried out below the order–disorder temperature for β and, if so, whether the massive α product was disordered?

Professor CAHN: For the compositions studied the order–disorder temperature was ~ 200° C and we could never succeed in getting the massive transformation there.

Dr. BAR-OR: Can I ask Dr. Kittl what is the difference between his calculated and experimental pre-exponential terms.

Dr. KITTL: We used experimental results to obtain the value of the pre-exponential term. We did not calculate this term.

Professor CAHN: Could Dr. Kittl interpret Fig. 2 in his paper?

Dr. KITTL: We consider that the surface upheaval shown in Fig. 2(*c*) is the result of the volume difference between the two phases β′ and ζ°. This is readily transmitted to the free surface and reflects the depth of the ζ° grains.

Mr. M. E. BROOKES (University of Birmingham) (*written discussion*): Dr. Kittl reports activation-energy (*Q*) values for the β′ → ζ° reversion in AgZn which show a rather random variation with composition. It might be expected that, since the number of A-B bonds varies with composition, the tendency to ordering would be maximized at the 1 : 1 atomic ratio, where the greatest number of A-B bonds is present. This is supported by a recent evaluation of mine of *Q* for the reversion, which shows a maximum value of *Q* at the stoichiometric composition and a variation of *Q* with zinc content:

Zn, at.-%	*Q*, kcal mole^{-1}
50	38·9
48	28·6
46	21·9

These values agree with those of Buckley,* who has also shown the monatonic variation of *Q* with composition. Thus, the β → ζ° reversion is order-dependent; the maximum value of *Q* and of the temperature of the reversion† occur at the stoichiometric composition.

Dr. KITTL and Mr. CABO (*written reply*): We do not consider that our *Q* values reveal a "rather random variation with composition"; in fact our Table I gives a variation

* J. I. Buckley (Brunel University), private communication.

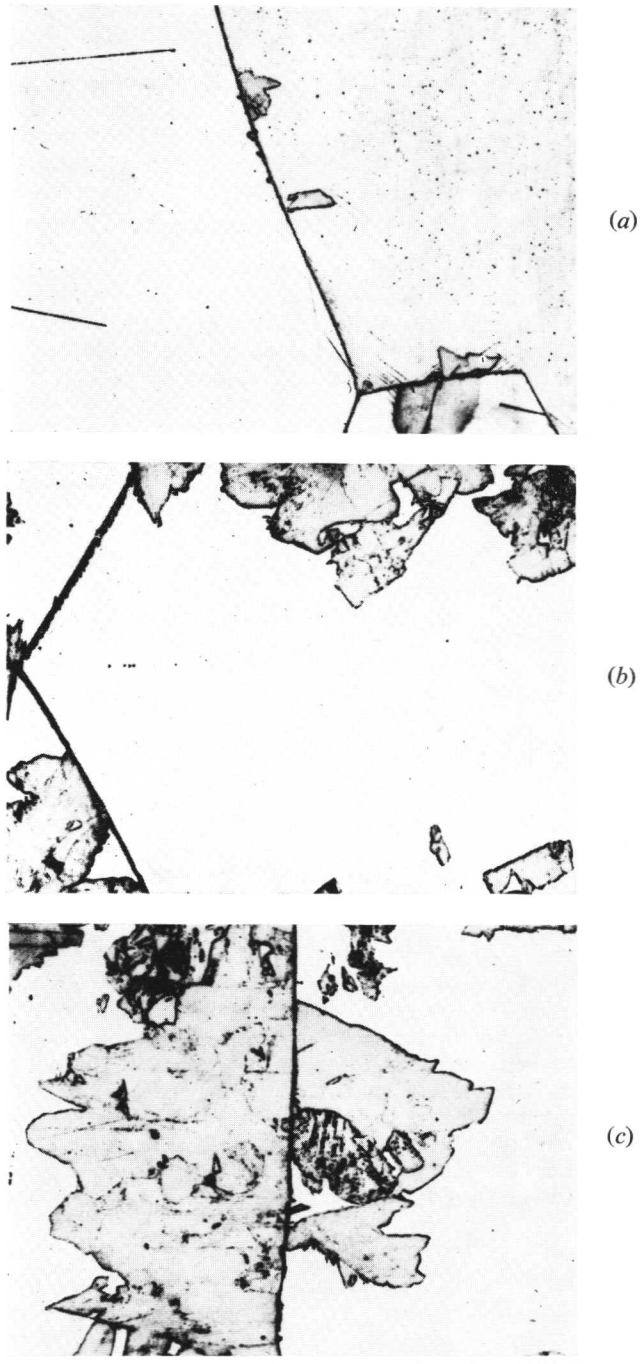

Fig. D.VI.4 *The extent of massive growth in three* 38% *Zn specimens held at* 480° *C for:* (a) 8, (b) 10, *and* (c) 14 *msec. Note the apparent delay time and rapid growth thereafter.* NH_4OH/H_2O_2 *etch.* × 160. (Cahn.)

† M. E. Brookes and R. W. Smith, *Trans. Met. Soc. A.I.M.E.*, 1968, **242**, 31.

in Q for the 45–50 at.-% Zn alloys that is rather similar to the variation shown by Mr. Brookes in his discussion. We agree that Q depends on order in this transformation.

Dr. AARONSON (*written discussion*): The authors explain the structure and migration mechanisms of β'/ζ° boundaries on the basis of the Kitchingman and the Mott models of interfaces. An alternative viewpoint on these aspects of interphase boundaries in massive transformations has recently been presented.* It appears to provide both a simpler approach to the problem and one that lends itself to a more direct test by experiment. This view, adapted from a previously presented theory of precipitate morphology, proposes† that there are two basic types of interphase boundary structure: the disordered type and the dislocation type. Unless strong boundary adsorption of a low-diffusivity solute occurs,‡ the disordered boundaries should be able to migrate freely at rates limited only by those of trans-interphase boundary diffusion. A dislocation boundary, on the other hand, is considered to have no mobility whatsoever in the direction normal to itself. This results from the kinetic difficulty of a change in crystal structure at a detectable rate, across the coherent regions between misfit dislocations. Such a change is difficult because it requires the creation of interstitial atoms in the matrix plane abutting these regions.§ All migration of dislocation interphase boundaries in both massive and precipitation reactions is therefore considered to take place by means of the ledge mechanism.

A dislocation boundary is most likely to develop at that boundary orientation corresponding to the least atomic mismatch across the boundary. In the $\beta' \rightarrow \zeta^\circ$ transformation, this is evidently the one corresponding to $(111)_\beta \parallel (0001)_{\zeta_0}$. It has been pointed out that the most direct test of this view of the growth aspect of the massive transformation would be to ascertain whether or not a misfit dislocation structure is present at this boundary orientation.‖ This demonstration has already been successfully accomplished for several precipitation reactions.¶ Analysis of the overall kinetics of growth in the direction normal to the $(111)_{\beta'} \parallel (0001)_{\zeta_0}$ boundary orientation on the basis of the ledge mechanism, as was recently carried out for a precipitation reaction,** would also be a valuable test of these concepts.

Dr. KITTL and Mr. CABO (*written reply*): We agree that the ideas proposed by Aaronson on the morphology of precipitates could be applied to interface-controlled transformations. However the " atomistic model " we presented for the transformation describes the interface displacement as well as Aaronson's model.

In other similar transformations (CuGa $\beta \rightarrow \zeta$ and AgCd $\zeta \rightarrow \beta'$) the interface appears to be part incoherent and part coherent as judged from metallographic observations. In these cases it has been observed that incoherent interfaces are highly mobile and, as for coherent interfaces, their mobility is due mainly to ledge displacements. These ledges are in fact " superledges ", since their thickness is in the micron range.

We can draw two conclusions from the available information:

(1) The displacement of the planar interfaces does not make a substantial contribution to the amount of phase transformed; hence the growth of these flat interfaces by displacement of submicroscopic steps or ledges appears not to contribute substantially to the overall growth process, but, following Aaronson's work this growth model is operative in certain cases.

(2) The planar interfaces move by super-ledge displacement or bulging out of a large portion across the planar interface.

We agree with Aaronson that the determination of the presence of a misfit dislocation structure is of importance but a determination of the contribution of submicroscopic ledge growth to the total growth must also be made to ascertain whether or not this contribution to growth is significant.

For future work we consider the analysis of the superledges and their contribution to growth to be of great interest. Their height and frequency are probably connected with the instability of the coherent interface to large fluctuations.

Dr. BROOM: Dr. Clark has given us a nice description of the natural history of these cubes with corners on and has implied that it is the internal stresses that determine the morphology. I wonder whether we know enough about the elastic constants to propound a quantitative theory.

Dr. H. McI. CLARK (University of Illinois, U.S.A.): No, we do not know anything about the elastic constants of the ζ° and the β' phases. However, our suggestion was based on the fact that the distortion of the lattices must be accommodated somehow. At the temperature of transformation 2–3% distortion is too much for elastic accommodation and it must be accommodated plastically.

Professor C. S. BARRETT (University of Chicago, U.S.A.): As one who likes to think of martensite as a thing with a shape change, how do your studies differentiate between a martensitic and an equilibrium phase?

Dr. CLARK: Perhaps it is a little confusing to use the term " shape change " but the martensite crystallographers have

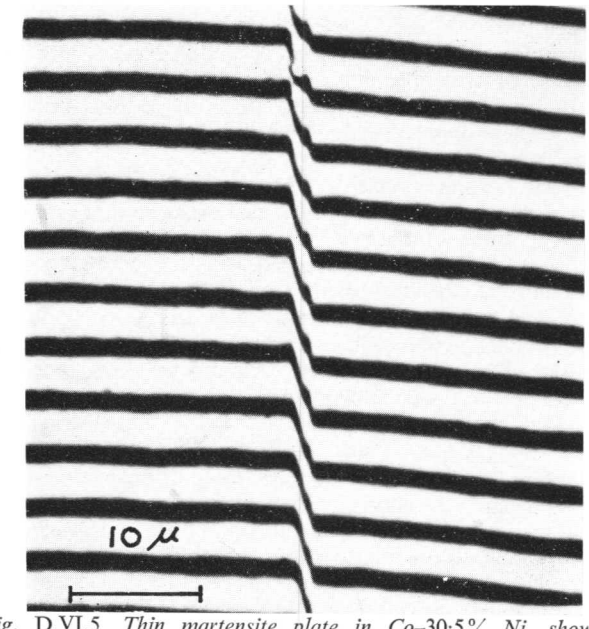

Fig. D.VI.5 *Thin martensite plate in Co–30·5% Ni, showing displacement across plate.* (Clark.)

* H. I. Aaronson, C. Laird, and K. R. Kinsman, *Scripta Met.*, 1968, **2**, 259.

† H. I. Aaronson, " Decomposition of Austenite by Diffusional Processes ", p. 462. **1962:** New York and London (Interscience Publishers).

‡ K. R. Kinsman and H. I. Aaronson, " Transformation and Hardenability in Steel ", p. 13. **1967:** Ann Arbor, Michigan (Climax Molybdenum Co.).

§ H. I. Aaronson, K. R. Kinsman, and N. A. Gjostein, unpublished research.

‖ H. I. Aaronson, C. Laird, and K. R. Kinsman, *Scripta Met.*, 1968, **2**, 259.

¶ J. L. Whitton, *J. Nuclear Mat.*, 1964, **12**, 115.

** C. Laird and H. I. Aaronson, *Acta Met.*, 1967, **15**, 73. G. C. Weatherly and R. B. Nicholson, *Phil. Mag.*, 1968, **17**, 801; H. I. Aaronson and C. Laird, *Trans. Met. Soc. A.I.M.E.*, 1968, **242**, 1437.

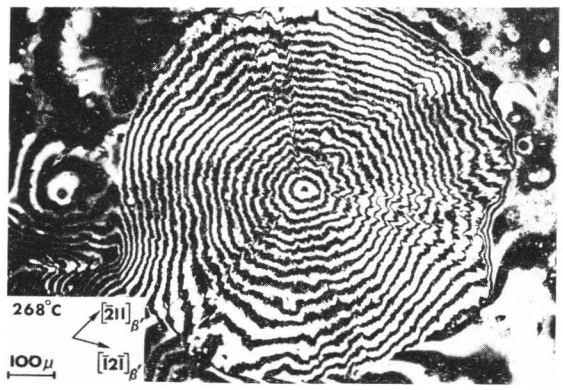

Fig. D.VI.6 *AgZn* $(111)_\beta$ *surface.* ζ° *particle with* c *axis normal to specimen surface, showing symmetrical upward displacement.* (Clark.)

only themselves to blame. I feel that " shape change " should be taken to mean a change in shape and this is certainly apparent on the surface of crystals partly transformed to the ζ° phase.

To answer your question specifically, a martensitic change would be one that shows a displacive nature across the plate, as in Fig. D.VI.5. What one sees on interference pictures of this material is, in general, rather complicated. However, a bull's-eye appearance is fairly typical (Fig. D.VI.6). The surface is pushed up in a rather symmetrical manner and this is quite consistent with the length increase involved in the lattice transformation.

Dr. KITTL: We disagree with the statement in the paper by Clark *et al.* that the critical ordering temperature is 240° C. We think it should be at least 255° C. Particles of ζ° still have more or less the same shapes when β' is transformed at 250° C, or at lower temperatures. Our present data are not consistent with a critical ordering temperature as low as 240° C.

Dr. CLARK: We made an experiment, both up-quenching from the β' phase to 250° C and down-quenching the β phase from 270 to 250° C and we observed exactly the same morphology, which is quite typical of that formed at the high temperature, namely the two obtuse-angle cones. There was no preferred growth and I would regard that as typical of growth from a disordered phase and not from an ordered phase. Therefore, I feel that the phase change must occur below 250° C.

Dr. M. J. COLLINS (Central Electricity Research Laboratories, Leatherhead): I have obtained some results that are similar to those of Berry *et al.* Fig. D.VI.7 is of an Fe–0·5% V–0·1% C alloy transformed at 840° C, showing rods and a fibrous carbide growth near an α/γ interface. Can your model be used to explain this structure?

Dr. A. T. DAVENPORT (University of Cambridge): We have also looked at this sort of structure and we think that the rods are part of the lamellar structure. I cannot say anything other than that at the present time. We do not understand what causes the fibrous structure to form on the interface.

If you have sheets of precipitates, then virtually no matter how you section the sheets in extracting your replica they will appear as lines. I must admit that those lines do not appear to run parallel to the interface, but this could be a sectioning effect. The only way one can study this reaction is from the very beginning, not when the pro-eutectoid ferrite has developed a long way from the austenite grain boundary.

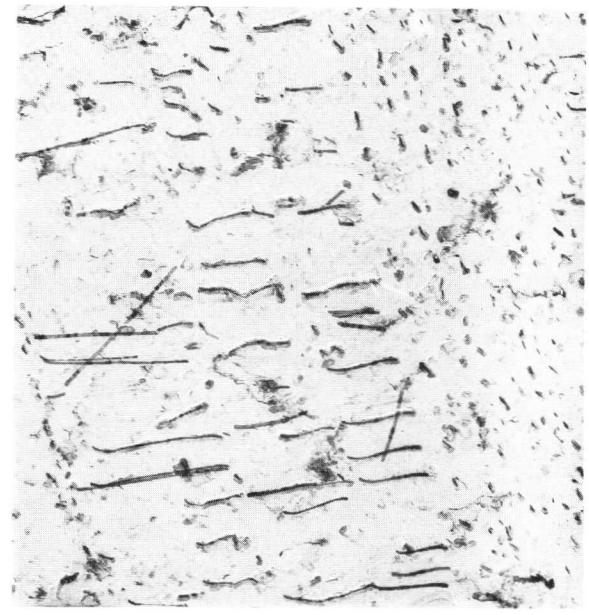

Fig. D.VI.7 *Carbon replica of Fe–0·5% V–0·1% C steel transformed at* 840° *C, showing rods.* × 15,000. (Collins.)

Dr. BAR-OR: Is Dr. Aaronson directly supporting our work by proposing an atomic jump on the bainite interface? Surely, even the ledges have to be controlled by interatomic jumps in the interface?

Dr. AARONSON: One requires ledge growth because the broad faces are immobile. Certainly, the atomic mechanism of the transformation is by diffusional jumps across the boundary at the ledges; that is why the term diffusional transformation is used, instead of glide or a martensitic transformation.

Dr. BAR-OR: I suggest that these ledges can also be formed by step-by-step diffusion.

Dr. AARONSON: If you could form them in that way there would be no need for them in the first place; you just have what Cahn calls continuous growth.

Dr. C. M. WAYMAN and Dr. G. R. SRINIVASAN (University of Illinois, U.S.A.) (*written discussion*): It is always nice to be able to sort things out on the basis of classification, and Dr. Aaronson is to be commended for his attempts to categorize more clearly than before bainite—a transformation, as he puts it, enveloped by an " aura of confusion " and, as Professor Christian interprets it, one " meaning all things to all men ". A number of interesting points have been made in his extensive survey which will hopefully provide stepping stones, rather than stumbling blocks, in clarifying the bainite dilemma. In our opinion, however, some of the points raised by Dr. Aaronson are subject to discussion, and we should like to take exception to them here.

In the first place—like it or not and whether correct or otherwise—we are at present, according to the literature, confronted with two forms of bainite, upper and lower. It is not clear from Dr. Aaronson's paper how these two forms should be distinguished and if, in fact, he considers them to exist as separate entities.

In a general way, it can be agreed that kinetics provides a difficult basis for classification of phase transformations. Research workers concerned with the martensite transformation have generally come to abandon as all-pervasive

such kinetic descriptions as fast, slow, isothermal, athermal, anisothermal, audible clicks, &c. (and, in addition, such mechanical descriptions as hard, brittle, &c.).

Concerning the microstructural definition of bainite, which seems to apply to conventionally prepared polished and etched specimens, we should note that certain inconsistencies can arise from the purely microstructural point of view. As Owen and Wilson have pointed out,* very similar microstructures can be obtained after different transformation mechanisms have operated. Among other comparisons, they note that blocks of massive product (no surface relief) formed from β-CuZn appear microstructurally similar to those observed in Fe–29% Ni, in which case the transformation is martensitic. Indeed, removal of the observed surface shears by polishing and etching somewhat obscures the character of the transformation in the latter case.

Coming now to the matter of surface relief and its relevance to bainite, it seems that Dr. Aaronson wants to " discard " a hard core of information that may ultimately be useful. It should be made clear that Dr. Aaronson's surface-relief definition of bainite apparently stems from the work of Ko and Cottrell (his Ref. 16), who noted that the surface-relief effects attendant on bainite formation are " similar to that due to the formation of martensite " and could be used to study bainite. It should be emphasized, however, that their observation is at best qualitative, and the nature of the strain (i.e., shape deformation) was not stated. This is understandable since it was not until a few years later that the invariant-plane-strain description of martensite became widely accepted.

In his paper Dr. Aaronson repeatedly refers to " martensitic relief effects ", " martensitic-like surface relief ", " relief effect of the martensitic type ", and " truly martensitic transformation ", yet it is not clear what he means or what he considers to be martensite-like relief, particularly since reference is not made to an invariant plane strain. Although he regards the surface-relief definition of bainite as including plates, needles, rods, and laths, clearly an invariant plane strain characteristic of martensite cannot apply to needles or rods, which have no habit *plane* and therefore cannot be described by an invariant plane strain. Furthermore, Dr. Aaronson refers to Fig. 3 of his paper, an interference micrograph " with martensite-like relief effect displayed with exceptional clarity ", which he claims applies to *a* Widmanstätten ferrite plate. If this relief is indeed martensitic, *two* adjoining plates must be involved. However, it should be pointed out that similar relief effects occur from α rod (not plate) precipitation from β-brass, in which case a composition difference exists and the transformation is acknowledged to be non-martensitic in nature.

Finally, we turn to a recent crystallographic study and analysis of lower bainite† (in which case Dr. Aaronson acknowledges the analysis to be at least partially successful !). In addition to having clearly established the plate-like morphology of lower bainite we were able to show both experimentally and theoretically that this transformation results in a body of self-consistent information, as is the case for martensite in steels. For example, the habit plane (different from martensite in the same material) is *irrational*, as is the orientation relationship between austenite and bainitic ferrite. In addition a martensitic shape change was established that was consistent in both character and magnitude, as evidenced by interferometry and scratch displacements. The point to be made here is that all this information fits together in a crystallographically consistent way; the right displacements go with the right variants, and the predictions of these features following the phenomenological theories of martensite crystallography not only parallel those which are observed but also yield irrational " quantities ", as are found experimentally and theoretically for the martensite transformation in steels. A further point is that the observed (and predicted) orientation relationship between austenite and bainitic ferrite is virtually identical to the irrational one (approximate Greninger–Troiano) found for martensite in steels, in which case the orientation relationship is considered to verify that a unique (Bain) correspondence exists between the two lattices. It should in addition be pointed out that the rather wide variation in the (irrational) bainite habit plane in steels with transformation temperature is not readily explained in terms of a microstructural definition. However, from the martensite crystallography point of view, habit-plane variations (as well as other changes in crystallography) can be considered as a result of varying elements of the inhomogeneous shear or dilatation parameter of the formal theories. Admittedly, the bainite transformation is rendered complex (relative to martensite in steels) by carbides, but it will be of great interest and importance to see what crystallographic results are obtained in future investigations of bainite.

Dr. Aaronson (*written reply*): It will be convenient to reply to this discussion on a paragraph-by-paragraph basis, beginning with the second.

The question of upper and lower bainite is a finer-scale problem than those with which this paper was intended to deal. Suffice it to say, then, that I do not consider that there is any fundamental difference in the reaction mechanisms of these two products. Their development may be the result of changes in ferrite crystallography with temperature, due perhaps to the changing difference in the lattice parameters of austenite and ferrite (with the high carbon content of the extrapolated Ae_3 at low temperatures as well as the different thermal-expansion coefficients of the two phases being involved). Alterations in the growth kinetics of individual ferrite plates, in the kinetics and crystallography of sympathetic nucleation (and thus in the morphology of sheaves—a more obvious difference between the two structures), and also in the various aspects of carbide precipitation follow readily from the changes in ferrite crystallography. At most carbon and alloy contents both structures fall in the " microstructural bainite " category; when carbides are absent, these structures can be considered simply as different groupings of Widmanstätten (proeutectoid) ferrite crystals.

Kinetics may no longer be a useful means of classification for martensite as is now accepted for nucleation and growth transformations. In the latter type of transformation, however, recognition that detailed studies of the kinetics of growth allow information to be obtained on the structure and the mechanism of migration of the interphase boundary has rendered such studies an important tool for understanding the atomic mechanisms through which the transformation takes place. It is possible that kinetic studies will eventually become equally useful in adding to our understanding of the martensite reaction.

A " purely microstructural point of view ", like any other, must be used carefully to be of value. For example, the

* W. S. Owen and E. A. Wilson, " Physical Properties of Martensite and Bainite " (Special Rep. No. 93), p. 53. **1965:** London (Iron Steel Inst.).

† G. R. Srinivasan and C. M. Wayman, *Acta Met.*, 1968, **16**, 609, 621.

experienced microscopist makes every effort to avoid deductions on transformation mechanisms solely on the basis of microstructures developed during the later stages of transformation; the difficulties that Wayman and Srinivasan mention appear to have arisen at least in part from this cause. One emphasizes, instead, the early and the intermediate stages of transformation, and tries to include kinetic, compositional, and even crystallographic studies of the microstructure, in order to obtain a more complete understanding of the phenomena under consideration. As to the microstructural definition of bainite itself, this pertains to a specific reaction mechanism; the technique aspect should not be overemphasized.

I am not proposing that we " discard a hard core of information ", but rather a definition. I did point out however, that this information, i.e., surface-relief effects, which relates to the growth mechanism of Widmanstätten ferrite, may be rather less useful than in the case of martensite, as it has led to the deduction of a mechanism of growth that does not appear to be correct.

Wayman and Srinivasan are concerned with my description of martensite-like relief effects. In particular, they seem insistent that martensite should exhibit an invariant plane strain. As Christian* points out, however, martensite in low-carbon, low-nickel alloys develops as needles or laths, rather than as plates. Klostermann† reports that surface martensite in Fe–30% Ni forms as needles, and makes it clear that the invariant-plane-strain concept is inapplicable. Yet, in both cases, the reaction product is undoubtedly martensite. For the present purpose, therefore, a quite general definition is used: tilting of an initially planar surface is taken to be a martensite-like relief effect, whereas " surface rumpling" (giving rise to a more or less continuously curved surface) is not.

The final point made by Wayman and Srinivasan is that they have successfully accounted for the crystallography of lower bainite in a high-alloy steel in terms of martensite crystallography theory, though not without appreciable (and sometimes unmartensite-like) assistance from the theory's disposable parameters. They suggest that the microstructural definition would be hard to do as well. However, since the microstructural definition of bainite has now been freed from restrictions with regard to the morphology of the ferritic component, and is concerned instead primarily with carbide precipitation, this challenge is irrelevant. What they really seem to be saying is that they have evidence that the ferritic component of lower bainite forms by shear. As the arguments of this paper and of my discussion on Christian's paper indicate, however, the shear mechanism (whose unit process is transport by dislocation glide), and the diffusional-growth mechanism (whose unit process is a thermally activated diffusional jump), can sometimes produce the same crystallography. Thus, additional evidence is needed to establish the mechanism of transformation. Admittedly, at very much higher temperatures, the analysis of data on the thickening kinetics of ferrite plates given in this paper seems to rule out the participation of a shear mechanism in the growth process. If the effects of carbides can be avoided, a similar study on lower bainite would be of great importance. I agree with Wayman and Srinivasan that further crystallographic information would also be of value. But I would remind them that when one is concerned with the mechanism of a transformation, one is dealing with a dynamic process. Hence kinetic studies, which provide a means of looking at growth while it is actually taking place, cannot be ignored.

Dr. P. M. KELLY (University of Leeds): Although I know it will be hopeless, could I plead with Dr. Aaronson to change his shear definition of bainite slightly to make it " a ferrite–carbide aggregate, where the ferrite plates exhibit a martensite-like relief effect "?

Dr. AARONSON: That is just a sub-definition. What you are doing is combining part of the microstructural definition with the surface-relief definition. In the work of Ko,‡ Flewitt and Towner,§ and Garwood,‖ there was no carbide or any second phase, yet this is clearly established in the literature as bainite. I think you are just adding an extra dimension of complexity to a situation that perhaps has already gone beyond retrieval!

Professor CHRISTIAN: This will probably be a minority view and possibly a minority of one. It really arises out of a comment in Dr. Kittl's paper when he talks about a transformation where half the atoms involved change places. He says that this requires extensive diffusion.

I would like to reserve the word " diffusion " for the situation where there is a differential equation of the type given in Cahn's paper, and to cut it out for situations where we are talking about atoms moving one or two atomic distances. In the latter case we are really talking about thermally activated migration.

I was brought up in the belief that diffusion meant diffusion, that is to say mixing of things, and did not mean migration.¶ If, ignoring this distinction, one talks about thermally activated transformations which involve no change in composition, these transformations are diffusionless and yet diffusion-controlled! I think this is wrong.

Dr. KITTL: Do you not like the classification of transformations controlled by short-range or long-range diffusion?

Professor CHRISTIAN: I do not like the way in which this classification is now used. Short-range diffusion means diffusion over relatively small distances, but " diffusion " over atomic distances seems to me to be nonsense.

* J. W. Christian, this vol., p. 129.
† J. A. Klostermann, this vol., p. 143.

‡ T. Ko, *J. Iron Steel Inst.*, 1953, **175**, 16.
§ P. E. J. Flewitt and J. M. Towner, *J. Inst. Metals*, 1967, **95**, 273.
‖ R. D. Garwood, " Physical Properties of Martensite and Bainite " (Special Rep. No. 93), p. 90. **1965:** London (Iron Steel Inst.).
¶ See, e.g., A. H. Cottrell, " Theoretical Structural Metallurgy ". **1955:** London (Edward Arnold).

Transformations in Solidified Gases

Charles S. Barrett

Transformations in solidified gases have been studied in very few laboratories yet they are governed by factors of wide scientific interest, some of which are very different from those involved in the commonly studied transformations of metallic substances. The principal methods used in the present work have been X-ray diffraction (diffractometry and photography) applied to fine-grained and coarse-grained samples frozen from the liquid state in a cell in which embedded metal wires assure temperature homogeneity. The samples have been subjected to thermal and mechanical treatments analogous to those used by metallurgists, within the temperature range from 4·2° K to the melting point. With these methods transformations of the following types have been studied: thermally activated first-order without orientation relationships; martensitic, with orientation relationship to the parent phase, both on cooling and on heating; order → disorder transformation in a superlattice; change in the degree of orientational disorder of diatomic molecules; change in the degree of antiferromagnetic alignment of molecules with magnetic moments; precipitation from solid solution, involving long-range diffusion; and transformations involving only short-range diffusion or none at all.

Many elements that are gaseous at ordinary temperatures solidify at low temperatures with crystal structures of very simple types (sometimes of low symmetry) that undergo various transformations. Among these solids and their mixtures can be found examples of every type of transformation and accompanying property changes that have been seen with metals and alloys. In addition there are types of transformations involving molecular reorientation and perhaps also libration or rotation of molecules. (However, experimental information on changes in libration or rotation is almost entirely missing, and single crystals that could provide it have seldom been grown.) The binding forces in these crystals are weaker than those in metallic, covalent, and ionic crystals; consequently the stabilities of some phases are influenced by perturbing forces that are likely to be less influential in the more familiar phases.

There are many reasons for interest in these solids. The van der Waals solids (particularly the solidified rare gases) have been the subject of a great many theoretical studies in the last 20 years, including frequent attempts to compute the relative stability of the phases. The advantage of such calculations is that the relative stability of the face-centred cubic and the hexagonal close-packed structures of these elements should be more readily calculated than for other classes of crystals or for more complex crystals. Nevertheless there has been a spectacular lack of success in these attempts.

It has now become possible to compute electron-density contours for diatomic molecules using molecular-orbit theory, and this accomplishment has increased the interest in intermolecular distances and other structural details of such crystals as solid N_2, O_2, and F_2 and their solid solutions. Despite the lack of reliable computations of the relative free energies of the phases, some of the structural details of the phases appear to be understandable in terms of packing and the postulated oscillation or rotation of molecules using the computed sizes, shapes, and electron-density gradients. These crystals are of increasing interest to spectroscopists, as more crystal structures become known and as more single crystals of the phases are prepared. Investigations of the O_2 phases have been stimulated by knowledge of the antiferromagnetism of the α phase.

Despite such reasons for scientific interest in these low-temperature phases, there have remained some phases with structures that are either unknown or uncertain, even among the pure elements. Oxygen, for example, has been the subject of numerous structure determinations in the last 40 years,[1] yet only in the last few years have the structures of the last of the three solid phases of this common element become known. It is remarkable also, that as recently as 1963, when Professor Lothar Meyer and the present author began to study mixtures of gases in the solid state, no phase diagrams had been studied by X-rays nor had any been published that could be considered trustworthy. There was a corresponding lack of data on transformations in the solid state.

It is the difficulty of getting meaningful data on phase diagrams or transformations by using thermal analysis and other indirect methods that accounts in large part for these gaps in our knowledge. Cooling curves have been used for locating liquidus and solidus lines and transformation temperatures and these are quite unable to disclose many of the transformations and precipitation reactions that involve only *small* latent heats or small changes in specific heats. Furthermore, thermal analysis is not likely to distinguish between a second-order transformation and a martensitic transformation or to deal effectively with metastable phases such as may result from supercooling. For example, the question of whether the $\alpha \rightarrow \beta$ transition in oxygen was a first-order or second-order transformation remained unclear until 1967. No phase diagram can be trusted unless it has been determined by appropriate diffraction methods, preferably X-ray or neutron diffraction, since with electron diffraction there is usually an uncertainty of several degrees in the effective temperature of the specimen and there is no

Manuscript received 12 February 1968. Professor C. S. Barrett, Ph.D., is at the James Franck Institute, University of Chicago, U.S.A.

opportunity to cold work the specimen. The preparation of the specimens is also important for confusion can arise from inhomogeneity and from phases remaining untransformed when they are cooled or heated into a temperature range where they are metastable. These are familiar pitfalls in phase-diagram determination and the means of avoiding trouble from them are well known, particularly among metallurgists. In the work with solidified gases it has proved to be particularly effective to use specimens frozen from the liquid state rather than vapour deposits, to cool rapidly through temperature regions in which segregation can occur, and to hold in single-phase regions for times long enough for diffusion to provide homogeneity. It has often been effective also, to subject the specimen to cold work at controlled temperatures, or to study the tendency for a phase to increase or decrease during annealing after the mechanical deformation.

Phase Diagrams Determined by X-Rays

The transformations to be discussed are found in pure elements and in the binary mixtures covered by phase diagrams that will be briefly introduced in this section. Details of the diagrams that remain uncertain are indicated by broken lines.

The argon–nitrogen diagram,[2] Fig. 1, has a solid solution with h.c.p. structure that extends over all compositions at high temperatures but which becomes unstable at lower temperatures with both low and high concentrations of N_2. Near the solidus the argon-rich mixtures are h.c.p. in structure with $c/a = 1{\cdot}635 \pm 0{\cdot}003$ and the nitrogen-rich compositions are based on pure N_2 which has molecules with centres on an h.c.p. array and molecular axes tilted at 54·5° to the c axis precessing around it, in space group $P6/mmc$.[3] The phases stable at low temperatures, f.c.c. Ar and α-N_2, are both cubic yet *intermediate* compositions remain stable in the hexagonal structure at all temperatures and do not transform to cubic even during plastic deformation.

The low-temperature phase α-N_2 has molecular centres very nearly on f.c.c. lattice points, and has the axes of the molecules pointing in [111] directions ($P2_13$, 4 molecules per cell, $a_0 = 5{\cdot}65$). The axes of nearest-neighbour molecules are therefore at an angle of 54° to each other. The same type of crystal structure is found in the low-temperature phase, α, of carbon monoxide.

The argon–carbon monoxide diagram,[4] Fig. 2, differs appreciably from Fig. 1 even though the molecule of CO is physically very similar to N_2 except for having a small dipole moment. The molecules CO and N_2 are isoelectric and are very similar in size, melting point, boiling point, and intermolecular distances in the solid state.[5] There is a $\beta \rightarrow \alpha$ transformation in N_2 at 35·6° K and in CO at 61·2° K. As shown in Fig. 2 however, the h.c.p. phase stable with all compositions at high temperatures decomposes eutectoidally at 53° K into the f.c.c. Ar-rich phase and the primitive cubic CO-rich phase of α-N_2 structure (these are labelled I and II respectively in Fig. 2). Unlike the Ar–N_2 system, the h.c.p. phase is unstable for all compositions at low temperatures.

The argon–oxygen diagram[6] is more complex than the ones just mentioned because O_2 exists in three modifications which will be discussed later. As indicated in Fig. 3, the solid solutions with the γ structure extend from the melting point down to a reaction isotherm at 40° K, slightly under the $\gamma \rightarrow \beta$ transition in pure O_2 at 43·8° K. The β-phase

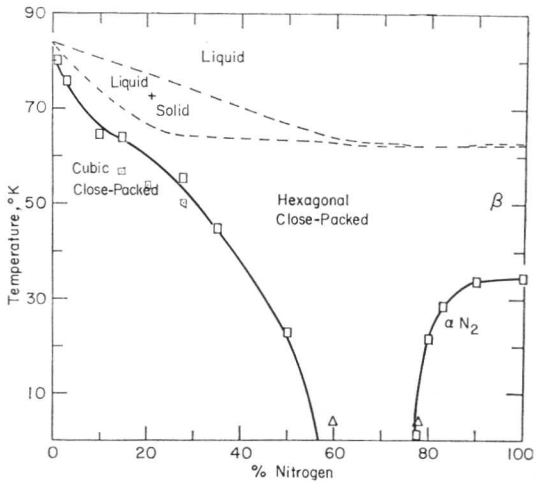

Fig. 1 *The Ar–N_2 phase diagram.*

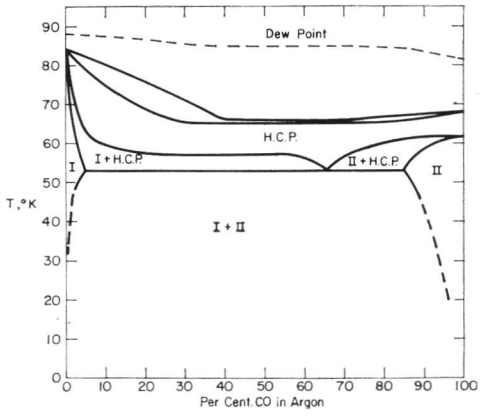

Fig. 2 *The Ar–CO phase diagram.*

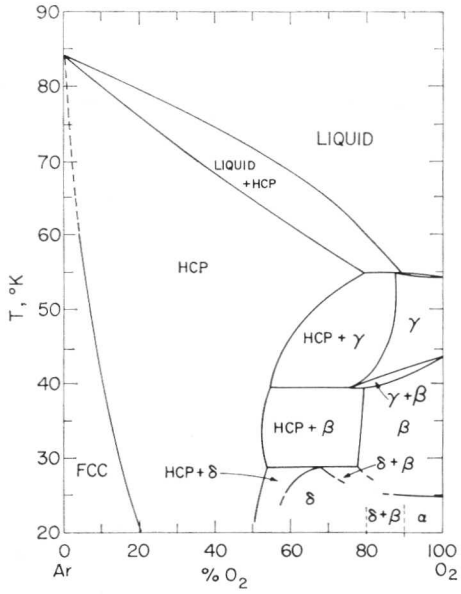

Fig. 3 *The Ar–O_2 phase diagram.*

region extends down to the temperature of the $\beta \rightarrow \alpha$ transition of O_2 at 23·8° K. The Ar-rich solid solutions of f.c.c. structure are of limited composition range in Ar–N_2, Ar–CO, and Ar–O_2, decreasing in width as the melting point is approached. The line of equal free energy between f.c.c. and h.c.p. phases on these diagrams, when extrapolated upwards, suggests that pure Ar would have the h.c.p. structure at temperatures just a few degrees above the melting point if melting had not occurred. A striking feature of the Ar–O_2 system is the occurrence of a previously unknown intermediate phase of cubic symmetry, δ, below ~ 28° K in the range ~ 55–90% O_2. Between this region and the Ar-rich region, the h.c.p. phase is stable at all temperatures.

The argon–fluorine system,[7] Fig. 4, differs from each of the preceding figures. Despite the very great similarity between the cubic structures of the high-temperature modification of F_2 and O_2 (discussed later) the h.c.p.-phase region that is a prominent feature of the Ar–O_2 system and of each of the other systems does not exist at all in the Ar–F_2 system. There is one eutectoid reaction at 40° K and there are no intermediate phases.

The nitrogen–oxygen system,[8] Fig. 5, is perhaps the strangest we have encountered. There are four reaction isotherms below the eutectic at 50° K. An unexpected phase has been found to be stable in part of the region 18–37% N_2 and 34–45° K; its powder diffraction pattern is accounted for by an orthorhombic unit cell which is under further investigation. This single-phase region terminates at the 34° K eutectoid line, and below this line there is a narrow region with a temperature range only 1·5° K wide in which β-O_2 coexists with β-N_2. Below the 32·5° K reaction line β-O_2 coexists with α-N_2, and below the 23° K reaction α-O_2 coexists with α-N_2.

Hydrogen (ortho H_2), frozen from the liquid in the h.c.p. form, undergoes a strain-induced martensitic transformation to f.c.c. over a range of temperature extending at least as high as 4·2° K when cold worked in this temperature range,[9] yet on simple cooling it appears to have a transformation temperature as low as 1·3° K.[10] The temperature at which h.c.p. and f.c.c. phases have equal free energies appears to be at least as high as 4·2° K, but is lower in para-H_2 and in D_2.[9] We found no solid solubility of neon in H_2 or D_2.[9]

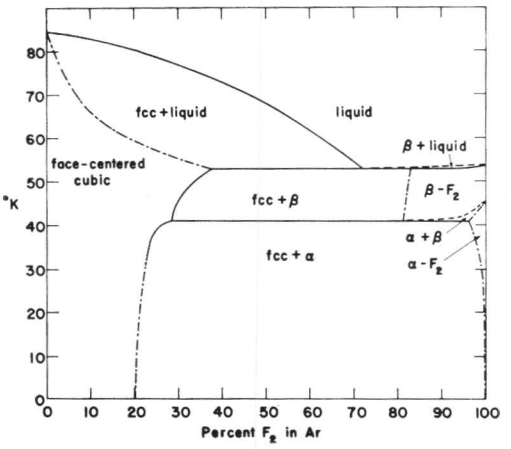

Fig. 4 The Ar–F_2 phase diagram.

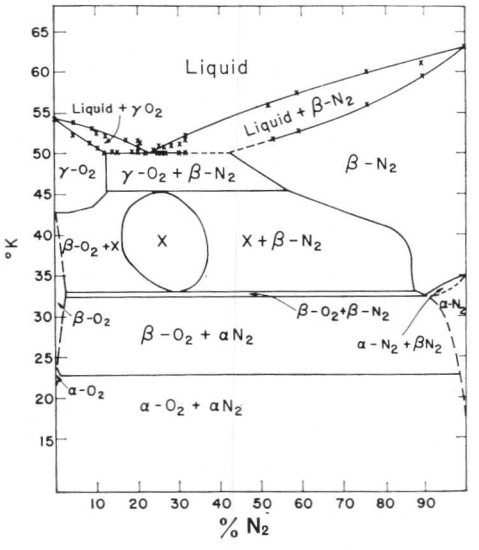

Fig. 5 The O_2–N_2 phase diagram.

Martensitic Transformations

The Ar-rich solid solutions in the Ar–N_2 and Ar–O_2 systems, Figs. 1 and 3 respectively, are stable in the f.c.c. form but the h.c.p. phase can be quenched to the lowest temperatures (even in pure Ar[11]) and then remain indefinitely as a metastable phase unless subjected to cold work. The passage of dislocations over the slip planes (which doubtless include (0001) h.c.p.) during plastic deformation permits the transition from h.c.p. to f.c.c. whenever the temperature of the specimen is below the line separating f.c.c. and h.c.p. phases in Figs. 1 and 3, and permits the opposite transformation during plastic deformation whenever the specimen temperature is above this line. This behaviour is exactly analogous to that in Co–Ni alloys[12] except that in Co–Ni alloys the *high*-temperature phase is f.c.c. and the *low*-temperature phase is h.c.p. The transition cannot be other than a strain-induced martensitic transformation. Reversion from f.c.c. to h.c.p. in Ar–N_2 can also be made to occur in a thermally activated fashion in the upper ranges of temperature.

An unexpected characteristic was observed during the experiments on this transformation in Ar-rich Ar–N_2 specimens; repeated hammering of the sample while it was maintained near the f.c.c./h.c.p. equal free energy line reduced the diffraction pattern to that of an amorphous sample.[3] Lesser cold working introduced many stacking faults judged by the weakening of the powder diffraction lines, but the process of freezing from the liquid seemed to introduce very few faults since (10.3), (10.2), and (10.1) lines were sharp.

The $\alpha \rightarrow \beta$ transformation in pure oxygen is clearly a martensitic one, as was proved by the fact that a large-grained specimen of α produced a spotty Debye picture with spots from $(001)_\alpha$ reflections remaining unchanged in position when the α-O_2 was transformed to β-O_2 on heating. These spots also remained upon cooling to α-O_2 again and survived even after repeated $\alpha \rightarrow \beta \rightarrow \alpha$ cycles, although they became somewhat more diffuse.[13] This established that the (001) plane of the monoclinic α-O_2 became the (111) plane of the rhombohedral β-O_2, as in analogous martensitic transformations among metals and alloys. Orientation relationships were not noted in polycrystalline experiments on the $\beta \rightarrow \gamma$ transformation of O_2 or in the $\alpha \rightarrow \beta$ transformation of N_2 or CO.[13] (No experiments using single crystals have been carried out.)

The $\alpha \rightarrow \beta$ Transformation in N_2

The $\alpha \rightarrow \beta$ transformation in N_2 appears to be thermally activated; it occurs very rapidly when the transformation temperature is reached on slow cooling or heating and is completed in a few seconds.[3] In the solid solutions of Ar in N_2 this transformation is too fast for bulk diffusion and segregation to occur.[8] In view of these characteristics and the fact that spotty Debye patterns have indicated that the $\beta \rightarrow \alpha$ transition eliminates all traces of the spots from β, it appears probable that the transformation is of the type known as *massive* and takes place by the rapid motion of high-angle grain boundaries with no regular orientation relationship between the old and new phase. However, there remains some possibility that it could be a martensitic transformation with an extremely narrow temperature range between initiation and completion, and with orientation relationships that would remain undetectable unless single-crystal techniques were used.

Quadrupole/quadrupole interactions have been cited as an important factor in stabilizing α-N_2. The downward trend of the $\alpha \rightarrow \beta$ transition line as Ar is added may be attributed to weakening of these quadrupole/quadrupole interactions. However, there appears to be no reliable quantitative information on the effects of the quadrupole moments either in the solid solutions or as a function of temperature in the pure element.

The Transformations in O_2

The structure of β-O_2 remained uncertain until 1962, when electron diffraction indicated that it was rhombohedral ($R\bar{3}m$; the equivalent hexagonal cell has $a = 3{\cdot}307$ Å, $c = 11{\cdot}256$ Å, and has 3 molecules per cell with their axes parallel to the hexagonal three-fold axis).[14] This structure has now been confirmed by several investigators. The variation of a and c with temperature is also now known.[13]

The structure of α-O_2 remained unknown even longer, partly because there was serious doubt[15] that a single-phase preparation of α had ever been produced. Certain reflections were practically identical for specimens above and below 23·88° K, as if coming from portions that had not transformed. The similarity of certain lines in the patterns of α and β, however, finally led to the discovery of the correct structure[16] when it was postulated that (0001) planes of β (hexagonal axes) became prominent planes of α without undergoing much distortion. The structure proposed on the basis of neutron-diffraction patterns[16] has now been confirmed with X-rays.[17] It has been shown that single-phase preparations can readily be obtained and X-ray photographs confirm that the (0001) planes of β do indeed become the (001) planes of α when α is described as C-face-centred monoclinic, $C2/m$, with two atoms per cell as indicated in Fig. 6; the structure has $a = 5{\cdot}403$ Å, $b = 3{\cdot}429$ Å, $c = 5{\cdot}086$ Å, $\beta = 132{\cdot}53°$.

Detailed calculations of electron density for the O_2 molecule have now been made[18] which are in accord with this monoclinic structure of α. The structure is now seen to consist of tightly packed rows of molecules along the [110] and [$\bar{1}$10] directions and also tightly packed rows along two directions in the ($\bar{2}$01) plane, when the molecules are assumed to have the calculated electron distribution (Fig. 7) and an effective size indicated by the 0·002 electron-density contour (in units of 67·49 e/Å^3), a contour enclosing 95% of the total charge.[19] The molecules are 3·18 Å wide and 4·18 Å long, and stand with their axes within a few degrees of the normal to the (001) plane. They are spaced more widely in the [010] direction than in the [110] and [$\bar{1}$10] directions, but in transforming from α to β these spacings between molecular centres are equalized and the plane containing them acquires a truly hexagonal array. These layers also shift over each other so as to make the periodicity of the stacking and the symmetry become those of a rhombohedral crystal.

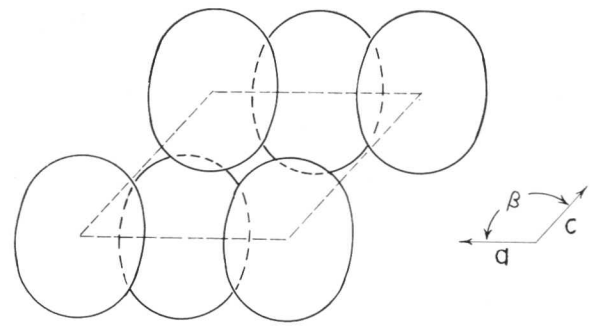

Fig. 6 The monoclinic unit cell of α-O_2 *projected along the* b *axis (normal to the paper) on to the* ac *plane. Size, shape, and orientation of molecules indicated; molecular axes lie parallel to* ac *plane; molecules with broken lines lie* b/2 *behind those in the front face of the cell.*

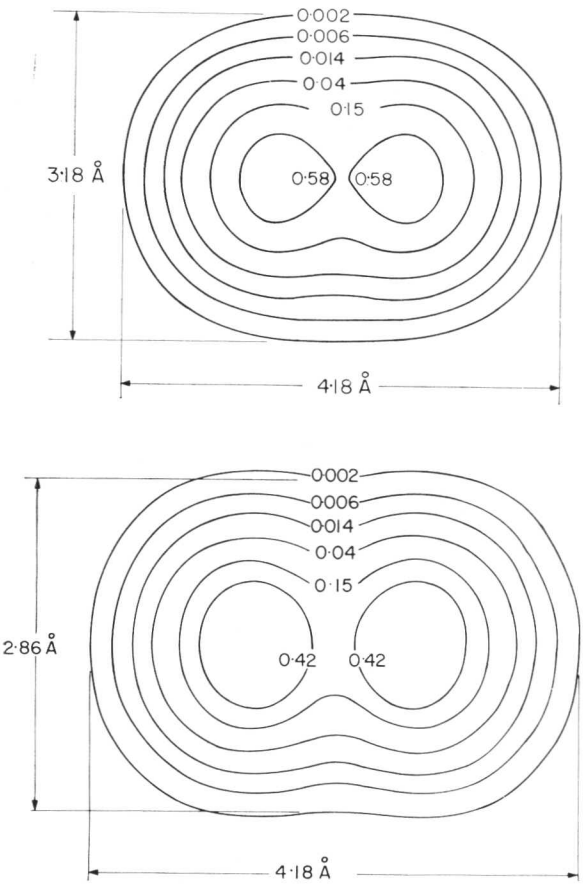

Fig. 7 Electron-density contours from self-consistent Hartree–Fock molecular-orbital calculations;[18] (a) *for the* O_2 *molecule* (3·18 × 4·18 Å) *and* (b) *for the* F_2 *molecule* (2·86 × 4·18 Å).

The wider spacing between molecules in the [010] direction suggests that in α-O_2 there may be vibrations of greater amplitude along [010] than along [110] or [$\bar{1}$10], or of greater amplitude of oscillation about [100] than about other axes in the basal plane. However, the corresponding spacings in β-O_2, which are equal in all three rows in the rhombohedral (111) plane, suggest that all molecules may be tilted from the three-fold axis and precess around the axis.

The $\beta \rightarrow \gamma$ transformation in O_2 involves a much more drastic alteration of structure than the $\alpha \rightarrow \beta$ transition; the latent heat is known to be $\sim 50\%$ greater than the latent heat of melting both in this high-temperature transition in O_2 and in the transition in F_2. As mentioned earlier, no indication has been seen in large-grained Debye patterns of any orientation relationship between the phases.

Oxygen is antiferromagnetic at the lowest temperatures with the magnetic moments of nearest neighbours in antiparallel arrangement,[16,17] a structure that accounts for the neutron-diffraction lines that have been obtained with the α phase.[19] Upon warming into the β-phase region the long-range antiferromagnetic order is lost. The lack of long-range order in β-O_2 can be attributed to the greater intermolecular distances in the β phase. It was first assumed that the magnetic moments in α were perpendicular to the $(001)_\alpha$ plane since the axes of the molecules are within a few degrees of this direction, but this assumption is not necessarily correct and some theoretical work now begun at the University of Chicago may or may not result in its confirmation.

The $\alpha \rightarrow \beta$ transformation has been classified as second order because of failure to detect unambiguously an abrupt change in the volume[21] or in the latent heat,[22] although the classification was uncertain in view of discrepancies between these experiments and earlier work by others. The change in molar volume is so small that X-ray determinations have not characterized it reliably. However, the change in symmetry that occurs at this transformation is such that it must be a first-order rather than a higher-order transformation.[13]

The δ Phase in the Ar–O_2 System

The phase labelled δ in Fig. 3 is a cubic phase that appears to form more readily from the γ-O_2 phase which is cubic, than from the β-O_2 phase which is rhombohedral.[6] The unit cell ($a_0 = 13{\cdot}23$ Å at 22° K) is very close to 8 times the volume of the unit cell of γ-O_2.[23] These two characteristics have led us to postulate a structure that is a superlattice of the δ phase and that predicts intensities in moderately good agreement with those of the observed X-ray powder diffraction pattern. Apparently the reaction in Ar–O_2 when held long enough below 28° K is the formation of this superlattice.

The F_2 Transformation

The high-temperature form of fluorine is very similar to that of oxygen.[24] It is cubic, *Pm*3*n*, with eight O_2 molecules per cell. It seemed likely that the low-temperature form was similar to α or β oxygen, particularly since recent measurements have shown[25] that the molar volume of γ-O_2 is related to the volume of β-O_2 or α-O_2 in the same manner that the volume of β-F_2 is related to α-F_2. However, the X-ray powder diffraction patterns could not be interpreted with a rhombohedral or other high-symmetry cell. When a monoclinic structure similar to α-O_2 but related to the calculated dimensions of the molecule 2·86 Å wide and 4·18 Å high (Fig. 7) was assumed, it was found that the positions of many diffraction lines were accounted for. Then, when a monoclinic cell with a height of two interplanar spacings of (001) planes, as in Fig. 8, instead of the height of one, as in Fig. 6, was taken, the positions of *all* reflections were accounted for.[26] A study of how the molecules might best fit together suggested that the axes might be tilted from positions normal to the (001) plane. We have recently found that the relative intensities of the powder diffraction lines of α-F_2 are such as to indicate that there is in fact a tilting of a few degrees from the perpendicular position of the molecules (see Fig. 8). The intensities are accounted for by assuming the same orientation for all atoms of a given layer, produced by a small tilt of molecules in one direction about an axis, and a rotation of the next (001) layer an equal amount in the opposite direction from the position normal to (001). The axis of rotation for this tilt was assumed to be the *b* axis.[26]

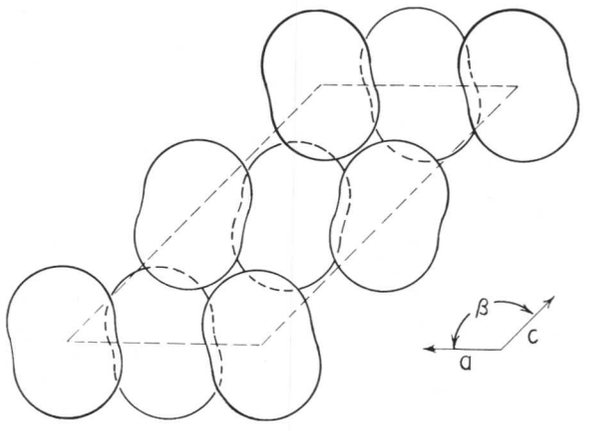

Fig. 8 The monoclinic unit cell of α-F_2 *projected along* b *on to the* ac *plane, with molecular size, shape, and orientation indicated; molecules with broken lines are* b/2 *behind those in the front face of the cell.*

Conclusions

In conclusion, it is well to emphasize that knowledge of these various structures and transformation characteristics developed very slowly with many incorrect postulates at first, but when two fundamental principles were recognized, progress was greatly accelerated. These principles are:

(1) That concepts of molecular packing, space filling, and molecular oscillation and rotation form a useful basis for understanding the structures and transformations of crystals of this type.

(2) That it is helpful to make use of the calculations of electron-density contours now available from self-consistent Hartree–Fock calculations of molecular orbitals carried out on large-scale digital computers, and particularly of the molecular sizes and shapes indicated by these calculations. Examples are found among these molecular crystals in which there is contact between molecules in certain directions (to an accuracy of 0·1 Å or perhaps better) when the crystals are assumed to have the calculated sizes, and some in which a transformation on heating results in equalizing intermolecular distances that were slightly different in the low-temperature phase.

References

1. J. C. McLennan and J. O. Wilhelm, *Phil Mag.*, 1927, **3,** 383; L. Vegard, *Z. Physik*, 1935, **98,** 1; E. M. Hörl, *Acta Cryst.*, 1962, **15,** 845; see also Ref. 24.
2. C. S. Barrett and L. Meyer, *J. Chem. Physics*, 1965, **42,** 107.
3. W. E. Streib, T. H. Jordan, and W. N. Lipscomb, *ibid.*, 1962, **37,** 2962.
4. C. S. Barrett and L. Meyer, *ibid.*, 1965, **43,** 3502.
5. B. C. Kohin, *ibid.*, 1960, **33,** 882.
6. C. S. Barrett, L. Meyer, and J. Wasserman, *ibid.*, 1966, **44,** 998.
7. C. S. Barrett, L. Meyer, and J. Wasserman, *ibid.*, 1967, **47,** 740.
8. C. S. Barrett, L. Meyer, S. Thomason, and J. Wasserman, *ibid.*, in the press.
9. C. S. Barrett, L. Meyer, and J. Wasserman, *ibid.*, 1966, **45,** 834.
10. A. F. Schuck and R. L. Mills, *Phys. Rev. Letters*, 1966, **16,** 616.
11. C. S. Barrett and L. Meyer, *J. Chem. Physics*, 1964, **41,** 1078.
12. J. B. Hess and C. S. Barrett, *Trans. Amer. Inst. Min. Met. Eng.*, 1952, **194,** 645.
13. C. S. Barrett, L. Meyer, and J. Wasserman, *Phys. Rev.*, 1967, **163,** 851.
14. E. M. Hörl, *Acta Cryst.*, 1962, **15,** 845.
15. R. A. Alikhanov, *J. Phys. Radium*, 1964, **25,** 449.
16. R. A. Alikhanov, *Zhur. Eksper. i Teoret. Fiziki*, 1963, **45,** 812; English translation: *Soviet Physics-JETP*, 1964, **18,** 556. Also private communication, 1966.
17. C. S. Barrett, L. Meyer, and J. Wasserman, *J. Chem. Physics*, 1967, **47,** 592.
18. R. F. W. Bader, W. H. Henneker, and P. E. Cade, *ibid.*, 1967, **46,** 3341.
19. C. S. Barrett and L. Meyer, *Phys. Rev.*, 1967, **160,** 694.
20. M. F. Collins, *Proc. Roy. Soc.*, 1966, [A], **89,** 415.
21. J. W. Stewart, *J. Phys. Chem. Solids*, 1959, **12,** 122.
22. C. H. Fagerstroem and A. C. Hollis Hallett, *Ann. Acad. Sci., Fennicae*, 1966, **AVI,** 210.
23. C. S. Barrett, T. H. Jordan, and L. Meyer, unpublished work.
24. T. H. Jordan, W. E. Streib, H. W. Smith, and W. N. Lipscomb, *Acta Cryst.*, 1964, **17,** 777; T. H. Jordan, W. E. Streib, and W. N. Lipscomb, *J. Chem. Physics*, 1964, **41,** 760.
25. J. A. Jahnke, *ibid.*, 1967, **47,** 336.
26. C. S. Barrett, L. Meyer, and C. Greer, unpublished work.

Research Note

A Band Structure for G.P. Zones and Its Effects

P. Wilkes and A. Hillel

It has long been known that clustering of solute atoms in a solid solution is associated with a resistivity anomaly. In spite of the decrease in the number of scatterers implicit in clustering, the resistivity increases, reaching a maximum for a cluster of $\sim$ 20 Å dia. for aluminium-base alloys.[1]

The assumption is often made that the resistivity maximum represents a standard state of the alloy with the same zone-size distribution irrespective of ageing temperature. The time to the maximum may then be used as a measure of clustering rate in the early stages, so giving an activation energy for the process. The results of this approach for aluminium[2,3] and copper[4] alloys give reasonable values for the energies of formation and motion of vacancies, both of which may control the clustering rate.

In view of the use being made of the resistivity anomaly it is clearly important to understand its origin. Until recently the generally accepted explanation has been due to Mott,[5] who proposed that enhanced scattering arose when the zones have a size comparable with the wavelength of the conduction electrons.

In aluminium this wavelength is $\sim$ 2·5 Å, which is clearly too small. A detailed calculation[7] using the formal transport equation confirms this, the critical scattering-zone size being less than one atom in diameter.

Labusch[7] has offered an explanation in terms of *Umklapp*—scattering from the G.P. zones. He shows that the anomalous resistivity could be due to this type of process in the case of spherical zones in aluminium-base alloys.

It has been proposed independently that the source of the extra scattering is Bragg reflection from the G.P. zones.[6] A simple one-dimensional treatment of this has shown[6] that a resistivity maximum can be explained in principle. This theory differs from that of Labusch in that the microstructure of the G.P. zones is the cause of the scattering rather than the Bloch character of the electron wave-functions. We believe this to be the correct explanation since, in a simple metal like aluminium, the wave function will approximate very closely to a single orthogonalized plane wave (i.e. free electrons) except at points on the Brillouin-zone boundary, so that *Umklapp* processes should be unimportant. However, in the case of G.P. zones, the two effects are qualitatively almost identical, since the periodic structure of the zones is coherent with that of the matrix.

In the present calculations we allow free electrons to scatter from a concentration of N_0 single solute atoms, which cluster into zones of size N atoms and concentration z/cm^3, leaving a concentration $(N_0 - Nz)$/cm^3 of single solute atoms. The resistivity (ρ) is given by

$$1/\rho = \frac{ne^2}{m} < \tau(\mathbf{k}) >_{\text{Fermi surface}} \qquad \ldots (1)$$

where $1/\tau(\mathbf{k}) = W(\mathbf{k})$ is the probability/sec that an electron in state k loses its momentum by collision.

Then

$$W(\mathbf{k}) = W_0 + (N_0 - Nz)W_1 + z\,W_N(\mathbf{k}) \qquad \ldots (2)$$

Simple transport theory leads to

$$W_N(\mathbf{k}) = \frac{mk}{(2\pi)^2 \hbar^3} \int_F d\Omega_{\mathbf{k}} (1 - \cos\theta_{\mathbf{k},\mathbf{k}'}) \mid v(\mathbf{k} - \mathbf{k}') \mid^2 \chi_N(\mathbf{k} - \mathbf{k}')$$

where the structure factor $\chi_N(q) \equiv \mid \sum_{\text{zone}} e^{iq.r} \mid^2$

Here $\Omega_{\mathbf{k}}$ is a volume in k space, $q = (\mathbf{k} - \mathbf{k}')$, θ is the angle between $\mathbf{k}$ and $\mathbf{k}'$, and W_0, W, and W_N are the scattering probabilities for the pure matrix, a single solute atom, and a zone of N atoms, respectively.

The form factor $v(q)$ is the Fourier transform of a single impurity potential.

As N increases, $\chi_N(q)$ develops Bragg peaks due to the microstructure of the zone. The peaks are at large momentum transfer, and so lead to an important additional contribution to ρ, increasing with N. Whether or not the resultant ρ increases with N depends on the shape of $v(q)$, and care was taken to make this accurate.

With spherical G.P. zones, Bragg scattering occurs at q_{Bragg} = a reciprocal lattice vector, which would appear to rule out any effect in a monovalent solvent where $2k_F < \mid q_{\text{Bragg}} \mid$. However, with a large mismatch in atomic sizes (as in copper–beryllium), the G.P. zones are flat. Then only the component of q in the plane of the zone enters $\chi_N(q)$, and as a result, the Bragg peaks are more diffuse and $\mid q_{\text{Bragg}} \mid$ is reduced.

It may be helpful to regard this as an early stage in the development of a separate Brillouin-zone structure for the G.P. zones superimposed on that of the matrix. The new, diffuse, Brillouin-zone structure is coincident with that of the matrix in the case of spherical zones, but not in the case of flat zones.

We simplify the calculation by making an approximation that is valid in the early stages of ageing.
From equations (1) and (2)

$$1/\rho = \frac{ne^2}{m} \left\langle \frac{1}{W(\mathbf{k})} \right\rangle = \frac{ne^2}{m} \left\langle \frac{1}{[W_0 + (N_0 - Nz)W_1 + zW_N(\mathbf{k})]} \right\rangle \qquad \ldots (3)$$

Manuscript received 3 July 1968. P. Wilkes, M.Sc., Ph.D., is in the Metallurgy Department, and A. Hillel, B.A., is in the Theoretical Physics Department, Faculty of Science, Manchester University. A. Hillel is at present working in the Theoretical Physics Department, Carnegie–Mellon University, U.S.A.

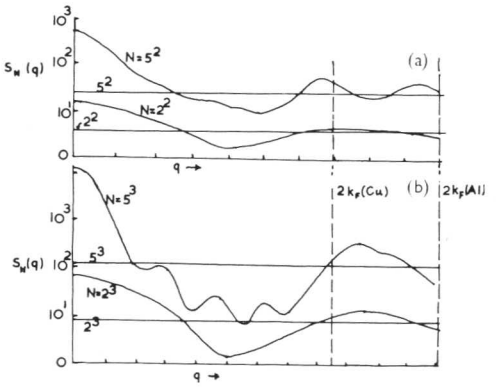

Fig. 1 *Structure factors for:* (a) *flat zones;* (b) *spherical zones.*

When $W(\mathbf{k})$ is fairly uniform one can put

$$\left\langle \frac{1}{W(\mathbf{k})} \right\rangle \simeq \frac{1}{\langle W(\mathbf{k}) \rangle}$$ This always *overestimates* ρ.

Then

$$\rho = \frac{m}{ne^2} \langle W(\mathbf{k}) \rangle = \rho_0 + (N_0 - Nz)\rho_1 + z\rho_N \qquad \ldots (4)$$

where $$\rho_N = \frac{4m^2 k_F}{\pi \hbar^3 n e^2} \int_0^1 dq\, q^3 \mid v(q) \mid^2 S_N(q)$$

$$S_N(q) = \langle \chi_N(q) \rangle \text{ orientations of zone}$$

and the notation for ρ is the same as for W in equation (2).

Figs. 1(*a*) and (*b*) show $S_N(q)$ for flat and spherical zones, respectively, (note logarithmic scale), for a f.c.c. structure.

We are interested in $\Delta\rho = z(\rho_N - N\rho_1)$. This is plotted in Fig. 2, with $z = 1$ zone/10^5 atoms $\sim 10^{18}$/cm^3, which is known to be an approximate upper limit to the zone concentration.

No maximum appears in Fig. 2, because the ultimate decrease in ρ is associated with the breakdown of our approximation (equation (4)). When N is large, equation (3) must be used for ρ. $W_N(\mathbf{k})$ becomes highly localized, so that the Bragg peaks affect $\langle 1/W(\mathbf{k}) \rangle$ to a decreasing extent. The resistivity now depends on z in a complicated way (equation (3)), which implies that the diameter of the zone associated with $\rho_{max.}$ cannot be truly independent of ageing temperature. This question has not yet been fully investigated.

The results show a much larger effect in Cu–Be than in Al–Cu, in agreement with experiment. A large effect is also predicted for Al–Ag.

Comparison with experimental determinations of $\Delta\rho_{max.}$ would lead one to conclude that the optimum zone diameter $D_{max.} \simeq 15$ atomic diameters for spherical zones, which is consistent with direct measurements.[1] For flat zones, the results imply that $D_{max.} > 20$ atomic diameters.

It is clear from these preliminary results that the resistivity anomaly can be explained by Bragg scattering from G.P. zones. The effect is relatively independent of temperature so that Matthiessen's rule will be obeyed. In many experiments ageing is interrupted by quenching and the resistivity is measured at the lower temperature. This has the advantage of reducing the resistance of the matrix so that scattering from the zones is greater in proportion. In the case of Cu–Be alloys it has been experimentally confirmed that Matthiessen's rule is obeyed during ageing.[4]

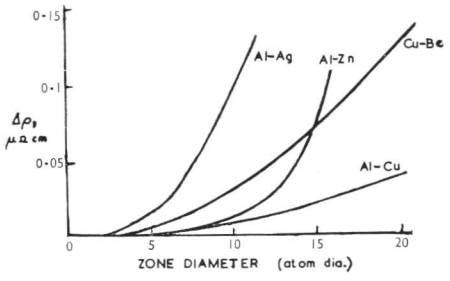

Fig. 2 *Resistivity increase for* 1 *zone*/10^5 *matrix atoms.*

The present calculation refers to nearly free electrons, where scattering is between points on an almost spherical Fermi surface. The conclusions cannot be applied to iron-base alloys where the principal scattering mechanism is from *s* to *d* states. The stronger dependence of the matrix scattering on composition may give deviation from Matthiessen's rule during ageing as the solution is depleted in solute. Anomalies of this kind have been observed.[8,9]

As the anomalous scattering arises from the new periodicity introduced by the presence of G.P. zones, any new periodicity should give a similar effect. It has long been suspected that the increase in resistance attributed to short-range ordering—the so-called *k*-effect—arises from the same cause as the G.P. zone resistivity anomaly. It can now be seen that the two effects are analogous. The requirements for observing a maximum are:

(*a*) A new periodicity within the lattice.

(*b*) The nucleus size for the new structure must be less than the critical size for maximum scattering.

The second condition is a stringent one, as the critical size is only a few atoms in diameter. Most precipitate nuclei are larger than this, so that maxima are not observed. This has given rise to the proposal that a resistivity maximum is unambiguous proof that G.P. zones are forming. The size of the nucleus is dependent upon its interfacial energy and a resistivity maximum therefore implies a very low interface energy. This in turn implies G.P. zones, but the possibility remains of a precipitate with such a small nucleus size that it will give a resistance maximum.

Finally, there is the interesting possibility that the energy of the G.P. zones may be qualitatively discussed in terms of the present analysis. The energy of a metallic structure is to some extent dependent upon the energy evaluated at points in reciprocal space where the structure-factor is non-zero.[10] In the case of flat zones additional points are produced. When suitable pseudopotentials are available for solid solutions the energy released by the formation of such zones should be calculable.

References

1. H. Herman and J. B. Cohen, *Nature*, 1961, **191**, 63.
2. C. Panseri and T. Federighi, *Acta Met.*, 1960, **8**, 218.
3. D. Turnbull, H. S. Rosenbaum, and H. N. Treaftis, *ibid.*, 1960, **8**, 277.
4. P. Wilkes, *ibid.*, 1968, **16**, 153.
5. N. F. Mott, *J. Inst. Metals*, 1937, **60**, 267.
6. P. Wilkes, *Acta Met.*, 1968, **16**, 863.
7. R. Labusch, *Physica Status Solidi*, 1963, **3**, 1661.
8. F. G. Wilson, private communication.
9. J. Higgins, unpublished work.
10. D. Weaire and J. E. Inglesfield, this vol., p. 321.

Research Note

Phase Changes and the Pseudopotential Method

D. Weaire and J. E. Inglesfield

In the last few years the model potential of Heine and Abarenkov[1] has been applied with considerable success to the problem of the relative energies of different crystal structures of non-transition metals.[2–4] By success we mean not only the development of plausible arguments that explain the observed structures, but also calculations that support them. The formalism used has been basically that of Harrison,[5] in which the energies of the electrons are treated in second-order perturbation theory and distortions of the Fermi sphere are neglected. While arguments may be adduced for the validity of such approximations, they are really justified by the measure of success achieved. It appears that the most important factor in the dependence of energy upon structure for these metals is the variation of the band-gaps $|2v(g)|$ with g, the magnitude of the corresponding reciprocal lattice vector, the pseudopotential matrix element $v(g)$ being sufficiently small for higher-order effects to be generally insignificant if not negligible.

We write the energy (per ion) of a metal at constant density as a sum of two terms

$$U = U_{\mathrm{E\,W}} + \mathrm{w} \sum_{g}{}' |S(g)|^2 E(g) \qquad \ldots (1)$$

The Ewald term U_{EW} arises from the electrostatic interaction of the ions, and may be evaluated by well-known methods due to Fuchs.[5] The contribution of the electrons, often called the band-structure energy, is expressed in terms of an energy-wavenumber characteristic $E(q)$ which is proportional to the square of the pseudo-potential $v(q)$.[2] Such an expression for the energy may be re-expressed in real space.[5] The ions are then seen to interact with an effective pair potential $\phi(r)$. Examples of $E(q)$ and $\phi(r)$ are shown below for the particular cases of Sn and Ga. As in much of solid-state physics, both real space and reciprocal space points of view are useful. Several recent and current applications are briefly described.

Calculations with the model potential[3] have been successful in accounting for the variation of c/a for Be, Mg, Zn, and Cd. The explanation of the large deviations of c/a from its ideal value for Zn and Cd in terms of the behaviour of $\phi(r)$ at the nearest-neighbour distance is shown in Fig. 1, which is sufficiently self-explanatory to need little further comment. The idea that the anomalous c/a values can be attributed to an instability of the ideally packed structure due mainly to the forces between nearest neighbours explains a great deal. For instance, it is no longer surprising that Howie and Jouffrey[6] failed to observe any change in c/a at a stacking fault in Cd. The α-Hg structure is seen to occur for precisely the same reason as the anomalous c/a for the other divalent metals, since it is related to f.c.c. by a similar distortion. In this case the instability of f.c.c. also has a neat explanation in terms of

Manuscript received 3rd July 1968. D. Weaire, M.A., and J. E. Inglesfield, B.A., are at the Cavendish Laboratory, Cambridge.

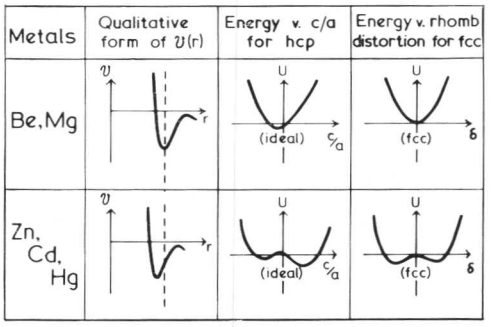

Fig. 1 Explanation of the occurrence of distorted structures for some divalent metals in terms of the interionic potential $\phi(r)$. (Broken line indicates nearest-neighbour distance for close-packed structures.)

$E(q)$. The (111) set of reciprocal lattice vectors is very close to the peak of $E(q)$ (which is similar to that shown in Fig. 3), so that a splitting of the set by rhombohedral distortion greatly lowers the band-structure energy. In a calculation using the model potential[3] the f.c.c. structure was found to be unstable with respect to such a distortion, and also metastable with respect to tetragonal distortion, in agreement with the observation of a tetragonal structure at low temperatures (β-Hg). Quantitative agreement with the observed magnitudes of distortion could be obtained only when the pseudopotential was reduced somewhat ($\sim 20\%$) but the agreement with experiment was then sufficiently convincing to invite speculation on the as yet undetermined structure of γ-Hg. It is suggested on the basis of the adjusted calculation that this might be the opposite rhombohedral distortion of f.c.c. to that which defines the α-Hg structure.[7]

The complicated crystal structures of Ga, and its pressure-induced phase change, may also be understood in terms of the pseudopotential.[4] Calculations show that the complicated orthorhombic structure of Ga I, stable at $T = 0°$ K, $p = 0$, has a band-structure energy lower than that of b.c.c., f.c.c., or h.c.p. metallic structures, this outweighing the raising of the Ewald electrostatic energy that results from departing from close-packed or nearly close-packed structures. The particular atomic arrangement leads to favourably placed reciprocal lattice vectors and, equivalently, in real space the neighbours tend to lie at the minima of $\phi(r)$.

The pressure-induced phase change from Ga I to f.c.t. Ga II may also be understood, and a very reasonable result for the atomic volume below which Ga II has a lower structural energy than Ga I has been obtained using a slightly modified pseudopotential. The corresponding effective pair potential enables us to understand the phase change in terms of interatomic distances (Fig. 2). On compression, the six neighbours in Ga I that lie at the first minimum of $\phi(r)$ move

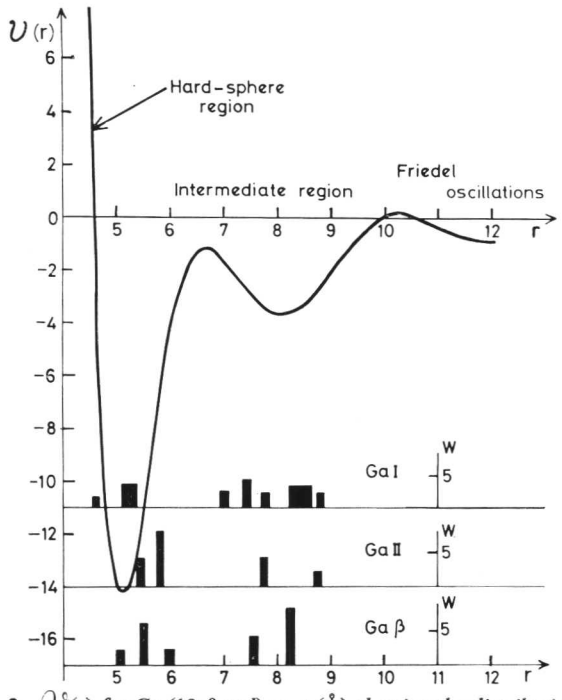

Fig. 2 $\mathcal{V}^{\circ}(r)$ *for Ga* (10^{-3} *ryd*) *vs. r* (Å) *showing the distribution of near neighbours in various structures.*

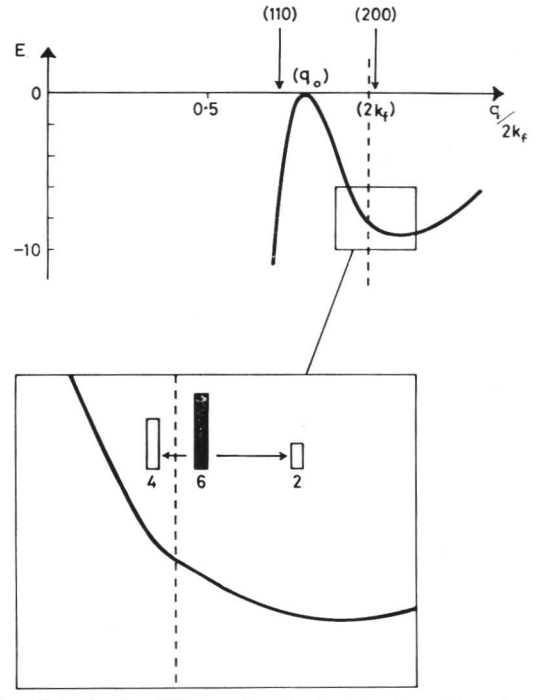

Fig. 3 E(q) *for Sn* (10^{-3} *ryd*) *calculated using Ashcroft pseudopotential,*[8] *and Hartree screening. The splitting of the* (200) *set of reciprocal lattice vectors of the b.c.c. structure for tetragonal distortion* (c/a ~ 0·92) *is indicated.*

out of the minimum, whereas the nearest neighbours in Ga II move into the minimum. Hence Ga II becomes energetically favoured.

Under pressure white Sn transforms to a structure related to b.c.c. by a small tetragonal distortion. This is at first surprising, since these (200) reciprocal lattice vectors lie near a *minimum* of $E(q)$ rather than the maximum and one would expect them to oppose such a distortion. A close examination (Fig. 3) shows that this is not the case owing to a slight wiggle in $E(q)$ near $2k_f$, where it has a very weak singularity in derivative. A preliminary calculation using the curve of Fig. 3 shows that this set of reciprocal lattice vectors actually contributes to instability for tetragonal distortions of the magnitude observed but strongly opposes larger distortions.

The perturbation-theory approach may be immediately applied to alloys of simple metals having the same valency, where the atoms have approximately the same size. The electronegativity difference appears through an " alloy potential ", which is the difference between the two model potentials. With this alloy potential alone, we can in some cases determine whether or not intermediate phases will form, and the width and ordering energy of such phases.

The configurational energy of an A–B alloy containing a concentration c of component B may be written as:

$$U_{\text{Config.}} = \frac{1}{2N}\left[c^2 \sum_{i,i'}{}' \mathcal{V}^{\circ}_A(|r_i - r_{i'}|) + (1-c)^2 \sum_{j,j'}{}' \mathcal{V}^{\circ}_A(|r_j - r_{j'}|) - 2c(1-c) \sum_{i,j} \mathcal{V}^{\circ}_A(|r_i - r_j|)\right] \quad \ldots (2)$$

The first double summation is over all A atoms, the second over all B atoms, and the third over all A and B. The potential $\mathcal{V}^{\circ}_A(r)$ may be derived from the alloy potential. Fig. 4 shows $\mathcal{V}^{\circ}_A(r)$ for the system Hg–Mg, and explains the ordering in HgMg.[9] Many problems still remain in cases where the

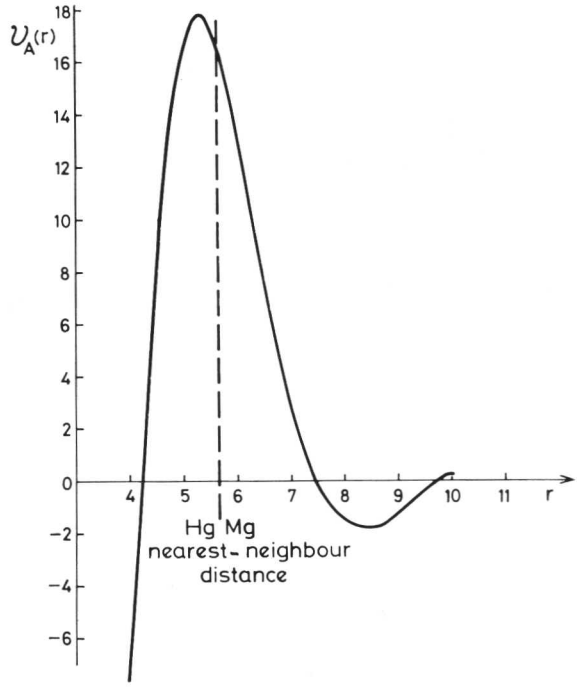

Fig. 4 $\mathcal{V}^{\circ}_A(r)$ *for Hg–Mg* (10^{-3} *ryd*) *vs. r* (Å).

atomic-size and valency differences are important.

Although higher-order perturbation terms (" covalency ") may in some cases be responsible for determining some of the details of structure, such as the precise value of c/a in a distorted structure, they are in general small. It is therefore appropriate for the discussion, inter alia, of martensite phase

transformations to consider a simple metal as made up of ions interacting with pairwise potentials. which have the appearance of a hard core at short range, and oscillate at medium and long range. The *quantitative* application of the method in this field will probably require pseudopotentials that are fitted to various structural properties, such as elastic constants, at the outset.

Acknowledgements

The authors would like to thank Dr. V. Heine for his help and advice. One of them (J.E.I.) received financial support from A.E.R.E. (Harwell).

References

1. A. O. E. Animalu and V. Heine, *Phil. Mag.*, 1965, **12,** 1249.
2. V. Heine and D. Weaire, *Phys. Rev.*, 1966, **152,** 603.
3. D. Weaire, *J. Physics* (*Proc. Phys. Soc.* (C)), 1968, **1,** 210.
4. J. E. Inglesfield, *ibid.*, 1968, **1,** 1337.
5. W. A. Harrison, " Pseudopotentials in the Theory of Metals ". **1966:** New York (W. A. Benjamin, Inc.).
6. A. Howie and B. Jouffrey, *Phil. Mag.*, 1966, **14,** 201.
7. D. Weaire, *ibid.*, 1968, **18,** 213.
8. N. W. Ashcroft, *Physics Letters*, 1966, **23,** 48.
9. J. E. Inglesfield, to be published.

Discussion

Dr. H. I. AARONSON (Ford Motor Company, Dearborn, U.S.A.): The pseudopotential is a more complex function than the Morse potential. Would Mr. Weaire explain in layman's language what kind of an advantage it possesses?

Mr. D. WEAIRE (University of Cambridge): The pseudopotential is the one seen by the electrons. It is put in at the start of the calculation of the interatomic potential, which is what is required. This is not all that complicated. Most of the oscillations at high r are not very important, but there is a considerable difference as compared with simple potentials in the intermediate region where you have that first bump. This is very important.

Professor J. W. CHRISTIAN (University of Oxford): I would like to ask Dr. Wilkes a question. It seems from what he said that one would expect a rather high resistance maximum to come from a spinodally decomposed structure with a high regularity. Would this be right?

Dr. P. WILKES (University of Manchester): Yes, but I have not measured it yet.

Mr. K. THOMAS (National Physical Laboratory, Teddington): I have some old results on ordering of $AuCu_3$ which seem to show that short-range ordering might in the same alloy give either an increase in resistivity or a decrease, depending on the temperature of formation. Now, does that put Dr. Wilkes to flight or would he be happy with such a situation?

Dr. WILKES: I think you could get either effect. The ordering produces a new diffuse Brillouin zone boundary and to predict an increase or decrease would require knowledge of the size of the ordered regions, the order parameter, the atomic spacing, and the pseudopotential of the system.

Professor V. GEROLD (Max Planck Institute, Stuttgart, Germany): I should like to mention that in the case of Cu–Au no resistivity increase was normally observed. However, within the first few seconds of ageing a very small increase was found.

Professor J. W. CAHN (Massachusetts Institute of Technology, Cambridge, U.S.A.): Is it possible to make phenomenological comparisons between electron-scattering or X-ray-scattering experiments and the resistance changes?

Dr. WILKES: In principle, the scattering factors are going to be the same. However, the electrons used for diffraction would be high-energy electrons considerably above the Fermi surface.

Dr. A. HILLEL (University of Manchester): As Dr. Wilkes said, it is just a question of the energy of the electrons. These energies are a few electron volts at the Fermi surface. Apart from that, what is happening here is simply a scattering of electrons from microcrystals.

Dr. WILKES (*written discussion*): The idea of eliminating the structure-factor calculation by using small-angle scattering results is very attractive. The intensity observed in such measurements is, however, confused by various background scattering processes. When these are eliminated, there remains the problem that the observed intensity is a multiple of the structure factor and the scattering factors involved. These latter for the high-energy electrons or X-rays are different from those for the conduction electrons. The best approach would probably be to compare the calculated structure factor with the observed intensity before going on to complete the resistivity calculations.

Professor J. NUTTING (University of Leeds): I want to ask Professor Barrett a question. If we can use the analogy of Mr. Weaire that atoms may be regarded as balls, I would have said metallurgy is essentially concerned with cricket balls, i.e., soft balls. I wonder what vacancy concentration is present in his " alloys "? In view of the fact that the atoms are such soft balls, can you get shuffling or interchange taking place without the help of vacancies?

Professor C. S. BARRETT (University of Chicago, U.S.A.): We do not know. We do know that you can have diffusion, homogenization, recrystallization, and recovery and all kinds of blacksmithing with which you are familiar, so we presume that there must be lots of vacancies. We would also like to study vacancies some day in these structures, but even to prove the presence of vacancies is not going to be so easy.

Dr. N. W. KING (Imperial College, London): I should like to ask Professor Barrett how slowly he cools his " alloys " when they have no two-phase region? He says he can quench his alloys and suppress the transformation, and then cold work them. How fast do you cool when you quench?

Professor BARRETT: Roughly, up to 10 deg/min. It is really not a quench. You do not need a quench to retain many of these phases down to the lowest temperatures. The slowest rate involves overnight holding at the most advantageous temperature.

Dr. A. G. CROCKER (University of Surrey): Mr. P. Marquis and I have performed some preliminary calculations on the atomic structure of boundaries. Eventually we plan to investigate transformation boundaries, as suggested by Dr. Aaronson, but initially we decided to examine the structure of twin boundaries in hexagonal close-packed crystals. Unfortunately, appropriate pair-potentials were not available for h.c.p. metals so we decided to use the Lennard–Jones potential for argon. As is well known, this potential predicts that argon should have the h.c.p. structure and perhaps, therefore, our results are more appropriate to some of the argon alloys examined by Professor Barrett, rather than to argon itself, which is of course f.c.c. A typical twin-boundary structure is shown schematically in Fig. D.VII.1, which indicates, as expected, that the atoms take up positions at the interface that are intermediate between parent and twin sites. Thus, we have established that interatomic potentials can be usefully employed to study the structure of boundaries. We now plan to use the pair-potentials developed by Mr. Weaire to examine twin boundaries in the h.c.p. metals and, if this proves successful, an investigation of transformation boundaries will follow.

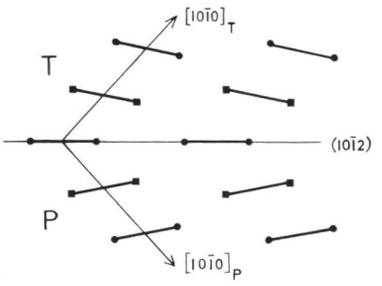

Fig. D.VII.1 *Schematic illustration of the structure a* $\{10\bar{1}2\}$ *twin boundary would have in hexagonal close-packed argon obeying a Lennard–Jones pair potential. The parent and twin structures, represented by P and T, respectively, are projected on to the* $\{1\bar{2}10\}$ *plane of shear. Motif pairs of atoms at each hexagonal lattice point are indicated by bars, atoms (represented by circles and squares) lying in the plane of the paper and at a distance* (a/2) *below the paper, respectively, where* a *is the lattice parameter. Note that the motif units at the twin boundary take up intermediate orientations between those in parent and twin.* (Crocker.)